TURUN
YLIOPISTO
UNIVERSITY
OF TURKU

THE HIDE-AND-SEEK CHAMPION:

Characterisation of ANO7 expression in prostate tissue and its role in cellular processes

Olli Metsälä

TURUN YLIOPISTON JULKAISUJA – ANNALES UNIVERSITATIS TURKUENSIS
SARJA – SER. D OSA – TOM. 1880 | MEDICA – ODONTOLOGICA | TURKU 2025

TURUN
YLIOPISTO
UNIVERSITY
OF TURKU

THE HIDE-AND-SEEK CHAMPION:

Characterisation of ANO7 expression in prostate tissue and its role in cellular processes

Olli Metsälä

TURUN YLIOPISTON JULKAISUJA – ANNALES UNIVERSITATIS TURKUENSIS
SARJA – SER. D OSA – TOM. 1880 | MEDICA – ODONTOLOGICA | TURKU 2025

University of Turku

Faculty of Medicine
Institute of Biomedicine
Medical Biochemistry and Genetics
Doctoral Programme of Molecular Medicine

Supervised by

Professor Johanna Schleutker, PhD
Institute of Biomedicine
University of Turku
Turku, Finland

Gudrun Wahlström, PhD
Institute of Biomedicine
University of Turku
Turku, Finland

Reviewed by

Alfonso Urbanucci, PhD
Faculty of Medicine and Health Technology
TAYS Cancer Centre and FICAN Mid
Tampere, Finland
Department of Tumor Biology
Institute for Cancer Research
Oslo University Hospital
Oslo, Norway

Adjunct Professor Tuomas Mirtti, MD, PhD
Finnish Cancer Institute and
Helsinki University Hospital
Department of Pathology
Helsinki, Finland

Opponent

Emeritus Professor G. Steven Bova, MD
Center for Cancer Eradication Research
Faculty of Medicine and Health Technology
Tampere University
Tampere, Finland

ISBN 978-952-02-0152-4 (PRINT)
ISBN 978-952-02-0153-1 (PDF)
ISSN 0355-9483 (Print)
ISSN 2343-3213 (Online)
Painosalama, Turku, Finland 2025

To my family

UNIVERSITY OF TURKU
Faculty of Medicine
Institute of Biomedicine
Medical Biochemistry and Genetics
OLLI METSÄLÄ: The hide-and-seek champion: characterisation of ANO7 expression in prostate tissue and its role in cellular processes
Doctoral Dissertation, 163 pp.
Doctoral Programme of Molecular Medicine
June 2025

ABSTRACT

Prostate cancer is one of the most prevalent cancers worldwide, imposing a significant burden on healthcare systems. Most cases are slow-growing; however, a minority progress to metastatic, lethal disease. Despite the relatively low mortality rate, high incidence of prostate cancer results in a substantial number of deaths.

Prognostication is primarily based on evaluating disease severity through clinical measurements, imaging, and histological evaluation. In localised prostate cancer, treatment decisions are informed by stratifying patients by the risk of disease progression. Low-risk cases are commonly managed through active surveillance, which helps avoid the morbidities associated with invasive treatments. By contrast, high-risk cases often undergo definitive local therapies, such as radical prostatectomy or radiotherapy, and adjuvant therapy. Cases presenting with intermediate-risk disease pose a more complex challenge for treatment selection. Consequently, there is a clear clinical need for additional prognostic tools for more precise differentiation between those who would benefit from invasive therapy with curative intention and those whose disease can be managed through active monitoring.

The *ANO7* gene is predominantly expressed in normal prostate tissue and prostate cancer. Genomic analyses have linked *ANO7* to the risk of prostate cancer and its more aggressive forms. Until recently, little was understood about the role of *ANO7* in cellular physiology and pathophysiology. We found that *ANO7* transcripts are enriched in the nuclei of prostatic luminal cells and prostate cancer cells, which indicates that *ANO7* is subject to post-transcriptional regulation via retained introns. We report that *ANO7* is highly expressed in luminal cells, but its expression is diminished in inflammation-induced club cell transformation in benign prostate glandular epithelium. We show that *ANO7* is associated with both androgen receptor signalling and lipid metabolism in luminal cells, as well as the presence of CD56bright natural killer cells in the epithelium. We present evidence showing that *ANO7* possibly serves a protective role and is particularly significant in low-grade cancer, where cancer-promoting lipid metabolism drives disease progression.

The results presented in this thesis bring information about the role of *ANO7* in prostate cancer. Further investigations about the cellular mechanisms of ANO7 is warranted for implementation of *ANO7* protein-altering germ-line mutations in clinical setting to improve risk stratification among prostate cancer patients.

KEYWORDS: ANO7, prostate cancer, AR signalling, lipid metabolism, prognosis

TURUN YLIOPISTO
Lääketieteellinen tiedekunta
Biolääketieteen laitos
Lääketieteellinen biokemia ja genetiikka
OLLI METSÄLÄ: Piiloleikin mestari: *ANO7*-ilmentymisen karakterisointi eturauhaskudoksessa ja rooli soluprosesseissa
Väitöskirja, 163 s.
Molekyylilääketieteen tohtoriohjelma
Kesäkuu 2025

TIIVISTELMÄ

Eturauhassyöpä on yksi maailman yleisimmistä syöpämuodoista. Useimmat eturauhassyöpätapaukset ovat hitaasti eteneviä, mutta pieni osa tapauksista kehittyy tappavaksi tautimuodoksi. Taudin suhteellinen kuolleisuus on alhainen, mutta silti suuri määrä miehiä kuolee eturauhassyöpään johtuen sen suuresta esiintyvyydestä.

Eturauhassyövän ennuste määritellään kliinisten mittausten, kuvantamisen ja histologisen arvion avulla. Paikallisen syövän tapauksissa hoito perustuu arvioon taudin etenemisriskistä. Matalan riskin syöpää hoidetaan tyypillisesti taudin aktiivisella seurannalla, mikä auttaa välttämään invasiivisten hoitojen aiheuttamia komplikaatioita. Korkean riskin potilaat hoidetaan usein eturauhasen poistoleikkauksella tai sädehoidolla, sekä liitännäishoidoilla. Keskisuuren riskin tapaukset ovat haastavia hoitovaihtoehtojen suhteen. Erityisesti näissä tapauksissa tarvitaan parempia taudinkuvaa ennustavia apukeinoja, jotta invasiivinen hoito voidaan kohdentaa siitä todellisuudessa hyötyville potilaille.

ANO7-geeniä ilmentyy pääasiassa normaalissa eturauhaskudoksessa sekä eturauhassyövässä. Genomianalyyseissa on löytynyt yhteys *ANO7*:n ja eturauhassyövän välillä. Tähän asti on tiedetty hyvin vähän *ANO7*:n vaikutuksesta normaalien ja sairaiden solujen toimintaan. Tuloksissa osoitamme, että *ANO7* transkripteja kertyy eturauhasen ontelosolujen (engl. luminal cell) ja syöpäsolujen tumaan, joka viittaa geenin luennan jälkeiseen lähetti-RNA:n säätelyyn intronipidätyksen vaikutuksesta. Näytämme, että hyvänlaatuisessa rauhasepiteelissä *ANO7* esiintyy pääasiassa ontelosoluissa, mutta sen ilmentyminen vähenee, kun solut muuttuvat nuijasoluiksi (engl. club cell), mikä tapahtuu tulehduksen yhteydessä. Osoitamme, että *ANO7*:n ilmentyminen on yhteydessä sekä androgeenireseptorisignalointiin että lipidimetaboliaan ontelosoluissa, sekä tietyn NK-solun alatyypin esiintymiseen rauhasepiteelissä. Esitämme aineisto, joka osoittaa, että *ANO7*:lla on suojaava vaikutus syöpää vastaan, erityisesti matala-asteisessa syövässä, jossa lipidimetabolia edistää taudin etenemistä.

Tässä väitöskirjassa esitetyt tulokset lisäävät tietämystä *ANO7*:n roolista eturauhassyövässä ja edellyttävät lisätutkimuksia proteiinin mekanistisesta toiminnasta soluissa. Tämä tieto vaaditaan, jotta *ANO7*:ssä sijaitsevia proteiinia muuttavia perinnöllisiä mutaatioita voidaan käyttää eturauhassyöpäpotilaiden riskiluokittelua.

AVAINSANAT: ANO7, eturauhassyöpä, AR-signalointi, lipidimetabolia, ennuste

Table of Contents

Abbreviations

5-ARI	5α-reductase inhibitor
ACC	acetyl coenzyme A carboxylase
ACLY	ATP citrate lyase
ACO2	aconitase 2, mitochondrial
ACP3	acid phosphatase 3
AKT	AKT serine/threonine kinase
ANO7	anoctamin 7
ANO7-L	ANO7 long isoform
ANO7-S	ANO7 short isoform
ATP	adenosine triphosphate
ATM	ATM serine/threonine kinase
AR	androgen receptor
BRCA2	BRCA2 DNA repair associated
BPH	benign prostatic hyperplasia
CD	cluster of differentiation
cDNA	complementary DNA
CoA	coenzyme A
COX	cyclooxygenase
cyt	cytoplasm
DAPI	4′,6-diamidino-2-phenylindole
DCXR	dicarbonyl and L-xylulose reductase
ddPCR	droplet digital polymerase chain reaction
DEG	differentially expressed gene
DHT	dihydrotestosterone
DSP	digital spatial profiler
EGF	epidermal growth factor
EGFR	epidermal growth factor receptor
ER (in ERα and β)	oestrogen receptor
ER	endoplasmic reticulum
FASN	fatty-acid synthase
FDR	false discovery rate

FF	fresh frozen
FFPE	formalin-fixed paraffin-embedded
GAPDH	glyceraldehyde 3-phosphate dehydrogenase
GO	gene ontology
GSEA	gene set enrichment analysis
H&E	haematoxylin and eosin
HOXB13	homeobox B13
HPA	human protein atlas
IF	immunofluorescence
IHC	immunohistochemistry
INF-γ	interferon gamma
KEGG	Kyoto encyclopedia of genes and genomes
KLK	kallikrein
KRT	keratin
MALAT1	metastasis associated lung adenocarcinoma transcript 1
MOI	multiplicity of infection
MPC	mitochondrial pyruvate carriers
MSMB	beta-microseminoprotein
mTOR	mechanistic target of rapamycin
mTORC	mTOR complex
MYC	MYC proto-oncogene, bHLH transcription factor
MUC2	mucin 2
NF-κB	nuclear factor kappa-chain-enhancer of activated B-cells
NK	natural killer
NKX3-1	homeobox protein Nkx-3.1
NTC	no template control
nuc	nucleus
PCa	prostate cancer
PET	positron emission tomography
PI3K	phosphatidylinositol-4,5-bisphosphate 3-kinase
PIA	proliferative inflammatory atrophy
PRAD	prostate adenocarcinoma
PSA	prostate-specific antigen
PSMA	prostate-specific membrane antigen
PPIB	peptidylprolyl Isomerase B
PTEN	phosphatase and tensin homolog
Rb	retinoblastoma protein
ROI	region of interest
RNAi	RNA interference
RNA-FISH	ribonucleic acid fluorescent in situ hybridisation

scRNA-seq	single cell ribonucleic acid sequencing
SCD	steroyl-CoA-desaturase
SDS-PAGE	sodium dodecyl sulphate polyacrylamide gel electrophoresis
shScr	shRNA with scrambled microRNA sequence
shRNA	short hairpin ribonucleic acid
SINE	short interspersed nuclear elements
siRNA	small interfering RNA
SNP	single nucleotide polymorphism
SPDEF	SAM pointed domain containing ETS transcription factor
SREBF	sterol regulatory element-binding transcription factor
SREBP	sterol regulatory element-binding protein
STN	solid tissue normal
ssGSEA	single sample gene set enrichment analysis
TBP	TATA binding protein
TCA	tricarboxylic acid
TCGA	the cancer genome atlas
TMPRSS2	transmembrane protease, serine 2
TNF-α	tumour necrosis factor alpha
TP53	tumour protein p53
UMAP	uniform manifold approximation and projection
wc	whole cell
WT	wild type

List of Original Publications

This dissertation is based on the following original publications, which are referred to in the text by their Roman numerals:

I Olli Metsälä, Gudrun Wahlström, Pekka Taimen, Pirkko-Liisa Kellokumpu-Lehtinen, and Johanna Schleutker. Transcripts of the Prostate Cancer-Associated Gene ANO7 Are Retained in the Nuclei of Prostatic Epithelial Cells. *International Journal of Molecular Sciences*, 2023, 24, 1052.

II Olli Metsälä, Gudrun Wahlström, Neha Goel, Mitro Miihkinen, Pekka Taimen, and Johanna Schleutker. Spatial profiling of *ANO7* in prostate tissue: links to AR-signalling-associated lipid metabolism and inflammation. *The Journal of Pathology*, 2025, 265(4), 518-531.

1 Introduction

Prostate cancer is one of the most common cancers affecting men worldwide. Autopsy studies suggest that prostate cancer prevalence is similar in all populations (Bell et al., 2015), however, the prevalence of diagnosed prostate cancers shows diversity, being more common in Western countries and men with West-African ancestry (Sung et al., 2021). The risk factors for prostate cancer include old age, lifestyle habits, and hereditary factors including family history of prostate cancer and inherited mutations. In fact, a substantial portion of prostate cancer risk is explained by genetic factors (Bergengren et al., 2023). The prognosis is generally good for prostate cancer at the time of diagnosis, however, due to the high prevalence of the disease, also the absolute number of prostate cancer-specific deaths is high (Sung et al., 2021). Prostate cancer originates in the prostate, a walnut-sized gland that produces seminal fluid, which nourishes and transports sperm. Prostatic epithelium contains secretory cells, that are specialised to produce citrate and other key component of the seminal fluid. These luminal cells of the prostate also harbour unique metabolism that cannot be found in any other cells of human body (Costello and Franklin, 2006). Luminal cells are also thought to be the cell type from which prostate cancer originates (Lee and Shen, 2015). The disease often progresses slowly and may initially present with mild or no symptoms. Prostate cancer is usually diagnosed in old men, therefore, with the slow progression, the patients usually die with prostate cancer and not because of it. However, when it advances, prostate cancer can develop into an aggressive form, which metastasises primarily to bone as well as liver, lungs and brain. If the treatments fail or the patient is not fit enough to tolerate treatments, metastatic prostate cancer eventually leads to death.

Prostate cancer treatment has taken major steps during the last decades leading to reduced mortality (Bergengren et al., 2023). However, especially the prostate-specific antigen (PSA) testing has led to detection of clinically non-significant cancers and overtreatment, which leads to patient's overtreatment and causes unnecessary adverse effects (Bell et al., 2015). Low risk cases can be treated with active surveillance while high risk cases are treated with surgery, radiation therapy, and/or chemotherapy, depending on the nature of the cancer (Cornford et al., 2024). The intermediate risk cases present a challenge for treatment decision making

(Cornford et al., 2024), and better prognostic tools are needed for improved risk stratification.

The *ANO7* gene (Anoctamin 7) encodes a protein that is predominantly expressed in the prostate gland. This gene is of particular interest in prostate cancer research due to its potential role in the disease's progression and its utility as a diagnostic and therapeutic target (Cereda et al., 2010; Marx et al., 2021). ANO7 has been shown to be involved in various cellular processes, including calcium-dependent ion channelling and phospholipid scrambling (Guo et al., 2021), and suggested to influence cell-cell interactions (Das et al., 2007). Several single nucleotide polymorphisms residing in *ANO7* associate with risk of prostate cancer (Conti et al., 2021) and aggressive form of prostate cancer (Kaikkonen et al., 2018). Moreover, the expression of *ANO7* is altered in prostate cancer, with lower levels observed in high-grade tumours compared to low-grade and benign tissues (Sinnott et al., 2017; Figiel et al., 2023). This evidence suggests that *ANO7* could serve as a biomarker for prostate cancer diagnosis and prognosis.

Better understanding of the functional role of *ANO7* in normal and cancerous prostate could pave the way for new therapeutic strategies aimed at targeting the treatments for patients that likely will benefit from them, *i.e.,* utilisation of *ANO7* in precision medicine.

2 Review of the Literature

2.1 The prostate

This chapter will outline the key developmental and structural features of the prostate relevant to this thesis, aiding to understand of the factors underlying prostate function.

The prostate is a glandular organ within the male reproductive system, located beneath the bladder and anterior to the rectum. During human embryonic development, the prostate begins to form between weeks 8 and 10, reaching a branched structure by week 11, after which ductal canal formation occurs. Within these canals, the epithelium organises into basal and luminal cell layers, enabling secretory cytodifferentiation (Cunha et al., 2018). At birth, the prostate has developed into a single-lobed structure, with full maturation occurring during puberty (Buskin et al., 2021). The adult prostate is the size of a walnut.

The prostate consists of four anatomical regions: peripheral zone, central zone, transition zone, and anterior fibromuscular stroma (Figure 1) (McNeal, 1968). Among the glandular regions, the peripheral zone constitutes over 70% of the prostate's volume, the central zone approximately 25%, and the transition zone 5% of the volume (McNeal, 1981). The anterior fibromuscular stroma is an integral part of the prostate, while it also maintains bladder pressure in conjunction with the bladder neck (Ehrlich et al., 2010). The androgen receptor (AR) functions as a master regulator in prostate development (Buskin et al., 2021). AR activation is mediated by circulating steroid hormones, primarily testosterone and dihydrotestosterone (DHT). DHT is a potent metabolite of testosterone (Baulieu, Lasnitzki and Robel, 1968) and exhibits an affinity for AR ten times greater than that of testosterone (Cunha et al., 2018). A deficiency in the enzyme 5-alpha reductase, which converts testosterone to DHT, leads to underdevelopment of the prostate and male external genitalia (Cunha et al., 2018). Additionally, without AR signalling activation, male embryos develop female genitalia, underscoring the pivotal role of AR and androgens in male sexual differentiation (Buskin et al., 2021).

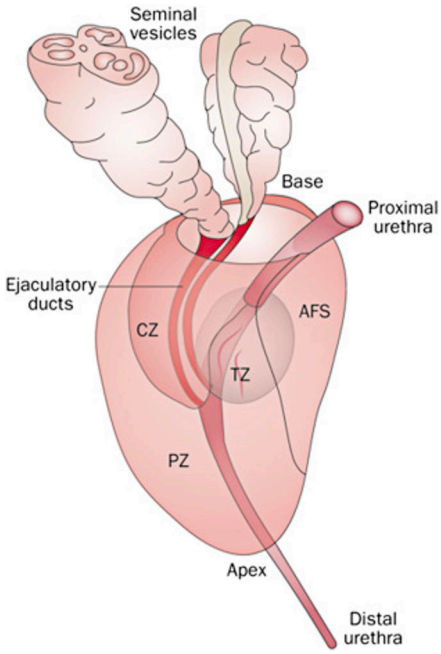

Figure 1. The zonal anatomy of the prostate. The prostate consists of transition zone (TZ), central zone (CZ), peripheral zone (PZ), and anterior fibromuscular stroma (AFS), with ejaculatory ducts and urethra traversing the organ. The figure is reproduced from Risbridger (2018) with permission.

During prostate development, the activation of AR signalling initiates and maintains the expression of various genes and pathways essential for the formation of the tissue's ductal structure. The andromedin hypothesis posits that, in response to AR activation, mesenchymal cells produce paracrine factors that regulate epithelial growth and differentiation (Toivanen and Shen, 2017). Such factors are suggested to include for example fibroblast growth factors (FGFs) 7 and 10, and Wnt agonists (Buskin et al., 2021). However, this regulatory mechanism likely involves more than a straightforward upregulation of growth factors to drive epithelial development (Pletcher and Shibata, 2022). Another hypothesis focuses on the role of smooth muscle in modulating epithelial growth. According to this view, AR signalling activation orchestrates smooth muscle differentiation, with a uniform smooth muscle layer acting as a barrier that separates the epithelium from growth factor-producing mesenchyme, thereby halting branching morphogenesis within the developing prostate (Toivanen and Shen, 2017). These developmental processes are also studied in relation to pathological conditions, aligning with the embryonic reawakening theory. This theory suggests that the reactivation of stromal components in adulthood may contribute to epithelial hyperplasia, underscoring the

critical role of the stromal compartment in prostate pathogenesis (Buskin et al., 2021).

In the mature adult prostate, several critical genes are directly regulated by AR, primarily expressed within epithelial cells, and are implicated in prostate pathology. These genes include for example *NKX3.1*, *TMPRSS2*, and *VEGFA* (Lucas et al., 2014; Gross et al., 2020; Saydullaeva, Butuner and Korkmaz, 2023; Wang et al., 2023). Conversely, other well-known genes associated with prostate pathology, such as *PTEN*, *TP53*, *BRCA2*, and *AKT*, are not regulated by AR (Gross et al., 2020; Mizuno and Beltran, 2022).

2.1.1 Function of the prostate

The primary function of the prostate, as an exocrine gland, is to produce prostatic fluid, which comprises 20-30% of the total volume of seminal fluid, or semen. Other components of seminal plasma include seminal vesicle fluid, sperm cells, as well as epididymal and bulbourethral fluids (Verze, Cai and Lorenzetti, 2016). The main functional components of prostatic fluid include zinc, citrate, glucose, kallikreins, phosphatases, and polyamines (Verze, Cai and Lorenzetti, 2016). These elements in prostatic fluid contribute to nourishing sperm and liquefying semen, thereby aiding sperm movement (Costello and Franklin, 2006).

2.1.2 Cellular composition of the prostate

In prior morphological and immunohistochemical studies, three distinct cell types have been identified within the prostatic epithelium: luminal cells, basal cells, and neuroendocrine cells. These cells are characterised by specific epithelial markers: keratin (KRT) 8 and 18 mark luminal cells, KRT5 and 6 along with tumour protein p63 (TP63) identify basal cells, and chromogranin A (CgA) and serotonin distinguish neuroendocrine cells (Cunha et al., 2018). The stroma is predominantly composed of smooth muscle, interspersed with blood vessels, nerve bundles, and immune cells in varying densities.

Recent advancements, particularly through single-cell RNA sequencing (scRNA-seq) analyses of healthy prostate tissue, have yielded a more detailed understanding of cell type composition in the adult prostate. Henry et al. (2018) identified additional epithelial cell types, namely hillock and club cells. These cell types were previously unrecognised in the prostate and were identified by comparing transcriptomes from the prostatic cells with mouse lung scRNA-seq data. Furthermore, the distribution of these cell types varies across different prostate zones in healthy tissue: hillock and club cells are more prevalent in the central and transitional zones compared to the peripheral zone.

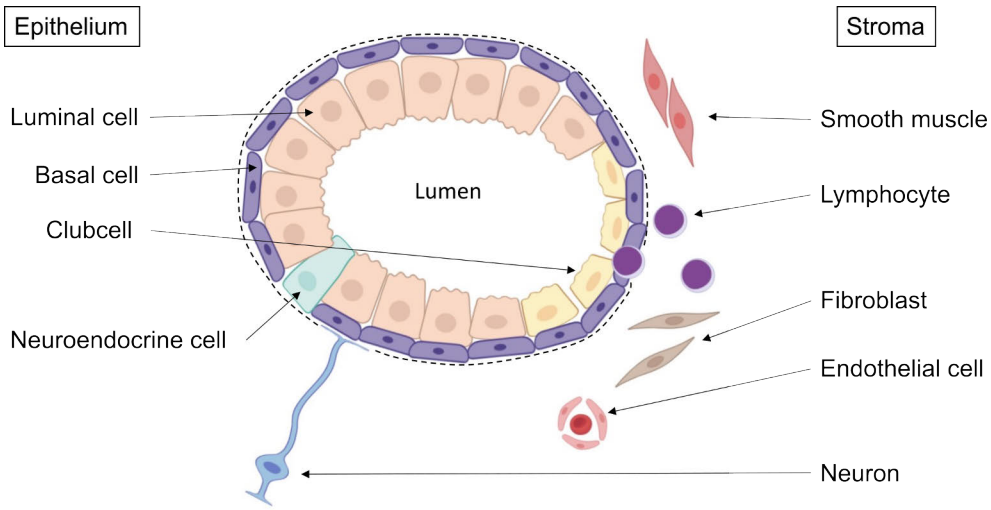

Figure 2. Cellular composition of the peripheral zone of the prostate. A healthy epithelium consists of double layer of basal and luminal cells with few neuroendocrine cells sparsely scattered. Club and hillock cells are rare in healthy peripheral zone epithelium, however club cells become more frequent as a result of an injury or other stress such as inflammation. Hillock cell are not visualised due to their rarity in the peripheral zone. Stroma consists of smooth muscle, fibroblasts, lymphocytes, endothelium (blood vessels), and neurons. Epithelial and stromal compartments are separated by a dashed line. Modified from Harris et al. (2022). Image created in Biorender.com.

Luminal cell

When discussing the luminal cells of the prostate, it is necessary to clarify the following: in tissue structure, luminal cells refer to the lumen-facing cell layer of the glandular epithelium, in contrast to basal cells, which are located between the luminal cell layer and the stroma (Figure 2). A similar epithelial structure, with a basal and luminal double cell layer, is found in the mammary glandular epithelium (Kumar et al., 2023) and lung epithelium (Hewitt and Lloyd, 2021). The luminal cell layer may contain several different types of cells with various functions. In this thesis, the term "luminal cell" refers to cells with a transcriptomic profile identified as luminal cells, as described by Henry et al. (2018) in normal prostate tissue and later used by Song et al. (2022) in localised prostate cancer tissue. This is in contrast to club cells, which are also located in the lumen-facing cell layer of the epithelium (Henry et al., 2018; Joseph et al., 2022; Huang et al., 2023).

Luminal cells perform the primary function of the prostate gland: the production of prostatic fluid. These cells are marked by the expression of *KLK3*, *KLK2*, *MSMB*, and *ACP3*, among other secreted proteins (Henry et al., 2018). Furthermore, luminal cells have a distinct cuboidal morphology, being tall and "fluffy," as described by

Joseph et al. (2022). The acinar structures containing luminal cells are infolded, providing more acinar area, which is likely related to their function in secretion. Luminal cells express high levels of AR targets genes (Joseph et al., 2022) and exhibit certain metabolic features related to the tricarboxylic acid (TCA) cycle and lipid metabolism (Giafaglione et al., 2023). The metabolism of the prostate is discussed in detail in chapter 2.1.3.

Club cell

Club cells were initially identified in the human lungs and were previously known as Clara cells, an eponym with a dark history (Parad, 2022). Henry et al. (2018) identified these cells in the prostate by comparing an unknown epithelial cell population in their human scRNA-seq data to mouse scRNA-seq data, finding that these cells highly correlate with mouse club cells. In a study of benign prostate hyperplasia (BPH) tissues, prostatic club cells are characterised by the expression of genes *LTF*, *PIGR*, *OLFM4*, *SCGB1A1*, and *SCGB1A3*, along with nuclear factor kappa-chain-enhancer of activated B-cells (NF-κB) signalling. Morphologically, club cells can be distinguished from luminal cells as the cell layer is shallower and the cells appear atrophied and shrunken compared to normal luminal cells (Joseph et al., 2022) (Figure 2).

The function of club cells has been investigated in the lungs, where they contribute to the detoxification of exogenous substances (*i.e.*, xenobiotic metabolism), mitigation of inflammation-inducing oxidative stress, regulation of inflammatory responses, defence against bacteria, and maintenance of protease/antiprotease balance. The protein secretoglobin family 1A member 1 (SCGB1A1), expressed by club cells, has been shown to inhibit phospholipase A2 and interferon gamma (INF-γ) signalling, both of which are important factors in inflammation (Blackburn et al., 2023).

In the prostate, club cells have been associated with proliferative inflammatory atrophy (PIA) (De Marzo et al., 1999; Joseph et al., 2022). PIA in the peripheral zone of the prostate is suggested to form as a result of exposure to the urinary microbiome and pathogens. In response, club cells express antimicrobial proteins, such as lactotransferrin (LTF), polymeric immunoglobulin receptor (PIGR), and matrix metalloproteinase 7 (MMP7) (Huang et al., 2023). Moreover, PIA lesions containing club cells are hypothesised to be susceptible to transformation into a precancerous state, intraepithelial neoplasia (de Bono et al., 2020; Huang et al., 2023).

Neuroendocrine cell

Neuroendocrine cells comprise only approximately 1% of prostate epithelial cells, sparsely scattered within the epithelium (Figure 2). The developmental origin of neuroendocrine cells is not well known. Previously, they were thought to migrate to prostate tissue during embryogenesis; however, there is some evidence suggesting that neuroendocrine cells may also arise from basal progenitor cells. Neuroendocrine cells secrete various peptide hormones and cytokines, such as serotonin, neuropeptide Y, histamine, calcitonin, vascular endothelial growth factor, and interleukin 8. Luminal cells have been shown to express the corresponding receptors to these hormones, suggesting that neuroendocrine cells regulate nearby cells in a paracrine manner. Two types of neuroendocrine cells have been identified: an open type with long microvilli reaching the lumen of prostate glands, sensing changes in prostate secretion content, and a closed type that receives stimuli from nerve cells, blood vessels, and smooth muscle. Neuroendocrine cells can be distinguished from other prostatic cells by markers such as CgA, neural cell adhesion molecule (NCAM/CD56), and forkhead-box A2 (Butler and Huang, 2021).

Hillock cell

Similarly to club cells, hillock cells were identified in normal prostate tissue through scRNA-seq by comparing the transcriptome to mouse lung scRNA-seq data. Hillock cells are marked by the expression of *KRT13* (Henry et al., 2018). A recent report on lung hillock cells stated that hillocks possess high resistance to physical, chemical, and pathogenic insults. Furthermore, hillock cells have a regenerative potential, being capable of regenerating the whole airway epithelium, including all cell types (Lin et al., 2024). However, while the hillock cell type was discovered in the lungs very recently and they are rare in the prostate, there are yet no reports on the potential role of hillock cells in the prostate. The role of hillock cells in prostate pathophysiology is unknown. They have been suggested to be depleted (Song et al., 2022) and enriched (Henry et al., 2018) in prostate cancer.

Stromal cells

The stroma is the other abundant structural compartment of prostate tissue besides the epithelium, and it plays a crucial role in supporting and nurturing the epithelium, aiding in its secretory function (Figure 2). The prostatic stroma consists of several cell types: fibroblasts, smooth muscle cells, endothelial cells, and neurons (Risbridger, 2018). Fibroblasts are more common in the anterior fibromuscular region, near the urethra, as well as in the central and transition zones, while smooth muscle cells are more common in the prostate peripheral zone (Henry et al., 2018),

where they provide contractility for pressing the prostatic fluid out of the gland (Risbridger, 2018). Stroma serves a role in hormonal regulation of the epithelium, providing precursor steroids for DHT synthesis, while the primary cell type for testosterone-to-DHT conversion are the luminal cells (Pelletier, 2008). Additionally, the stroma plays a significant role in prostatic diseases, and the emergence of differentiated stromal cell types, such as cancer-associated fibroblasts and myofibroblasts, promotes a tumorigenic environment for epithelial neoplasia (Di Carlo and Sorrentino, 2024). While not being an integral component of prostate tissue, immune cells are also present in the prostate (Henry et al., 2018). There is no literature about the distribution of immune cells in truly healthy prostate tissue compartments; however, Andersen et al. (2021) reported that immune cells localise in both epithelial and stromal compartments in cancerous prostate tissue.

2.1.3 Metabolism

Extensive work by Costello and Franklin defined the distinct metabolic features of the secreting prostate epithelium in the peripheral zone of the prostate. The prostate epithelial cells harbour metabolic features primarily found in the prostate epithelium. This unique metabolism is related to the production of citrate, which is secreted into the acini. The prostatic fluid is notable for its high concentration of citrate and zinc, ranging between 40-150 mmol/gram and 8-10 mmol/gram, respectively. These values are tens or hundreds of times greater than in blood plasma or other tissues (Costello and Franklin, 2006).

Citrate is an intermediate of the TCA cycle, also known as the citric acid cycle or Krebs cycle, which occurs in the mitochondria and is the main source of adenosine triphosphate (ATP) in human cells. ATP functions as an indispensable energy transfer molecule in cellular reactions (Rajendran et al., 2016). Zinc plays a central role in citrate production. High mitochondrial zinc concentration inhibits the function of mitochondrial aconitase (ACO2), an enzyme in the TCA cycle that transforms citrate into isocitrate. This inhibition leads to the accumulation of citrate, which is utilised by alternative means in prostate cells. In addition to pyruvate, prostate cells also use aspartate to be incorporated into the TCA cycle. A normal secretory prostate cell uses two molecules of aspartate and one molecule of glucose to produce two molecules of citrate and approximately 14 ATPs. In contrast, human cells normally use one glucose molecule to produce about 38 ATP molecules, meaning that while producing citrate, prostatic cells sacrifice approximately 60% of the potential energy produced compared to other cells in the body (Costello and Franklin, 2006) (Figure 3).

AR signalling regulates some of the key enzymes and transporters to maintain citrate production. AR is shown to induce the expression of pyruvate dehydrogenase

(PDH) E1 component subunit α (PDHE1α), resulting in enhanced conversion of pyruvate into acetyl-CoA (CoA, coenzyme A), and the aspartate transporter (EAAC1), which carries aspartate into the cell, as well as aspartate aminotransferase (mAAT), which converts aspartate into oxaloacetic acid (OAA). Both acetyl-CoA and OAA serve as precursors to the TCA cycle. Additionally, AR also induces zinc uptake into the cell to inhibit the enzyme ACO2 (Mah et al., 2020) (Figure 3).

In the cytosol, citrate serves as a precursor to the production of fatty acids and cholesterol. Normal prostate lipid metabolism is not extensively studied; however, studies in rodents and primates have shown that androgens regulate the expression of lipogenic genes such as fatty-acid synthase (FASN), ATP citrate lyase (ACLY), and acetyl-CoA carboxylase (ACC). FASN and ACC are essential in the synthesis of fatty acids from citrate via acetyl-CoA and malonyl-CoA (Figure 3). However, in normal prostate cells, only a small share of the citrate pool is used for this alternative route, while the majority is secreted into prostatic fluid (Mah et al., 2020)

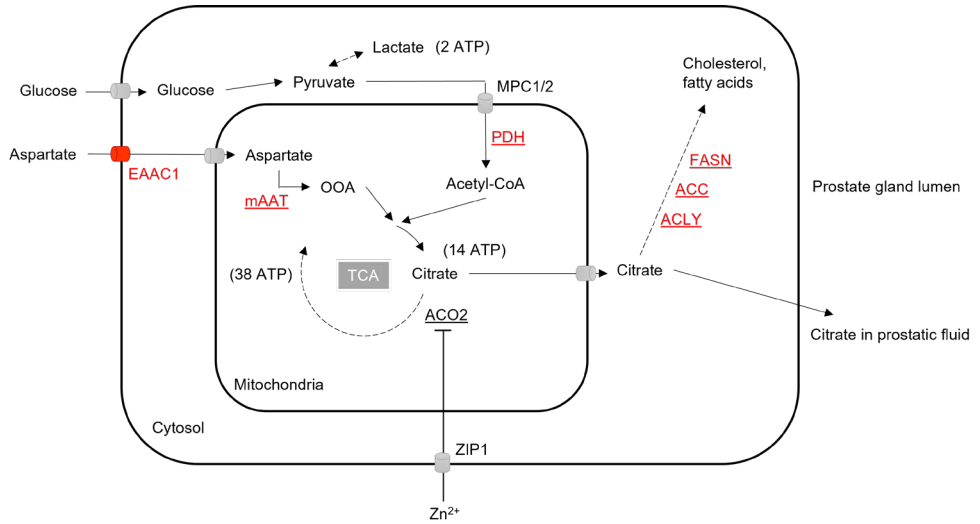

Figure 3. Metabolic features of prostatic luminal cells. Luminal cells (prostatic secretory cells) utilise a combination of glucose and aspartate to fuel the TCA cycle. Key enzymes in this process include mitochondrial aspartate aminotransferase (mAAT) and pyruvate dehydrogenase (PDH). The TCA cycle is truncated by high concentrations of zinc, leading to the accumulation of citrate. Citrate is either secreted into the prostatic fluid or used as a precursor for lipid synthesis. Red colour denotes AR regulated transporters and enzymes, the latter of which are underlined. Modified from Costello and Franklin (2006) and Mah et al. (2020).

2.2 Prostatic diseases

The prostate gland is susceptible primarily to three pathological conditions: prostatitis, BPH, and prostate cancer.

Prostatitis

Prostatitis is an inflammatory disease of the prostate with heterogeneous symptoms and aetiology. Histologically, prostatitis is marked by the presence of immune cells in the tissue and increased inflammatory markers. In prostatitis cases, only 5-10% have demonstrated bacterial infection, while the rest are caused by other factors such as prostatic calculi, or small stones obstructing the ducts and causing symptoms (Hyun, 2017; Yebes et al., 2023). A study conducted during autopsies showed that 70% of prostates contain signs of chronic inflammation (Zlotta et al., 2014), indicating that prostatic inflammation is very common, at least in elderly men. Prostate inflammation is associated with androgen levels, as AR signalling regulates the tight junctions of the prostate epithelium, maintaining the epithelial barrier and protecting the epithelium from external insults (Meng et al., 2011). Furthermore, lower serum testosterone correlates with inflammatory markers tumour necrosis factor alpha (TNF-α), cyclooxygenase 2 (COX2), and MIP-1 (Jia et al., 2015), and an increased number of immune cells (CD3+ lymphocytes and CD68+ macrophages) are detected in the stroma and epithelial basal membrane of castrated mice and men compared to normal controls (Meng et al., 2011).

Prostatitis may cause urinary tract symptoms, sexual dysfunction, and pain around the prostate, negatively affecting the quality of life of patients (Yebes et al., 2023). Moreover, prostatitis has also been linked with an increased risk of developing prostate cancer (de Bono et al., 2020).

Benign prostate hyperplasia

BPH is also a common pathological condition in elderly men. It usually resides in the transition zone of the prostate and causes urinary symptoms due to the expanded volume of the prostate pressing on the urethra. The prevalence of BPH increases with age, with 50% of men between the ages of 51 and 60 showing pathological features of BPH (Devlin, Simms and Maitland, 2021).

As androgens play an important role in the development and maintenance of prostate tissue, they have also been implicated in BPH pathogenesis. Despite declining serum testosterone levels with age, DHT levels in BPH tissue remain stable, supporting prostate cell growth via saturated androgen receptors. 5α-reductase inhibitors (5-ARIs) are the mainstay treatment for BPH, but while 5-ARIs effectively reduce prostate volume and improve symptoms over time, their delayed

effect suggests that additional factors may drive BPH progression (Devlin, Simms and Maitland, 2021).

In addition to androgens, oestrogens may also play a significant role in BPH pathogenesis by acting through oestrogen receptors (ERα and ERβ) and the aromatisation of androgens to oestrogens, particularly in men with large volumes of adipose tissue or altered androgen:oestrogen circulating hormone ratios due to ageing. While ERα is associated with prostate stromal proliferation and ERβ with pro-apoptotic effects, the dominance of ERα and increased aromatase activity in stromal cells may drive hyperplasia. However, clinical attempts to target ERα and aromatase activity have failed (Devlin, Simms and Maitland, 2021).

A study of over 8,000 men showed a correlation between chronic inflammation and BPH-related urinary symptoms, suggesting that inflammation is a driver for BPH progression (Nickel et al., 2008). Inflammation-induced cytokines, such as proinflammatory INF-γ and ILs 8, 15, and 17, as well as inflammation-induced release of reactive oxygen species (ROS), promote stromal and epithelial cell proliferation via the release of growth factors FGF-2, FGF-7, and transforming growth factor β1. As a disease progression mechanism related to inflammation, it has been suggested that proliferating cells create a hypoxic environment, which in turn promotes the production of ROS and enhances the release of growth factors, creating a vicious cycle of growth (Devlin, Simms and Maitland, 2021). Supporting evidence for the role of inflammation in BPH progression includes the use of nonsteroidal anti-inflammatory drugs, which are inhibitors of COX1 and COX2 enzymes. These drugs show inhibitory effects on metabolism and induce apoptosis in BPH cell lines (Minnery and Getzenberg, 2005). COX enzymes convert the fatty acid derivative arachidonic acid into prostaglandin G2, which is further converted into other inflammatory mediators with various disease-promoting effects. Clinical studies on the use of COX inhibitors have shown promising results in mitigating symptoms in prostatitis and BPH, as well as lowering the risk of prostate cancer (Ishiguro and Kawahara, 2014).

Prostate cancer

In 2020, prostate cancer accounted for 7.3% of all new cancer cases globally, behind only of female breast cancer and lung cancer, which accounted for 11.7% and 11.4% of cases, respectively. Prostate cancer is the most commonly diagnosed cancer in men in all Americas, most European and sub-Saharan African countries, Japan, Australia, and New Zealand. The age and population-standardised incidence rate is highest in Northern Europe, followed by Western Europe, the Caribbean, Australia, New Zealand, and North America. Similarly adjusted mortality rates are highest in

the Caribbean and African regions, while mortality is lowest in Asian regions (Sung et al., 2021).
In Finland, the incidence rate (adjusted to 100,000 person-years) of prostate cancer in 2022 was 125.8 in men aged 20-69 years old, and 823.7 in men of 70 years old and above (Pitkäniemi et al., 2024). The lifetime probability of developing prostate cancer in Finnish population was 13.9% in data collected between 2018 and 2022 (Pitkäniemi et al., 2024), which is similar to the United States population with lifetime probability of 12.9% in data from 2017-2019 (Siegel, Giaquinto and Jemal, 2024). A meta-analysis of incidental prostate cancers found in autopsy studies around the world estimated that the prevalence of prostate cancer is 5% in individuals under the age of 30 and increases to 59% in individuals over 79 years old (Bell et al., 2015).

As an interesting side note, although women do not have a prostate, there is a periurethral, fluid-secreting organ in women that is homologous to the prostate, called Skene's gland. This organ can also develop cancer, although it is extremely rare. Skene's gland cancer has been reported to have striking similarities with prostate cancer, and treatments used against prostate cancer are also effective for treating Skene's gland carcinoma (Gao et al., 2022).

2.2.1 Prostate cancer

2.2.1.1 Risk factors for prostate cancer

The aetiology of prostate cancer remains largely unknown despite its high prevalence. Established risk factors for prostate cancer include advanced age, family history of prostate cancer, and protein-impairing mutations in DNA-repair genes BRCA1 and BRCA2, along with a condition called Lynch syndrome (Sung et al., 2021). Lynch syndrome is caused by heritable germline variants in DNA mismatch repair genes *MLH1*, *MSH2*, *MSH6*, and *PMS2*, and additionally deletions in *EPCAM* that cause silencing of *MSH2* (Maratt and Stoffel, 2022). Population-based risk of prostate cancer is highest in black men with Western African ancestry (Rebbeck et al., 2013), indicating a significant genetic factor contributing to prostate cancer risk. Furthermore, a study comparing monozygotic and dizygotic (identical and non-identical) twins found that prostate cancer has the second highest risk attributable to genetic factors (57% of cases), with skin cancer and leukaemia having similarly high rates (Mucci et al., 2016). However, many, if not most, of these factors remain unknown for prostate cancer.

Regarding other factors, there is strong evidence that obesity and developmental factors leading to greater linear growth (greater height) increase prostate cancer risk, while some evidence suggests that consumption of dairy products and diets high in

calcium increases the risk for prostate cancer (Continuous Update Project panel, 2018). A recent systematic review of prostate cancer epidemiology and risk factors compiled many known and suspected factors in detail (Bergengren et al., 2023). Selected factors from this publication and their effects on prostate cancer risk are listed in Table 1.

Table 1. Prostate cancer risk factors. Selected from (Bergengren et al., 2023).

FACTOR	EFFECT
ANCESTRY	The higher PCa incidence in men with ancestry from northwestern sub-Saharan Africa is suggestive of higher prevalence of PCa predisposing genetic factors. This may also result from environmental influences causing inflammation and subsequent carcinogenesis.
FAMILY HISTORY	Brothers and sons of men with PCa have a 2.5-fold increased risk of PCa. Having a first-degree relative with breast cancer increases the risk of PCa by 1.2-fold.
GERMLINE VARIANTS	Mutations in the following genes are linked with increased risk of prostate cancer: *HOXB13*, *BRCA2*, *BRCA1*, *ATM*, *CHEK2*, *NBS1*, *MLH1*, *MSH2*, *MSH6*, and *PMS2*.
BALDNESS	Baldness in general does not correlate with PCa risk, however, vertex pattern baldness is found to associate with an increased risk to PCa.
HEIGHT	Taller height is correlated with an increased risk of PCa. This may be associated with insulin-like growth factor levels during puberty.
PHYSICAL ACTIVITY	High physical activity may reduce the risk of PCa as well as increase the cancer-free survival from PCa.
DIET	Vegetarians compared to meat eaters have a lower risk of PCa, moreover, plant-based diet shows a positive short-term effect on PCa outcomes. Inflammatory diet increases the risk of PCa. Dairy protein intake (≥30g/d) increase the risk for PCa. Phytoestrogens (found in many types of beans) reduce the risk of PCa.
SMOKING	Smoking tobacco as well as smokeless tobacco increase the risk of lethal PCa.
FERTILITY	Infertility and subfertility are associated with an increased the risk of PCa.
INFLAMMATORY DISEASES	Prostatitis may increase the risk of PCa. Sjögren's syndrome, periodontitis, and ulcerative colitis have been found to associate with an increased risk of PCa.
METABOLIC CONDITIONS	Metabolic syndrome and obesity are associated with high-grade PCa.
ENVIRONMENTAL FACTORS	Sexual activity has a dual effect; high frequency of ejaculations reduces the risk of PCa, whereas high number of female sexual partners increase the risk of PCa. HPV infection (especially HPV-16) increase the risk of PCa.

2.2.1.2 Inflammation in carcinogenesis

Prostate is regarded as an immune privilege organ similarly to other reproductive organs, such as testes and uterus. Immune privilege organs have blood-tissue barriers and their immune responses vary from other organs such a way that inflammation is inhibited in immune privilege organs (Leibovitz, Baumoehl and Segal, 2004). Despite that, inflammation has been proposed to contribute to prostate cancer initiation through a sequence of events, including the presence of chronic inflammation, followed by the accumulation of DNA damage and dysregulation of the cell cycle and certain oncogenes that initiate carcinogenesis (de Bono et al., 2020).

The factors inducing inflammation are not fully understood; however, pathogens, dietary fats and obesity, chemical injury (caused by uric acid from urine reflux into the prostate), and physical trauma (caused by corpora amylacea or prostatic stones) are putative factors causing inflammation. The inflammatory response creates a feedback loop in which inflammation-induced formation of free radicals (reactive oxygen and nitrogen species) causes DNA damage, which enhances the inflammatory response, and the cycle continues, leading to chronic inflammation. DNA-repair proteins and other tumour-suppressor proteins, such as p53, play a key role in recovering from the inflammatory cycle. Prolonged activation of tumour-suppressor genes, in combination with DNA damage in inflammation-induced proliferating cells, eventually results in the loss of tumour-suppressors (such as *PTEN* and *TP53*), activation of the Wnt pathway, and amplification of *MYC*. These processes, summarised here, are suggested to initiate carcinogenesis in the prostate epithelium, first into prostatic intraepithelial neoplasia and eventually into carcinoma (de Bono et al., 2020).

The epithelium reacts to inflammation by adopting a club cell identity (Huang et al., 2023), in which NF-κB signalling plays a key role (Joseph et al., 2022). These club cells found in PIA are not completely comparable to club cells found in a healthy prostate; however, the PIA-associated club cells are suggested to play a similar protective role as their healthy counterparts. Moreover, they express the anti-apoptotic protein Bcl-2, which may increase the survival of club cells (Huang et al., 2023). NF-κB signalling also plays an important role in prostate cancer and contributes to AR-independent progression (Jin et al., 2014).

2.2.1.3 Hallmarks in prostate cancer

After initial changes from benign epithelial cells to precancerous lesions have occurred, several processes contribute to the progression of cells into more advanced cancer cells, or tumour progression. Several hallmarks of cancer have been depicted by Hanahan and Weinberg (2000; 2011), and Hanahan (2022), that recapitulate the

main features of cancer cells aiding growth and survival. The following chapters elucidate the role of a few of these hallmarks that occur in primary prostate cancer and are central to the thesis, including aspects in cell proliferation, metabolism, and the interconnection between metabolism and lineage plasticity. It is worth mentioning, however, that there are other important traits in prostate cancer that drive tumour progression and responses the therapy. These include for example non-mutational chromatin and epigenetic dysregulation (Hanahan, 2022), which affects all the hallmarks of cancer (Kukkonen et al., 2021), and the neural component in prostate cancer as it is prone to perineural invasion and neuroendocrine differentiation, which both are poor prognostic factors (Sigorski et al., 2021).

2.2.1.4 Sustaining proliferation

Cancer growth essentially revolves around the proliferation of cells, as exemplified by the six original hallmarks of cancer. In prostate epithelial cells, proliferation is induced by external cues triggering a proliferative cascade. This is also called mitogenic signalling, and in the prostate, key mitogenic pathways involve signalling via growth-stimulating receptors such as EGFR and AR (Guo, Luttrell and Price, 2000; Nussinov et al., 2024).

Growth factors, such as epidermal growth factor (EGF), fibroblast growth factor (FGF), or platelet-derived growth factor (PDGF), bind to cell surface-residing growth factor receptors (*e.g.*, epidermal growth factor receptor, EGFR). Upon ligand (growth factor) binding, receptor tyrosine kinase (RTK) or G-protein coupled receptor (GPCR) activates the intracellular signal transduction cascade via sequential activation of Ras, Raf, MEK, and ERK, also known as the MAPK/ERK pathway (mitogen-activated protein kinase, MAPK; extracellular signal-regulated kinase, ERK) (Nussinov et al., 2024). In the final stage of the cascade, ERK translocate into the nucleus and activates the transcription of cell cycle-promoting genes, such as *CCND* (encoding cyclin D) and *MYC* (Daksis et al., 1994; Weber et al., 1997).

Alternatively, the cell cycle promotion can be triggered via PI3K/AKT pathway. Akt is activated by several plasma membrane-residing RTKs or GPCRs via PI3Ks, while the PI3K is suppressed by PTEN. Additionally, AKT can be activated by DNA damage (via ATM and ATR), or mechanistic target of rapamycin (mTOR) complex 2 (mTORC2). AKT signalling affects several cellular functions, promoting growth, survival, metabolism, and more processes that contribute to tumour growth (He et al., 2021).

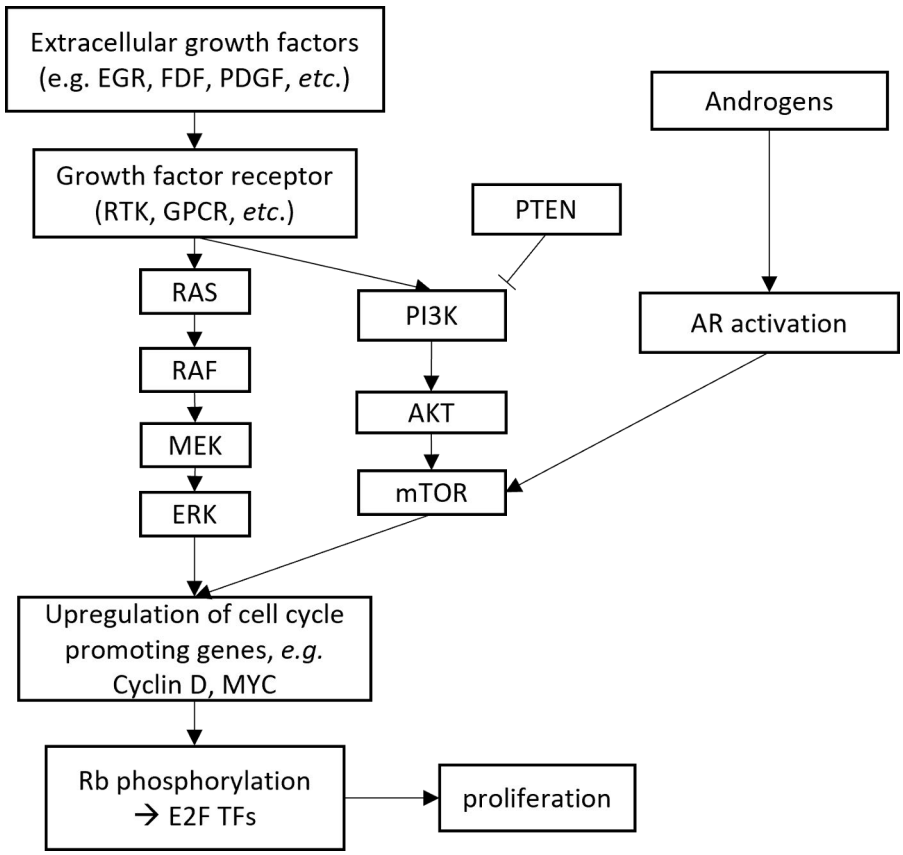

Figure 4. Growth-stimulating signalling in prostate cancer. Growth factors activate the signalling cascade either via RAS-RAF-MEK-ERK or PI3K-AKT-mTOR, while the latter route is inhibited by PTEN. AR is activated by androgens in the cytoplasm. These pathways activate cell cycle promoting genes leading to hyperphosphorylation of Rb and release of E2A transcription factors.

In prostate cancer, AR activated by androgens also promotes the cell cycle, albeit in a more complex manner compared to mitogens. The cell cycle-promoting function of AR is mediated via mTOR, which then upregulates cyclin D independently of PI3K/AKT pathway activation (Xu et al., 2006), while mTOR activation via the PI3K signalling cascade is also important in prostate cancer (Braglia et al., 2020).

Activated cell cycle regulators phosphorylate the retinoblastoma protein (Rb), which is a central regulatory axis connecting external growth and hormonal signals to E2F-dependent transcription and cell cycle progression. Normally, hypophosphorylated Rb restrains E2F activity, preventing S-phase entry until mitogenic and androgenic stimuli induce Cyclin/CDK complexes that phosphorylate and inactivate Rb, thereby releasing E2F and driving proliferation (Burkhart et al., 2019).

Genetic or functional alterations in the Rb pathway—including loss of Rb—are common in prostate cancer (Robinson et al., 2015). While indirect mechanisms, such as *PTEN* loss or *MYC* overexpression, may initially promote proliferation via E2F, direct Rb loss emerges as a recurrent event in advanced, metastatic disease, often under therapeutic pressures like androgen deprivation therapy (ADT). Overexpression of *MYC*, however, can initiate tumorigenesis independently of Rb (Burkhart et al., 2019). In prostate cancer, MYC drives AR regulated proliferation as well as AR-independent growth (Bernard et al., 2003) and induces lipogenic metabolism (Singh et al., 2021).

The most common genomic alterations during the course of prostate cancer progression include amplification and overexpression of *AR*, inactivation or loss of *TP53* and *PTEN*, as well as several fusions in the ETS transcription factor family (such as in *ERG*) (Grasso et al., 2012; Robinson et al., 2015; Abida et al., 2017). These alterations affect the mitogenic pathways, enhancing the nuclear activity of transcription factors and promoters that facilitate cell growth (Figure 4).

Primary prostate cancers exhibit a more heterogeneous mutational landscape compared to metastatic disease, showing that certain combinations of alterations are preferred to achieve metastatic potential. These alterations include amplification in *AR* and *MYC*, and deletions in *PTEN*, *TP53*, and DNA repair genes (Abida et al., 2017; Wedge et al., 2018). ADT treatment frequently results in altered *AR*, which drives metastatic castration-resistant prostate cancer, while SPOP mutation are suggested to sensitise primary tumours to ADT (Abida et al., 2017).

2.2.1.5 Metabolic rewiring

Metabolic rewiring, or deregulating cellular energetics as it is named in the hallmarks of cancer by Hanahan and Weinberg (Hanahan and Weinberg, 2011), plays a key role in prostate cancer progression from a very early phase. During prostate cancer development, the cells begin to utilise the full capacity of the TCA cycle. This has been shown by comparing benign prostate and cancerous prostatic tissue, where the zinc and citrate concentrations are markedly reduced in cancer. While the high production of citrate in benign prostatic cells is mediated via a truncated TCA cycle by zinc ions inhibiting ACO2 (Figure 3), it has been shown that the loss of the zinc transporter ZIP1 occurs early in cancer development, enabling the utilisation of the TCA cycle in full capacity (Costello and Franklin, 2006) (Figure 5).

In many other cancer types, cells produce energy by high uptake of glucose and converting it to pyruvate and lactate. Normally, this metabolic route would occur under hypoxic conditions; however, cancer cells prefer aerobic glycolysis, or glucose to lactate conversion, in normal oxygen conditions (Finley, 2023). This process, called the Warburg effect, produces excess lactate and greatly reduces the amount of

ATP produced per molecule of glucose (Warburg, 1956; Mah et al., 2020). The reason why cancer cells utilise aerobic glycolysis over maximising glucose oxidation to produce ATP is still somewhat unclear (Finley, 2023). However, a recent report showed that the Warburg effect is a superior way of producing energy (ATP) over mitochondrial respiration, providing evolutionary justification for aerobic glycolysis in rapidly growing cells (Kukurugya, Rosset and Titov, 2024).

Prostate cancer cells adapt to utilise the Warburg effect, *i.e.*, high glucose intake and production of ATP via pyruvate to lactate conversion, in late-stage cancers and especially in low-oxygen conditions (Mah et al., 2020). This is corroborated by data from positron emission tomography (PET) studies using the glucose analogue fluorodeoxyglucose (FDG). FDG-PET imaging highlights tissues with enhanced glucose uptake, such as inflamed tissue and tumours. In prostate cancer, FDG shows poor performance in detecting the metabolic activity of cancer lesions (Effert et al., 1996); however, FDG uptake shows prognostic value in detecting aggressive prostate cancer cases (Lavallée et al., 2019). Thus, in terms of the TCA cycle, low-grade prostate cancer differs from cancers in general since they gain additional ATP from the TCA cycle by running it similarly to normal human cells (Costello and Franklin, 2006). In late-stage prostate cancer, however, the cells adapt to a more flexible metabolism.

Along with the utilisation of the full capacity of the TCA cycle, prostate cancer cells also exhibit increased lipid metabolism. This was first noted by Swinnen et al. (1996) in an androgen-sensitive prostate cancer cell line, where androgen treatment caused the formation of intracellular lipid droplets containing fatty acids, phospholipids, and cholesterol. Prostate cancer cells are shown to be dependent on lipids as an energy source. Inhibition of a specific lipid, cholesteryl ester, affects only prostate cancer cells and not benign epithelial cells. This mechanism is AR-independent and mediated via the PI3K/AKT pathway, activating the sterol regulatory element-binding protein 1 (SREBP1) (Yue et al., 2014).

Additionally, AR and *SREBF1* (encoding SREBP1) regulate each other in prostate cancer cells, creating a positive feedback loop between the production of lipogenic genes and AR signalling (Huang et al., 2012; Audet-Walsh et al., 2018; Mah et al., 2020). In addition to lipid production, AR signalling increases the expression of transporters such as fatty acid binding protein (FABPpm) and fatty acid translocase (FAT/CD36) for the transport of extracellular fatty acids into cells. The genes *ACC*, *FASN*, and steroyl-CoA-desaturase (*SCD*) are regulated by androgens and contribute to *de novo* fatty acid synthesis (Figure 5). Fatty acids are used in energy production through fatty acid oxidation, where AR signalling again plays a role by increasing the expression of enoyl-CoA-isomerase (ECI2). Collectively, AR signalling promotes lipid metabolism by facilitating the intake and synthesis of fatty acids for use as energy sources, signalling molecules, and in

membrane synthesis. SREBP is the master transcriptional lipogenic regulator in prostate cancer cells (Mah et al., 2020) and promotes malignant lipid metabolism in tumours (Chen et al., 2018).

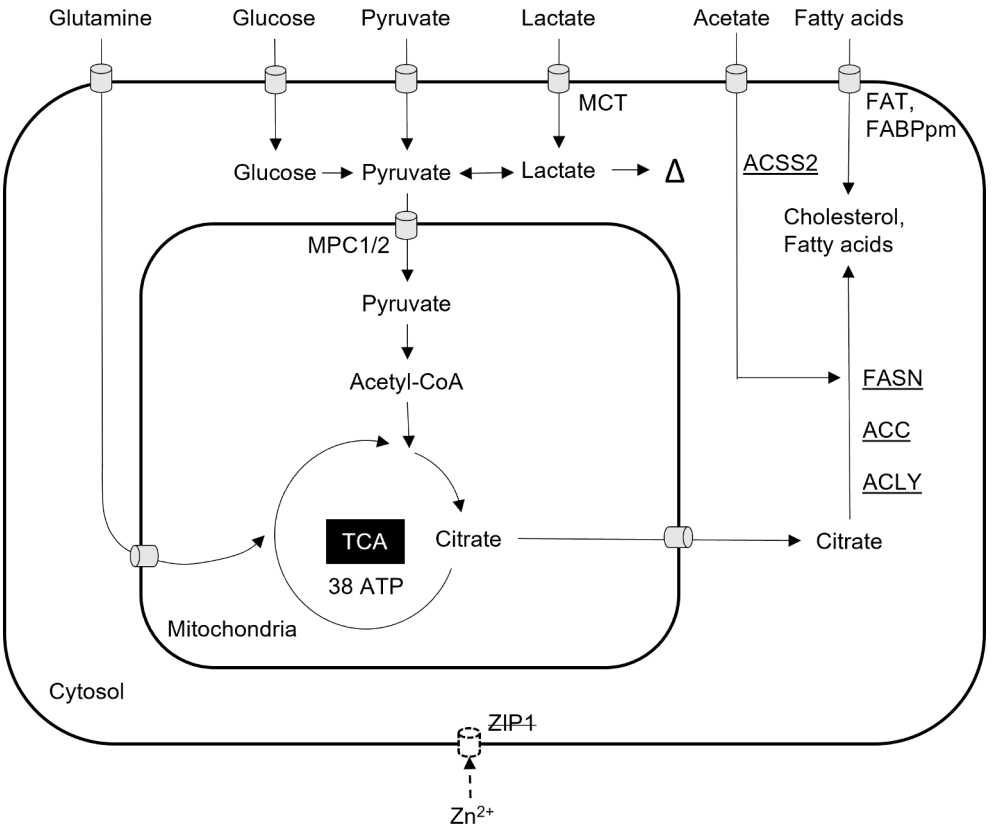

Figure 5. Nutrients used for TCA cycle and synthesis of lipids in prostate cancer. Glutamine, glucose, pyruvate, and lactate fuel the TCA. Loss of zinc transporters allow harnessing the full capacity of TCA cycle in prostate cancer. Citrate along with acetate are used for de novo lipid synthesis and circulating fatty acids are absorbed to increase the lipid pool. Lactate, which can be absorbed from outside of the cells or are accumulated as a result of truncated MPC function, causes a shift from luminal to basal transcriptome (Δ). Enzymes are denoted with underlining. Modified from (Ahmad, Cherukuri and Choyke, 2021) and (Sena and Denmeade, 2021).

For lipid production, prostate cancer cells can utilise several nutrients, including glucose, glutamine, acetate, pyruvate, and lactate (Sena and Denmeade, 2021). Acetyl-CoA is the primary building block for de novo fatty acid synthesis, which can be produced from citrate by or from acetate by acetyl-CoA synthetase (ACSS). The rate-limiting enzymes ACLY and FASN are upregulated in prostate cancer (Sena and Denmeade, 2021; Singh et al., 2021; Dairo et al., 2024), and these genes are suggested

to be regulated by MYC (Singh et al., 2021), which is a downstream target of AR (Gao et al., 2013). Enhanced lipid metabolism drives aggressive features in prostate cancer cells, and several studies have shown that lipogenic genes are essential for prostate cancer. Inhibition of several fatty acid synthesis genes has been shown to suppress cell growth and invasiveness in *in vitro* and *in vivo* experiments (Chen et al., 2012; Scott et al., 2012; Gao et al., 2014). Moreover, lipid metabolism appears especially enriched in the most advanced prostate cancer type, metastatic castration-resistant prostate cancer (mCRPC) (Zadra and Loda, 2019; Zadra et al., 2019).

While mTORC2 regulates the activation of AKT, mTORC1 plays a central role in anabolic metabolism in cells, including the increase of lipid synthesis (via SREBP), glucose metabolism, and mitochondrial biogenesis. mTORC1 is activated by an abundance of nutrients, oxygen, and growth factors. On the other hand, when cells are deprived of energy, mTORC1 is inhibited by AMP-activated protein kinase (AMPK). Increased mTORC1 signalling drives growth and proliferation in cancer, including prostate cancer (Saxton and Sabatini, 2017).

To summarise, this is a simplified presentation of the metabolic features in prostate cells, aiming to introduce some of the underlying mechanisms relevant to this thesis. These examples demonstrate how flexible prostate cancer is due to multiple means of producing energy, and that AR signalling and metabolism are tightly conjoined in prostate cells and are key to their function.

2.2.1.6 The effect of altered metabolism on epigenetic regulation

Although not abundantly produced in early-stage prostate cancer, lactate is an important factor modifying epithelial cell identity and cancer cell metabolism. A study by Ippolito et al. (2022) showed that lactate produced by cancer-associated fibroblasts in the tumour microenvironment rewires cancer cells via histone acetylation by BET proteins. This process activates ACLY, ACC, and cholesterol metabolism via SREBP regulation, making the cancer cells utilise lipids as an energy source more efficiently. Furthermore, the authors demonstrate the importance of the lactate transporter monocarboxylate transporter 1 (MCT1) in this process (Figure 5).

In a recent study, lactate was shown to alter transcription in cells by affecting the epigenome, inhibiting luminal cell differentiation. The authors also found that luminal-type cells use plenty of pyruvate in energy production, and that inhibition of mitochondrial pyruvate carriers 1 and 2 (MPC1/2), which carry pyruvate from the cytoplasm to the mitochondria to feed the TCA cycle (Figure 5), results in lactate accumulation in the cells. The lack of MPC in prostate cancer consequently renders the cells more dependent on glutamine for utilisation in the TCA cycle (Bader et al., 2019) (Figure 5). Epigenetic regulation also plays a role in individual metabolic genes, such as FASN, which has been shown to be upregulated by hypomethylation in cancer (Dairo et al., 2024).

These studies demonstrate that metabolites are not only utilised as a source of energy in prostate cancer but also affect cell identity through transcriptional modifications, subsequently influencing the therapy outcomes of AR-targeting therapeutics.

2.2.2 Diagnostics, prognostication, and treatment of prostate cancer

Prostate cancer diagnosis involves a combination of clinical evaluation, laboratory testing, imaging, and histopathological assessment. Population level screening for prostate cancer is not recommended due to the risk of overdiagnosis and overtreatment, especially related to the measurement of PSA. However, counselling is advised for individuals at high risk of prostate cancer, such as those with a family history of prostate cancer or genetic predisposition. In early detection, initial risk assessment includes combining PSA measurement, digital rectal examination as well as individual risk factors. Abnormal findings lead to evaluation of the need for biopsy sampling, which is determined by the risk of clinically significant prostate cancer. This is done by utilising risk stratifying tools, such as multiparametric magnetic resonance imaging (MRI) and PSA density (serum PSA divided by prostate volume). Prostate tissue biopsies are taken if there is a suspicion of clinically significant cancer. Ultrasound guided or systematic biopsies are options, and MRI findings guide in taking targeted biopsy for increasing accuracy and sensitivity of finding clinically significant cancer lesions (Cornford et al., 2024).

Tissue biopsies are evaluated for cancer cells using the Gleason grading system. The original system included five patterns, and the cancer was scored by combining the most and second most prevalent patterns, resulting in a score ranging from 2 to 10 (Gleason, 1966). Recently, however, the lowest assigned score has been 6, and there has been debate over whether this score should even be classified as cancer. Additionally, Gleason score 7 includes combinations of 3+4 and 4+3, with the latter shown to have a worse prognosis compared to the former. Therefore, a new grading system was proposed, stratifying the histological patterns into five grade groups (GG): GG1 (Gleason score ≤6), GG2 (Gleason score 3+4=7), GG3 (Gleason score 4+3=7), GG4 (Gleason score 4+4=8; 3+5=8; 5+3=8), and GG5 (Gleason score ≥9). These groups show a proportionally increasing risk of relapsing disease after radical prostatectomy, while all groups contain advancing cases (Epstein et al., 2016). The Gleason score and Gleason GG are recommended to be used parallelly (van Leenders et al., 2020). PET imaging targeting prostate-specific membrane antigen (PSMA, encoded by *FOLH1*) is used for further evaluating local and distant metastasis to guide treatment (Cornford et al., 2024).

Traditionally, prostate cancer cases have been stratified into low, intermediate, and high risk of developing advancing disease (D'Amico et al., 1999), with the intermediate risk group being the most challenging for treatment decisions regarding whether to proceed with invasive treatment or not (Cornford et al., 2024). The treatment options for localised disease are radical prostatectomy (prostate removal surgery), radiotherapy, active surveillance, chemotherapy and adjuvant treatments (Cornford et al., 2024). Low risk and some intermediate risk patients can be offered active surveillance before entering into invasive treatment. A recent study following prostate cancer patients diagnosed with localised prostate cancer found no difference in prostate cancer-specific death in cases treated with prostate removal surgery, radiotherapy, or active surveillance after fifteen years of follow-up. However, there were significant differences in disease progression and the appearance of metastasis, which were more frequent in the active surveillance group (Hamdy et al., 2023). Prostate cancer is a disease of older men, and usually, patients die with prostate cancer, not because of it, as demonstrated by the high prostate cancer-specific survival in the study by Hamdy et al. (2023). This highlights a shortcoming in the risk-assessment of advancing disease and treatment-decision making practice, while many patients that are undergoing early invasive treatments are likely suffering from adverse-effect related to the treatment while not getting enough benefits in terms of disease outcome. Therefore, better prognostic biomarkers should be utilised to help clinicians in treatment decision-making for localised low and intermediate risk prostate cancer.

2.2.3 Biomarkers in prostate cancer prognostication

PSA-based tests have been developed for a more accurate estimation of clinically significant prostate cancers. These tests include 4K (four-kallikrein) panel, PHI (prostate health index), and IsoPSA (James et al., 2024). Genetic factors, along with other parameters, are included in tests such as Stockholm3 (Grönberg et al., 2018). Biopsy-based gene expression classifiers, such as Oncotype DX, Decipher, and Prolaris, improve the accuracy of risk assessment and recommended in cases where they are likely to affect disease management (Eggener et al., 2020). Testing for germline mutations is not routinely utilised anywhere in the world; however, some high-risk patients might benefit from testing for cancer-predisposing mutations. It would likely be more feasible to generate polygenic tests for several genes that increase the risk at a low level than to use monogenic risk score testing (James et al., 2024). Currently, the European Association of Urology only recommends *BRCA2* germline mutations for early screening of prostate cancer in carriers and assessing homologous recombination deficiency to determine eligibility for poly ADP-ribose polymerase inhibitor (PARPi) treatment in patients with metastatic disease (Cornford et al., 2024).

2.3 Anoctamin 7

Anoctamin 7, encoded by the *ANO7* gene (also known as NGEP, New Gene Expressed in Prostate; TMEM16G, Transmembrane protein 16G), is a transmembrane protein predominantly expressed in human prostate epithelial cells and in prostate cancer (Bera et al., 2004). *ANO7* encodes two splice variants: a long isoform containing 25 exons (*ANO7*-L) and a short isoform comprising the first four exons and part of intron four of the long isoform (*ANO7*-S) (Figure 6). ANO7-L is a transmembrane protein that localises close to the apical membrane of the luminal epithelial cells of the prostate (Das et al., 2008; Wahlström et al., 2022). ANO7-S lacks the membrane-spanning regions and is therefore likely cytosolic (Bera et al., 2004); however, the presence of endogenous ANO7-S protein has not yet been confirmed in human tissue or cell lines.

In RNA sequencing (RNA-seq) of human tissue samples, several introns show a marked presence in addition to exonic reads in *ANO7*, specifically introns 3, 4, 5, 18, 19, and 22 (Wahlström et al., 2022) (Figure 6). Intron retention is a common regulatory phase between transcription and translation, and the biological roles it serves include building a reservoir of pre-mRNA for rapid post-transcriptional splicing in response to signalling, regulation of translation in cell developmental phases, or targeting mRNA for degradation (Gordon, Phizicky and Neugebauer, 2021). *ANO7* mRNA has been detected in HeLa cells to interact with heterogeneous nuclear ribonucleoprotein H1 (hnRNP H1), an RNA-binding protein that regulates RNA metabolism (Uren et al., 2016).

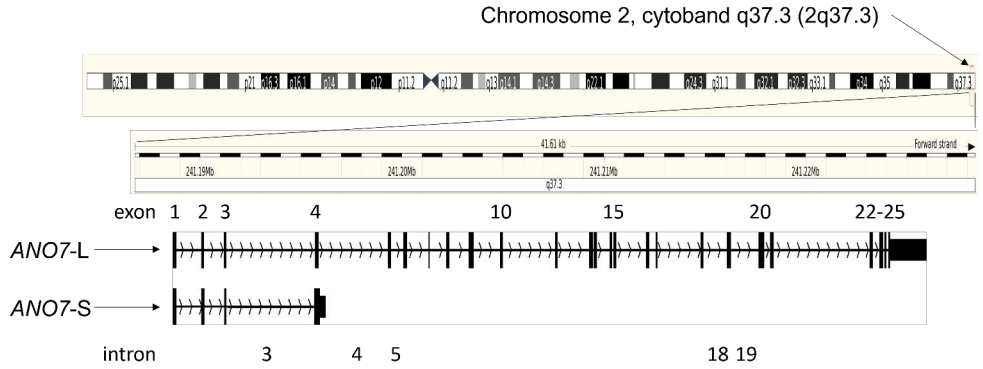

Figure 6. *ANO7* transcript variants. The *ANO7* gene, located on the q37.3 cytoband of chromosome 2, produces two transcript variants. These include *ANO7-L*, which has 25 exons, and *ANO7-S*, which comprises the first four exons of *ANO7-L* and extends into the fourth intron. Retained introns identified in patient tissue RNA-seq are numbered.

2.3.1 ANO7 and other anoctamin family proteins

ANO7 belongs to a family of 10 anoctamin proteins, named ANO1-10. These proteins were initially thought to be anion channels and contain eight (octa) transmembrane domains, hence the name anoctamin was coined (Hartzell et al., 2009). However, it was later found that these proteins exhibit dual functions: ANO1 and ANO2 are chloride channels, while many other family members act as unselective cation channels and additionally as phospholipid scramblases (Falzone et al., 2018). All anoctamin proteins contain calcium ion binding sites that, upon calcium binding, change the conformation of the transmembrane helices and open a channel or cavity for ions and/or phospholipids. Additionally, other factors, such as calmodulin, cholesterol, and phosphorylation, are reported to modulate anoctamin activity (Kalienkova, Clerico Mosina and Paulino, 2021). A model of the ANO6 homodimer and a predicted model of the ANO7-L protein are presented in Figure 7.

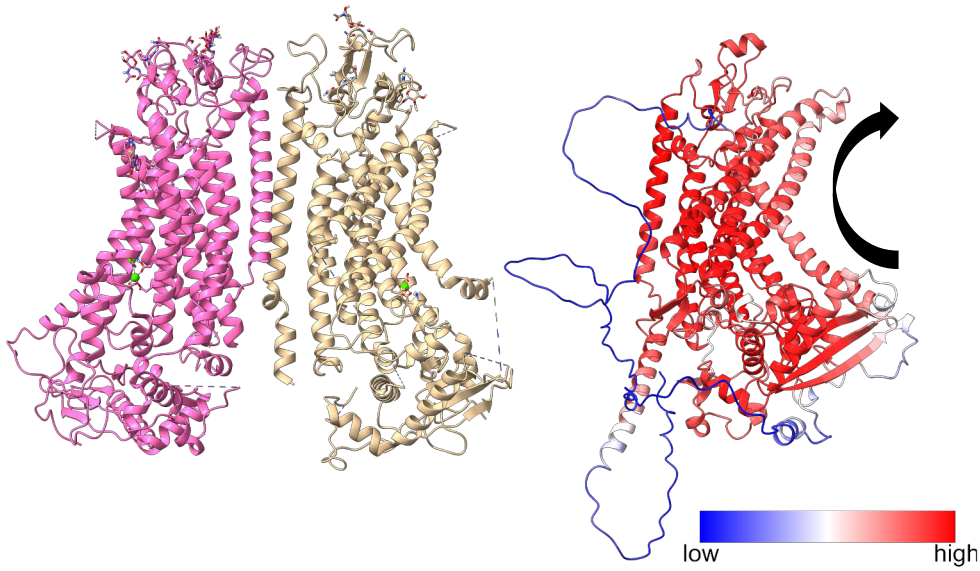

Figure 7. Protein structures of ANO6 homodimer and ANO7. The ANO6 homodimer structure (Protein data bank ID: 8SUN) on the left has been resolved with electron microscopy. The Alphafold predicted structure of ANO7 (AF-F1-v4) on the right. The predicted ANO7 model confidence is marked with blue-white-red gradient. The blue regions represent disordered domains that lack a fixed three-dimensional structure. The black arrow denotes for the putative region in the protein structure that facilitates scrambling of phospholipids. Citations of the protein models: 8SUN (Feng et al., 2023); AF-F1-v4 (Jumper et al., 2021; Varadi et al., 2022).

The mechanisms by which the anoctamin family proteins function in cells and tissues are diverse. The chloride channels ANO1 and ANO2 regulate neuronal excitability and are involved in nociception, sensory transduction, and smooth muscle contraction (Benarroch, 2017). These functions are mediated, for example, by tethering the endoplasmic or sarcoplasmic reticulum (ER/SR) with the plasma membrane via protein interactions, thus creating membrane contact sites. In these contact sites, signals from outside the cell cause the release of ER/SR calcium stores, which then activate anoctamins along with other calcium signalling-related effects (Schreiber, Ousingsawat and Kunzelmann, 2024).

Lipid scramblases are membrane proteins that mediate the translocation of phospholipids from one side of a membrane to the other in a calcium-dependent manner. This action is similar to that of flippases and floppases (facilitating flip-flop movement of specific lipids across membrane, inwards or outwards, respectively); however, these two consume ATP in the process, unlike scramblases (Wang and Kinoshita, 2023). ANO6 was first associated with scramblase function when impaired ANO6 was found in a rare bleeding disorder, Scott's syndrome. In Scott's syndrome, ANO6 is required in the cascade where platelets coagulate and clot blood as a result of the translocation of phosphatidylserine to the platelet outer membrane (Suzuki et al., 2010; Castoldi et al., 2011). This process is mediated by a scrambling domain identified in ANO6 (Yu et al., 2015) and this domain is also identified in other anoctamins (Gyobu et al., 2017). The most efficient scramblase activity has been reported for ANOs 3, 4, 5, 6, and 7, and they are able to scramble many types of phospholipids, including phosphatidylserine, phosphatidylcholine, sphingomyelin, and galactosylceramide (Gyobu et al., 2017).

Initially, ANOs 1-7 were reported to localise predominantly in the plasma membrane, while ANO8-10 were seen to localise in intracellular compartments, in experiments conducted in HEK293 cells (Tian, Schreiber and Kunzelmann, 2012). However, another study reported intracellular localisation for ANOs 3-7 in experiments also with HEK293 cells. Furthermore, ANO7 was not found to induce notable ion currents; hence, the authors argue that ANO7 is likely not a plasma membrane chloride channel (Duran et al., 2012). Our observations align with the intracellular localisation of ANO7, and the localisation appears close to mitochondria (Löf et al., 2025). However, it may still be possible that ANO7 protein resides both in the plasma membrane and intracellular organelles, at least in the endoplasmic reticulum, while the localisation depends on cellular polarisation or other factors.

Anoctamins are also shown to play a role in cancer. Several anoctamins, such as ANO1, ANO6, and ANO9, have been shown to affect oncogenic properties in cancers such as gastrointestinal stromal tumour, head and neck squamous cell carcinoma (HNSCC), breast cancer, oesophageal squamous cell carcinoma (ESCC),

and others (Kunisaki, 2020). Interestingly, the tumour-promoting effects have been shown to be mediated by promoting mitogenic signalling through EGFR in breast cancer, HNSCC, and ESCC (Britschgi et al., 2013).

As for ANO7, it has been suggested to take part in cellular adhesion since LNCaP cells over-expressing *ANO7* form cell aggregates, and this feature is attenuated with small interfering RNA (siRNA) silencing *ANO7* (Das et al., 2007). No other functional roles have been reported for ANO7 to date, except for those in the latest publications by our group (Löf et al., 2025; this study).

2.3.2 Tissue expression of *ANO7*

The Genotype-Tissue Expression (GTEx) and the Human Protein Atlas (HPA) databases contain bulk and single-cell RNA sequencing data from normal human tissues. The bulk RNA sequencing consensus data shows that *ANO7* is most highly expressed in prostate tissue, with notable expression also seen in the intestine and stomach (Appendix 1). At the single-cell level, three cell types are enriched for *ANO7*: prostatic glandular cells, intestinal goblet cells, and gastric mucus-secreting cells (Appendix 2). In cancer, *ANO7* is enriched in prostate cancer as compared to other cancer types in the TCGA (The Cancer Genome Atlas) dataset (Appendix 3).

In the prostate, a study of healthy tissue showed *ANO7* to be specific to luminal epithelial cells compared to other prostatic cells (basal epithelial, other epithelial, and fibromuscular stroma) (Henry et al., 2018).

2.3.3 Association of *ANO7* with prostate cancer

ANO7 has been associated with prostate cancer susceptibility through analyses comparing the genomes of prostate cancer patients to healthy individuals. The genomic location of *ANO7* (2q37.3) was first identified in a linkage analysis, which provides information about the association of regions at a resolution that does not allow for the detection of individual genes (Cropp et al., 2011). In a multi-ancestral meta-analysis of genome-wide association studies, single-nucleotide polymorphisms (SNPs) located in *ANO7* were shown to be associated with prostate cancer risk (Conti et al., 2021). Furthermore, some African-specific *ANO7* SNPs have been linked to prostate cancer risk (Chen et al., 2023; Jiang et al., 2024).

Our group has studied two *ANO7*-residing SNPs in detail. Patients carrying the rs148609049 (stop-gain mutation) have worse survival in prostate cancer, while rs77559646 has no effect on the survival of prostate cancer patients. However, the rs77559646 risk genotype G/A is correlated with higher *ANO7* expression in patients compared to non-carriers of the allele A and is more common in aggressive cases than in non-aggressive cases (Kaikkonen et al., 2018). The rs77559646 is a splice-

site variant that almost fully disrupts the splicing of *ANO7* mRNA, leading to a loss of protein in tissue (Wahlström et al., 2022).

Notably, a majority of these risk SNPs in *ANO7* are located in the coding region and are non-synonymous variants or introduce a stop codon (Kaikkonen et al., 2019; Conti et al., 2021; Jiang et al., 2024). The lower expression of protein and mRNA in prostate cancer has been linked with poor outcomes (Mohsenzadegan et al., 2013; Marx et al., 2021), although a contradictory result of higher mRNA expression associating with worse survival has also been reported (Kaikkonen et al., 2018).

2.3.4 *ANO7* as a biomarker for prognostication

ANO7 is already included in a commercial multigene panel, Decipher, which is used for predicting aggressive prostate cancer by measuring mRNA levels from biopsies (Erho et al., 2013). Despite the undisputed association with prostate cancer, very little is known about the role of *ANO7* in cellular processes. Our group has studied ANO7-interacting proteins using a proximity ligation assay, identifying proteins related to vesicle trafficking, among others (Kaikkonen et al., 2020). The study that identified risk SNPs in African populations suggested that some of these mutations affect the protein structure and cause obstruction in a predicted ion pore; however, no effects on cellular processes were hypothesised (Jiang et al., 2024). More information is required about the role of ANO7 and how it affects cancer progression, so that the risk SNPs could be utilised in the prognostication of prostate cancer.

3 Aims

The expression of *ANO7* and several of its SNPs have been strongly associated with prostate cancer across various populations worldwide. However, the function of this gene in prostate tissue and its contributions to tumour development remain poorly understood. The primary aim of this work was to investigate the role of *ANO7* in normal prostate physiology and in the progression of prostate cancer. This information is required to enable the application of *ANO7* as a prognostic biomarker and to inform treatment planning.

The main aims of this thesis were:

- To perform functional studies of *ANO7* in prostate cancer cell lines.
- To characterise of the spatial expression pattern of *ANO7* in prostatic tissue, including benign glandular and cancerous tissue.
- To explore the cellular processes that are associated with *ANO7* expression in human prostate tissue.

4 Materials and Methods

4.1 Human prostate tissue (I, II)

The patient material in Study I was a subset of seven formalin-fixed and paraffin-embedded (FFPE) tissue samples from seven patients enrolled in the Prosty study (Kellokumpu-Lehtinen et al., 2013). Tumour microarray blocks were made by drilling cylinder-shaped cores from the original FFPE blocks and assembling them in a cassette, followed by embedding in paraffin. The material included tissue chips from transurethral resection of the prostate and tissue samples from radical prostatectomies.

The patient material in Study II was from the Turku Prostate Cancer Consortium (https://tpcc.utu.fi/) sample collection. The patients underwent radical prostatectomy as part of their primary treatment for localised prostate cancer. The prostate organ was dissected in Auria Biobank, and tissue core punches were taken from the peripheral zone of the prostate. Tissue pieces were prepared either as FFPE or fresh frozen (FF) blocks.

The tissue preparations, including the preparation of the tissue micro-array block from the Prosty FFPE blocks as well as fresh tissue preservation, embedding, and sectioning, were performed by the Histocore services at the Institute of Biomedicine, University of Turku, Turku, Finland.

4.2 RNA fluorescent *in situ* hybridisation (I, II)

For the detection of transcripts in prostate tissue FFPE sections in Studies I and II, the RNAScope Multiplex Fluorescent kit v2 (323110, Advanced Cell Diagnostics, Newark, CA, USA) was utilised. The RNA fluorescent *in situ* hybridisation (RNA-FISH) method is based on Z-shaped probes complementary to the target mRNA, with each probe binding to approximately 50 bases. The probe mixture for each mRNA target contains up to 20 different probes covering a continuous region in the target transcript. For a signal to be amplified, two Z-probes need to bind adjacently, creating a secondary binding site for a pre-amplifier. Next, the amplifiers bind to the pre-amplifier, and fluorophores bind to the amplifier, thus creating a strong amplification for each mRNA molecule upon excitation in fluorescent microscopy.

The two Z-probe strategy decreases unspecific signals since the binding of only one probe does not create a signal. The hybridisation steps are illustrated in Figure 8.

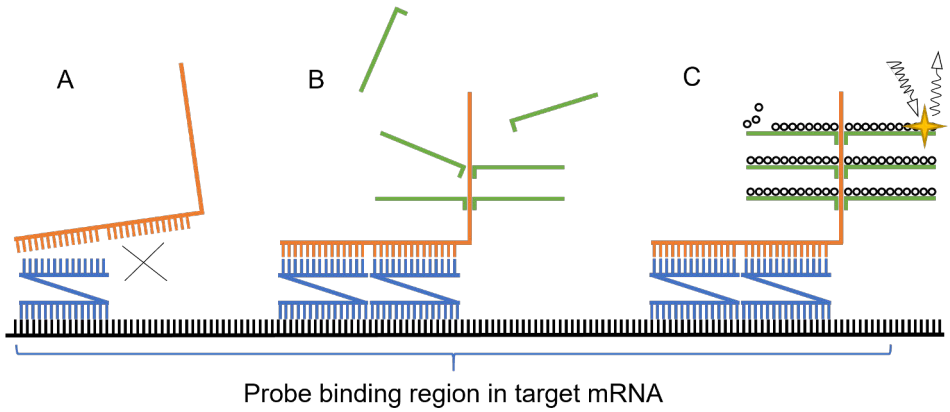

Figure 8. Fluorescent *in situ* hybridisation steps. Binding of one Z-probe (blue) does not allow the binding of a pre-amplifier (orange) (A). Once the Z-probes binds to the target mRNA adjacently, the pre-amplifier binds onto the Z-probes and amplifiers (green) bind onto the pre-amplifier (B). Fluorophores (white dots) attach onto the amplifiers and can be visualised with fluorescence microscopy (C).

The 20 Z-probes were designed to target nucleotides 1015-1979 of the transcript NM_001001891.2, encoding the long form of *ANO7* (transcript variant 1). This region overlaps with exons 9-17 of the *ANO7* long-form transcript and does not contain intronic sequences. Additionally, the RNAScope kit contains probes against human housekeeping gene mRNA *PPIB* (NM_000924.4) as positive control probes, and a negative control probe targeting B. subtilis mRNA *dabB* (EF191515).

The protocol was performed according to the RNAscope Multiplex Fluorescent Reagent Kit v2 Assay with Sample Preparation and Pretreatment (Document Number 323100-USM). Here, the protocol is described briefly. Five µm FFPE tissue sections were mounted on slides for the hybridisation, and separate slides were made for targeting ANO7, and positive and negative controls. The slides were baked for 1 hour at 60°C, followed by deparaffinisation with xylene and 100% ethanol washes. Endogenous peroxidase was inactivated with hydrogen peroxide treatment, and target retrieval was performed by incubating the slides in 1x Target Retrieval Reagents for 15 minutes at 100°C. To detach the proteins cross-linked with the nucleotides, the sections were incubated in Proteinase Plus for 30 minutes at room temperature. Next, the probes were hybridised by applying the probe mix on the sections and incubating for 2 hours at 40°C in a HybEZ oven. Then, the amplifiers were hybridised subsequently with 30-minute incubations at 40°C in between. Finally, the signals were developed by subsequently adding a probe-specific

Multiplex FL HRP solution and fluorophore with incubations (15 and 30 minutes at 40°C for HRP and fluorophores, respectively) in between. Lastly, the sections were mounted in Prolong Antifade Mountant with DAPI (P36931, Thermo Fisher Scientific, Waltham, MA, USA) and covered with a coverslip.

The fluorophores used for *ANO7* variant 1, *PPIB*, and *dabB* in the publications were Opal 570 (Akoya Biosciences, Menlo Park, CA, USA) (I) and Opal 650 (Akoya Biosciences) (II).

4.3 Immunohistochemistry and immunofluorescence (I, II)

The immunohistochemistry (IHC) staining of the FFPE sections in Studies I and II, as well as the FF sections in Study II, was performed by the Histocore services at the Institute of Biomedicine, University of Turku. The FFPE IHC protocol has been described (Wahlström et al., 2022). The FF sections were fixed with a 4% formalin solution, and then the FFPE protocol was followed from antigen retrieval onwards. The staining was conducted with ANO7 antibody (HPA035730, Sigma-Aldrich, St. Louis, MO, USA) diluted 1:200 for FFPE and 1:900 for FF.

The immunofluorescence (IF) protocol used in Study II has been described (Conway et al., 2023) and detailed in Study II, Supplementary Materials and Methods. Briefly, the FF sections were placed on slides, followed by fixation, blocking, permeabilisation, antibody incubations, DAPI staining, and mounting under a coverslip. The primary antibodies used in the IF were ANO7 (1:200, HPA035730, Sigma-Aldrich) and CD45 (1:200, ab8216, Abcam, Cambridge, UK). The secondary antibodies were anti-rabbit AF-488 (1:200, A21206, Thermo Fisher Scientific) and anti-mouse AF-647 (1:200, A31571, Thermo Fisher Scientific).

4.4 Cell culture (I)

The cell lines used in the studies were LNCaP, 22Rv1, MDA PCa 2b, and VCaP prostate cancer cell lines. The cell lines were acquired from American Type Culture Collection (ATCC).

22Rv1 was derived from a parental xenograft in mice, CWR22R. This xenograft was established from an androgen-sensitive, PSA-secreting xenograft CWR22, and following castration of the mice, the xenograft relapsed and became androgen-independent (Sramkoski et al., 1999). MDA PCa 2b was derived from a prostate cancer bone metastasis. MDA PCa 2b cells express AR and are androgen-sensitive; however, it is an androgen-independent cell line (Navone et al., 1997). The VCaP cell line was established by deriving cells from a castration-resistant prostate cancer metastatic lesion in a patient's vertebrae, followed by xenotransplantation in mice

and then cultured *in vitro*. VCaP cells harbour *AR* amplification and express high levels of AR and AR target genes, such as PSA (encoded by *KLK3*) and prostatic acid phosphatase (*ACP3*) (Korenchuk et al., 2001). LNCaP was established from a metastatic prostate cancer by needle aspiration biopsy from a lymph node metastasis. It is AR positive and expresses AR target genes, such as *KLK3* and *ACP3* (Horoszewicz et al., 1983).

All cell lines were grown in incubators at +37ºC, in a 5% CO2 air atmosphere, and supplemented with penicillin/streptomycin (50 U/ml, 50 µg/ml, respectively). The growth media with supplements for cell lines are listed in Table 2. Additionally, ultraglutamine (BE17-605E/U1, Lonza, Basel, Switzerland) was used at a 2nM concentration, if not already supplemented in the growth media.

Table 2. Cell lines and growth media.

CELL LINE	ATCC ID	GROWTH MEDIA	SUPPLEMENTS (FINAL CONCENTRATION)	USED IN
LNCaP clone FGC	CRL-1740	RPMI 1640 (Gibco)	10% non-heat inactivated FBS (Biowest, Nuaille, France)	I, II, shRNA exp.
22Rv1	CRL-2505	RPMI 1640 (Gibco)	10% non-heat inactivated FBS (Biowest)	I, II, shRNA exp.
MDA PCa 2b	CRL-2422	F12-K (Kaighn's modification) (Gibco)	20% non-heat inactivated FBS (Biowest), 25ng/ml cholera toxin (Sigma-Aldrich), 10ng/ml mouse EGF (Sigma-Aldrich), 0.005mM phosphoethanolamine (Sigma-Aldrich), 100pg/ml hydrocortisone (Sigma-Aldrich), 45nM sodiumselenite (Sigma-Aldrich), 0.005mg/ml human recombinant insulin (ThermoFisher)	II, shRNA exp.
VCaP	CRL-2876	DMEM (Lonza)	10 % non-heat inactivated FBS (Biowest)	II, shRNA exp.

4.5 Gene knockdown with short hairpin RNA

Lentiviral transduction of short hairpin RNA (shRNA) was used to generate stable silencing of *ANO7* in cell lines. The SMARTvector shRNA system (Horizon Discovery, Cambridge, UK) with three different target regions in the *ANO7* variant 1 transcript was used. The vector in all constructs was pSMART, containing an hCMV promoter, a puromycin-resistance insert for puromycin selection, and TurboGFP for visualisation of transduced cells under a fluorescence microscope. The mature microRNA sequences were: ACAGAACAGACATGCACAG (shANO7-1), CGGGAGACTTTTCTGGATA (shANO7-2), and ACTTCGTCCTCGTTTGGGA

(shANO7-3). For a negative control, a non-targeting shRNA construct provided by the manufacturer was used (shScr).

The transductions were performed following the manufacturer's instructions (SMARTvector Lentiviral shRNA Technical Manual, Horizon Discovery). The cell lines used in transductions were LNCaP, 22Rv1, MDA PCa 2b, and VCaP. Before the lentiviral transductions, each cell line was tested for polybrene (TR-1003-G, Sigma-Aldrich) tolerance with several seed densities in a 96-well plate (5K, 7.5K, and 10K cells per well), varying concentrations of polybrene (0-14 µg/ml, 2 unit increments), and with and without FBS in the medium in 6-hour and 24-hour incubations, after which complete media was added (2x volume of the polybrene medium) in the wells. The optimal condition was determined one day after the addition of the complete medium, aiming at selecting the well with the highest polybrene concentration, preferably without FBS, with >90% cell viability by visual inspection. Additionally, the cells were tested for puromycin killing efficacy by seeding the cells for 50% confluency in a 24-well plate prior to the treatment. Puromycin (P9620, Sigma-Aldrich) was added in varying concentrations (0-10 µg/ml, 0.5 unit increments), incubated for 48 hours, and visually inspected, aiming at 0% viability. The optimal conditions selected for transduction media are listed in Table 3 (the seed density was adjusted for the 24-well plate based on the results in the 96-well plate). A 0.01% poly-L-lysine (P4707, Sigma-Aldrich) solution diluted 1:3 in water was used for coating the well plates for MDA PCa 2b during the transduction to improve the attachment of the cells.

Table 3. Lentivirus transduction conditions.

CELL LINE	SEED DENSITY	POLYBRENE	FBS	INCUBATION	PUROMYCIN
MDA PCA 2b	50K per well	4 µg/ml	+	24 h	1 µg/ml
VCaP	50K per well	6 µg/ml	-	6 h	0,5 µg/ml
22Rv1	50K per well	8 µg/ml	-	24 h	0,5 µg/ml
LNCaP	50K per well	10 µg/ml	-	24 h	1 µg/ml

The optimal number of viruses per seeded cell, or the multiplicity of infection (MOI), for efficient gene knockdown is determined post-transduction; therefore, several MOI values were used in the transduction. The cells were seeded in 24-well plates two days prior to the transduction. A serial dilution of the viruses for each construct in MOI values was performed as follows: 25, 8.33, 2.78, and 0.93 (hereafter, MOI25, MOI10, MOI3, and MOI1, respectively). In addition to the three targeting shRNAs and the control shRNA, a sham transduction with no viruses was conducted to monitor the viability of the cells. The transfection media with or without the viruses was added to the cells, and after the determined incubation time,

normal media (2x the volume of the transfection media) was added to the wells. After three days, the puromycin selection was started and continued for at least six weeks before culturing the cells in normal growth media. The transduction efficacy and selection of transduced cells were monitored with an immunofluorescence microscope from the live cells. The cells were expanded until a sufficient number of cells was achieved for measurements and freezing down.

4.6 Cell fractionation (I)

In Study I and the shRNA experiments, the mRNA distribution was measured from whole cell lysate, and nuclear and cytoplasmic compartments. A cell fractionation protocol was developed for this purpose. The protocol is based on the incubation of the cells in hypotonic buffer, which causes the cells to swell due to water influx resulting from an osmotic pressure gradient. First, the cellular membrane was ruptured by incubating the cells in hypotonic buffer. The breakage of the plasma membrane was enhanced with mechanical shearing by passing the cells through a needle a few times. Nuclei were pelleted, allowing the collection of the supernatant containing the cytoplasmic fractions. Next, the nuclei were washed with buffer containing mild detergent to detach any cell organelle remnants from the nuclei. The cytoplasmic and nuclear fractions were then mixed with TRIsure (BIO-38032, Meridian Bioscience, Cincinnati, OH, USA) or SDS lysis buffer for the extraction of RNA or protein, respectively.

The fractionation protocol is provided in Appendix 4. The purity of the cell fractions was assessed by Western blot, detecting the nuclear transcription factor protein HOXB13 and a microtubule (cytoskeleton) protein beta-tubulin, which are localised in the nucleus and cytosol, respectively (https://www.proteinatlas.org/ENSG00000159184-HOXB13/subcellular, https://www.proteinatlas.org/ENSG00000196230-TUBB/subcellular).

4.7 RNA extraction (I)

Two methods were used for the extraction of RNA, as described below. The commercial kit (spin tubes) was used for the cell lysates without excess liquid in the sample. The cell fractionation protocol resulted in liquid samples, which are unsuitable for the spin tube method; therefore, phenol/chloroform extraction was used.

The purity of the resulting RNA from both methods was measured with NanoDrop One (Thermo Fisher Scientific), and poor-quality samples [determined by A260/A280 <1.8 (optimally >2) and A260/A230 <2 (optimally >2)] were

discarded. The integrity of the RNA in Study I was determined with TapeStation 2200 (Agilent Technologies, Santa Clara, CA, USA).

4.7.1 Commercial kit (shRNA experiments)

The RNeasy Plus Mini (74134, Qiagen, Venlo, Netherlands) RNA extraction kit was used for the shRNA samples according to the manufacturer's instructions. The cells were grown in 6-well plates and lysed with 350 µl of the lysis buffer provided in the kit. The kit is based on a porous matrix embedded into a spin column and involves multiple rounds of washes with buffers and ethanol to eliminate proteins and DNA, resulting in purified RNA.

4.7.2 Phenol/chloroform extraction (I)

TRIsure was used for the extraction of RNA from whole cells or cellular fractions in Study I. The protocol is based on phase separation of proteins, DNA, and RNA into aqueous and organic phases by centrifugation. RNA is extracted from the aqueous phase and precipitated with isopropyl alcohol, followed by washes with ethanol. A modification to the manufacturer's recommended protocol was made by adding a second chloroform phase separation. This decreases the yield but increases the purity of the samples.

4.8 Western blot (I)

In Study I, the samples were sonicated with a Sonoplus ultrasonic homogeniser (Bandelin, Berlin, Germany) and the protein concentration was measured with a Pierce BCA Protein Assay (Thermo Fisher Scientific). The samples were mixed with 2x Laemmli Sample Buffer (Bio-Rad Laboratories, Hercules, CA, USA) 1:1, and 20 µg of the protein was loaded into SDS-PAGE run using commercial gradient gels (4561023, Bio-Rad). The separated proteins were transferred into a 0.45µm polyvinylidene difluoride (PVDF) membrane (Merck, Darmstadt, Germany) and the overall protein amount was assessed with Ponceau S.

The shRNA protein samples were sonicated and 30 µl of lysate was loaded either in a commercial gradient gel (4561023, Bio-Rad Laboratories) or a self-made 7% acrylamide gel, then transferred into a 0.45µm PVDF membrane.

The antibodies were incubated overnight at +4°C and secondary antibodies were incubated for 1 hour at room temperature. Chemidoc MP Imaging System (Bio-Rad) or LAS-4000 Luminescent Image Analyzer (Fujifilm, Tokyo, Japan) were used for imaging. The primary antibodies used were HOXB13 (90944C, Cell Signaling Technology, Danvers, MA, USA), β-tubulin (sc-9104, Santa Cruz Biotechnology,

Dallas, TX, USA), and ANO7 (custom affinity purified rabbit antibody, targeting amino acids 451-468 in ANO7-L [UniProt accession number Q6IWH7-1]), and the secondary antibody was anti-rabbit-HRP (ab97080, Abcam).

4.9 Droplet digital PCR (I)

Droplet digital polymerase chain reaction (ddPCR) was used to quantitatively measure the amount of mRNA in the samples in Study I. The method is based on PCR with TaqMan probe chemistry, which includes primer pairs to enhance the DNA sequence of interest in addition to target sequence-specific probes containing a fluorophore and a quencher (a fluorophore-inhibiting molecule). The primers and probes bind to target regions, and when the polymerase reaction reaches the target-bound probe, which is designed to bind between the primer binding sites, the fluorophore-quencher conjugation is cleaved and the fluorophore can be detected with a fluorescence signal. The ddPCR method involves mixing reaction reagents with oil to create micelles, where the PCR reaction takes place during the thermal cycling. The PCR reaction is conducted as end-point PCR, which offers qualitative information on whether the target sequence was present in the droplet or not. By calculating the number of positive droplets and adjusting the ratio of positive versus negative droplets with the volume of the micelles, quantitative information is achieved about the amount of target sequence in the sample.

The QX200 ddPCR system (Bio-Rad Laboratories), used in Study I and the shRNA experiments, included a QX200 Droplet Generator, a QX200 Droplet Reader, and a C1000 Touch Thermal Cycler. The sample RNA was treated with DNase I (18068015, Invitrogen, Waltham, MA, USA) and cDNA was synthesised with the iScript Select cDNA Synthesis Kit (1708897, Bio-Rad Laboratories). ddPCR Supermix for Probes (no dUTP) (1863024, Bio-Rad Laboratories) was used to set up all master mixes. The assays used in experiments are listed in Table 4.

Table 4. ddPCR assays.

TARGET	CATALOGUE NO. AND FLUOROPHORE	PRIMERS AND PROBE TARGET SEQUENCE	TEMPLATE PER REACTION	USED IN
ANO7	dHsaCPE5026736 (FAM)	Undisclosed. The chromosomal context region: hg19|chr2:242135121-242135242:+	300ng (I) 110ng (shRNA exp.)	I, shRNA exp.
GAPDH	dHsaCPE5031596 (FAM)	Undisclosed. The chromosomal context region: hg19|chr12:6647153-6647379:+	6ng	I
MALAT1	custom ordered (FAM)	forward primer 5′-GGTCTAGGATCCTCTACGCA-3′ reverse primer 5′-AAGAAGGAAGGAGCGCTAAC-3′ probe 5′-ACGCCTGCTCGCCTCCTCCGT-3′	600pg	I
TBP	dHsCPE5058362 (FAM)	Undisclosed. The chromosomal context region: hg19|chr6:170871320-170876038:+	110ng	shRNA exp.

The thermal cycler program was optimised for each assay. The following program was used in Study I: step 1, 10 minutes at 95°C; step 2, 30 seconds at 94°C; step 3, 1 minute at 57°C; steps 2 and 3 were repeated 39 times; step 4, 10 minutes at 98°C; and step 5, hold at 4°C. The ramp rate at all steps was 2°C/s. In the shRNA experiments, the temperature in step 3 was 55°C. The plate was incubated overnight at 4°C before droplet reading. The raw data was analysed with QX Manager Software version 1.2 Standard Edition (Bio-Rad Laboratories). The values were normalised to copies of transcript per 1 µg of RNA (copies per µg RNA).

4.10 Microscopy

The imaging in Studies I and II was performed at the Cell Imaging and Cytometry Core at Turku Bioscience, Turku, Finland.

4.10.1 Slide scanners (I, II)

The haematoxylin and eosin (H&E) and IHC stained sections were scanned with a Pannoramic 1000 slide scanner (3DHISTECH, Budapest, Hungary) using a 20x Plan-apochromat objective. The RNA-FISH sections were scanned with a Pannoramic MIDI slide scanner (3DHISTECH) equipped with 20×/0.8 NA Plan-apochromat and 40×/0.95 NA Plan-Apochromat objectives. The filters for fluorophores are listed in Table 5. The images were captured using CaseViewer software (3DHISTECH).

Table 5. Details for imaging of fluorophores.

FLUOROPHORE	INSTRUMENT	FILTER	USED IN
DAPI	Pannoramic MIDI slide scanner	445nm [1]	I, II
DAPI	Spinning disc confocal (Marianas CSU-W1)	445nm [1]	I, II
AF488	Spinning disc confocal (Marianas CSU-W1)	525nm [1]	II
AF570	Spinning disc confocal (Marianas CSU-W1)	617nm [1]	II
Opal570	Spinning disc confocal (Marianas CSU-W1)	617nm [1]	I
AF647	Spinning disc confocal (Marianas CSU-W1)	692nm [1]	II
Opal650	Pannoramic MIDI slide scanner	387/485/559/649nm [2]	II

[1]Single-band filter
[2] Quad-band filter

4.10.2 Confocal imaging (I, II)

In contrast to conventional fluorescence microscopy, the confocal microscopy technique is used for enhanced optical resolution and contrast of signal. This is achieved by pinpointing the captured light signal to a very narrow layer in the sample, thus blocking light coming from outside the field of focus. In addition to better image resolution, the confocal technique also enables three-dimensional imaging of objects in a sample.

The RNA-FISH sections (Study I) and immunofluorescence-stained sections (Study II) were imaged with a Marianas CSU-W1 spinning disc confocal microscope (3i, Denver, CO, USA). The objective used in Study I was a 63×/1.4 NA oil-immersion Plan-Apochromat objective (Zeiss, Oberkochen, Germany). The objectives used in Study II were a 10×/0.45 NA Plan-Apochromat air (Zeiss), a 20×/0.8 NA Plan-Apochromat air (Zeiss), and a 40×/1.2 LD C-Apochromat water-immersion (Zeiss) objective.

The filters used in studies I and II are listed in Table 5. The images were acquired and image montages were created with the SlideBook6 software (3i).

4.11 Image analysis

4.11.1 RNA-FISH mRNA quantitation (I)

The quantitation of mRNA molecules in Study I was performed using ImageJ (NIH, Bethesda, Maryland, USA) and Imaris (Oxford Instruments, Abingdon, UK). First, for each series of image sections, the image stacks were transformed into maximum projection. Masks of the regions of interest were created on the maximum projection, and the original image stacks were cropped based on the masks to include only

epithelium or cancerous cells. The resulting image stacks were imported into Imaris image analysis software. The nuclei were segmented using the DAPI channel, and the mRNA molecules were segmented using the channel for probes (*ANO7*, *PPIB*, and *dabB*). After segmentation, the number of transcripts detected inside the nuclei was divided by the number of transcripts detected in the whole image to yield a ratio of transcripts located in the nuclei versus total mRNA. Each probe was imaged with varying exposure times, aiming at maximal sensitivity for quantitating the nuclear versus total number of transcripts; thus, comparing the absolute number of transcripts between conditions (*e.g.* low-grade cancer versus high-grade cancer) is not exact. Additionally, the negative control probe *dabB* was exposed for a longer time (250ms) compared to positive probes (*ANO7*, *PPIB*) (100-200ms) to enable evaluation of non-specific signal distribution. The assessment of cellular morphology determining the benignity or cancer grade was made from the H&E-stained sections adjacent to the RNA-FISH section.

4.11.2 ANO7 and CD45 distribution in prostate tissue (II)

In Study II, montages created from the IF images were processed with ImageJ (NIH). The whole tissue montages, as well as ROIs, were cropped, followed by creating maximum intensity projections from the image stacks. Then, to enhance the signal, a global contrast enhancement was applied for each channel (ANO7, CD45, DAPI). The localisation of the signal was evaluated visually.

4.12 Spatial profiling of prostate tissue (II)

For detailed, high-resolution analysis of the epithelial regions positive or negative for ANO7 expression, GeoMX Digital Spatial Profiler (DSP) (NanoString Technologies, Seattle, WA, USA) was employed with the Whole Transcriptome Atlas (WTA) (HWTA21003, NanoString Technologies) targeting the mRNA of more than 18,000 protein-coding genes. The technology is based on photocleavable barcodes linked with the mRNA-targeting probes. After the mRNA-targeting probes are hybridised with the tissue, user-defined areas are illuminated, releasing the barcodes, which are collected for sequencing and subsequent quantitation of gene expression.

Initially, 46 tissue samples were collected from 16 patients who were diagnosed with localised prostate cancer and underwent radical prostatectomy. Clinical parameters of the patients are provided in Study II, Supplementary Materials and Methods, Table S1. All tissue samples were screened for suitable regions of interest, which were defined as the tissue containing a high-contrast on/off-expression pattern and assessed by ANO7 protein staining. Ten tissue samples from four patients were

selected for the spatial profiling. Since the tissue pretreatment protocol has issues with tissue displacement from the slides, each tissue sample was prepared with a replicate section on the same slide to ensure the availability of intact tissue for sample collection.

Sets of four slides were prepared for each patient containing serially sectioned sample sections, as described in Study II, Supplementary Figure S1A. For each set, the slides were treated as follows: slides 1 and 3 were stained for ANO7 protein, slide 2 was used for GeoMX DSP sample collection, and slide 4 was stained with H&E for morphological assessment.

Slide 2 for each slide set was prepared according to the GeoMX DSP Manual Slide Preparation User Manual (version MAN-10150-02 Nov 2022). Briefly, the protocol involved fixation with 10% neutral-buffered formalin, antigen retrieval in Tris-EDTA (pH 9) solution, exposure of RNA-target to remove cross-linked proteins with proteinase K, and post-fixation in 10% neutral-buffered formalin. Then, the WTA probes were hybridised with the tissue overnight, followed by the application of morphological markers for the detection of nuclei (SYTO13, GMX-RNA-MORPH-HST-12, NanoString Technologies) and a pan-cytokeratin (panCK, GMX-RNA-MORPH-HST-12, NanoString Technologies) for the detection of epithelium. A detailed protocol is provided in Study II, Supplementary Materials and Methods.

The epithelial ROIs from slide 2 in each slide set were collected based on the ANO7 protein staining on the adjacent slides, 1 and 3, the ROIs being either positive or negative for ANO7 in both slides. The samples were collected using the GeoMX instrument at the Single Cell Omics core services in Turku Bioscience. The sequencing sample preparation was done by the Single Cell Omics staff and sequenced at the Finnish Functional Genomics Center at Turku Bioscience with a NovaSeq 6000 equipped with an S1 V1.5 flow-cell (Illumina, San Diego, CA, USA). The resulting FASTQ files were converted into files containing counts per probe (dcc-format) in BaseSpace Sequencing Hub (Illumina). The data preprocessing and quantile normalisation were performed by a bioinformatician in our group.

4.13 External data (II)

The publicly available TCGA PRAD (The Cancer Genome Atlas, Prostate Adenocarcinoma) dataset contains bulk RNA-seq data and has been widely used for discovery and validation purposes. The data, including gene expression and clinical data, was downloaded from UCSC (University of California Santa Cruz) Xena Browser (https://xenabrowser.net/). The RNA-seq data contain cancer and adjacent benign tissue samples.

4.14 Computational analysis tools

4.14.1 Differential gene expression (II)

An analysis of differentially expressed genes (DEGs) was used in Study II. DEGs were calculated in Chipster (Kallio et al., 2011) using linear mixed models (limma) (Smyth, 2004; Smyth, Michaud and Scott, 2005). P-values were adjusted using the Benjamini-Hochberg procedure, and false discovery rate (FDR) <0.05 was considered significant.

4.14.2 Gene set enrichment analysis (II)

The gene set enrichment analysis (GSEA) (Subramanian et al., 2005) was utilised to detect pathways or processes that are differentially expressed between sample groups. The gene sets were derived from the Molecular Signatures Database (https://www.gsea-msigdb.org/gsea/msigdb). The analysis was conducted with Hallmark gene sets, which contain 50 different human biological expert-curated gene sets designed to reduce redundancy in overlapping gene sets, with enhanced sensitivity in the GSEA whilst also capturing a large proportion of the biological processes related to cellular functions (Liberzon et al., 2015). The Hallmark gene sets serve as a good starting point to build hypotheses before moving on to more detailed analysis. The analysis was performed with the GSEA software version 4.3.2 for Windows (Broad Institute, Cambridge, MA, USA).

4.14.3 Single-sample GSEA (ssGSEA) (II)

The single-sample GSEA (ssGSEA), used in Study II, is an extension of the GSEA. Unlike comparing groups of samples, ssGSEA calculates the enrichment of a gene set within a sample and does not require normalisation of the data. The method has been described in detail (Barbie et al., 2009). The score resulting from the analysis represents a combined value for a set of genes in a sample. The ssGSEA was utilised to assess the enrichment of marker genes for prostate tissue cell types. The marker genes for the prostatic cell types were derived from a single-cell sequencing study, which profiled cell composition from patients' prostate needle biopsies (Song et al., 2022). The tissue comprised normal and cancerous cells thus representing a similar tissue type composition of the one used in the present study. In Song et al., the analysed cell types representing benign cells were luminal, basal, and club cells found in the epithelium, and fibroblast, smooth muscle, and endothelial cells found in the stroma, as well as myeloid and T-cells, which can be found in both the epithelium and stroma. For a detailed analysis of immune cells, marker gene sets

were used from a pan-cancer study for tumour-infiltrating lymphocytes (TILs) (Charoentong et al., 2017) for the assessment of 28 immune cell subtypes. The marker gene lists per cell type are provided in Study II, Supplementary Materials and Methods, Table S9. The values from the ssGSEA were standardised with z-scoring, which calculates the distance of a sample's value from the mean of the whole dataset.

4.14.4 Network analysis (II)

Cytoscape is designed as a network visualisation tool for complex data, integrating annotations and attributes within the network (Shannon et al., 2003). Cytoscape software version 3.10.1, with the ClueGO App (Bindea et al., 2009) version 2.5.10, was used in Study II to generate a network analysis of the pathways enriched in ANO7-positive epithelium in low infiltration regions. The 277 DEGs, upregulated in ANO7-positive epithelium in low inflammation regions, were uploaded into ClueGO. The DEGs were divided into two groups: genes correlating with ANO7 ($r > 0.4$) as Cluster 1, and the remaining genes as Cluster 2. Using gene sets in Gene Ontologies (GO), Kyoto Encyclopedia of Genes and Genomes (KEGG), and Reactome libraries, the pathways in which the marker genes were over-represented were calculated in ClueGO, resulting in 65 terms representing cellular pathways or processes. Next, the terms were grouped based on similarity per shared genes, using Cohen's kappa score ≥ 0.4 as a threshold for grouping. The network analysis provides a visualisation of the terms that are close to each other and can be used for the interpretation of complex data and redundancy in the results.

4.15 Artificial intelligence (thesis)

Microsoft Copilot was used to correct British English grammar and spelling, and to enhance readability of this thesis. Copilot was run within the University of Turku O365 environment.

5 Results

5.1 shRNA knock-down of *ANO7* in cell lines showed poor efficacy

The aim of the shRNA knockdown of *ANO7* was to evaluate the transcriptomic and phenotypic changes caused by *ANO7* knockdown in the cell lines. The silencing efficacy of *ANO7* in shRNA cell lines was measured with ddPCR. A housekeeping gene, *TBP* (TATA binding protein), was used as a positive control in the measurement, since the expression level of *TBP* is similar to *ANO7* in human prostate RNA-seq data.

We measured the expression of *ANO7* and *TBP* in all of the generated shRNA cell lines: 22Rv1, VCaP, LNCaP, and MDA PCa 2b. The expansion of VCaP cells was successful only with *ANO7*-targeting construct 3 (shANO7-3) and the corresponding non-targeting construct (shScr) with MOI values of 10 and 25. The expansion of LNCaP failed with shANO7-1 at MOI values of 10 and 25. The rest of the expansions were successful with all constructs (shScr, shANO7-(1/2/3)) and all MOI values (MOI1, MOI3, MOI10, and MOI25).

Figure 9 shows the results of the silencing efficacy measurements conducted with two technical replicates per sample. The *TBP* expressions were fairly stable in all samples. The *ANO7* values were normalised to *TBP* by dividing the mean of each *ANO7* value by the mean value of *TBP* in the same sample from two technical replicate measurements. The *ANO7* values were then normalised to the corresponding shScr sample within each MOI, and the results are presented as the percentage of *ANO7* transcripts in targeting constructs in relation to shScr.

The silencing efficacy was generally poor, with some ANO7-targeting constructs showing even higher values than the non-targeting control. The highest silencing efficacy was seen in MDA PCa 2b (shANO7-1, MOI1 and MOI3), with 62% efficacy. The highest efficacies for other cell lines were 34% in 22Rv1 (shANO7-2, MOI25), 43% in VCaP (shANO7-3, MOI25), and 55% in LNCaP (shANO7-3, MOI25) (Figure 9).

We ran a Western blot analysis from MDA PCa 2b samples with the highest silencing efficacies, but no changes were seen in signal bands that correspond to the size of ANO7 protein (Appendix 5).

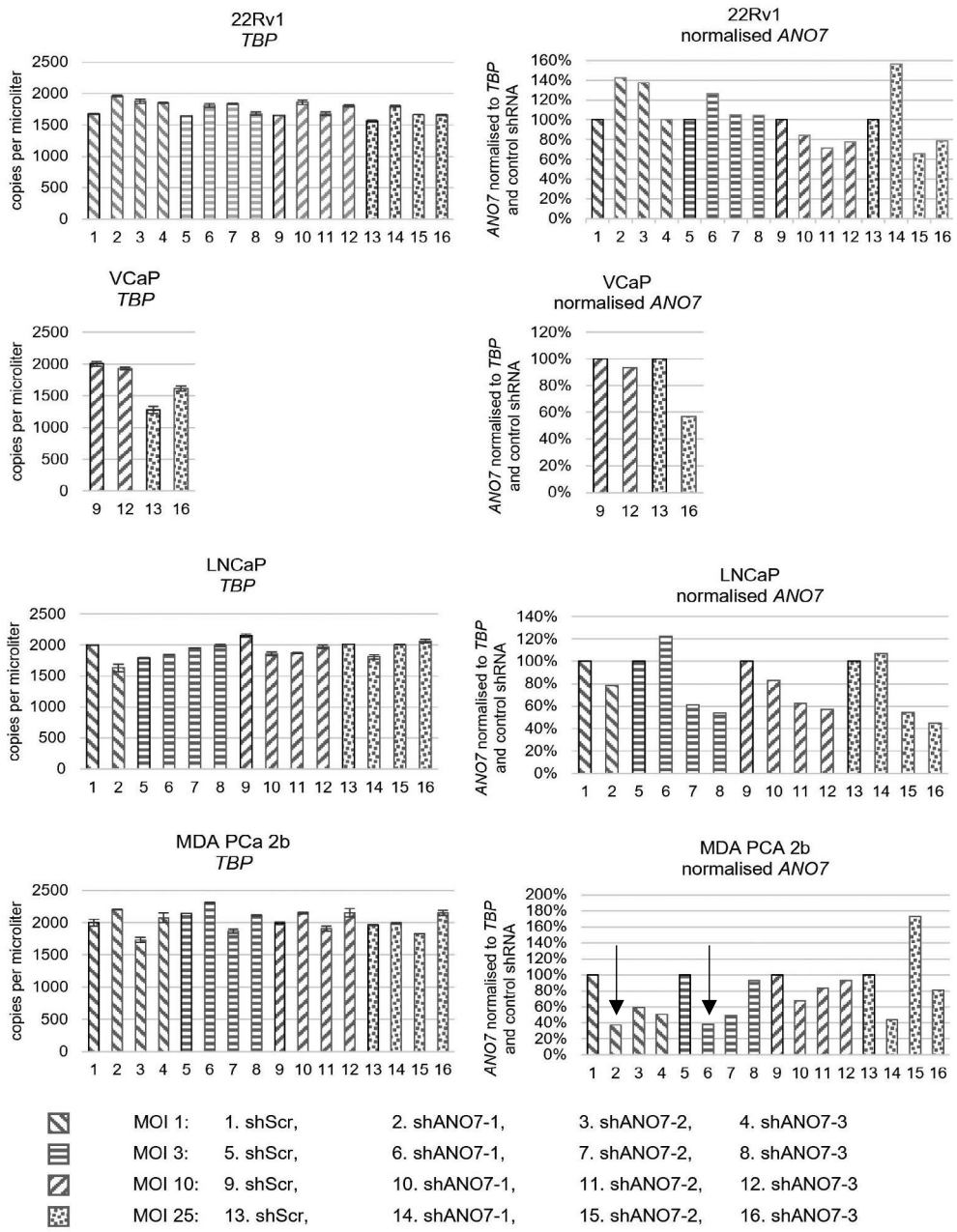

Figure 9. ShRNA silencing of endogenous *ANO7* expression in prostate cancer cell lines. The silencing efficacy was assessed by measuring *ANO7* and a housekeeping gene *TBP*. The *ANO7* transcript counts were normalised to *TBP* in each sample, after which the targeting shRNA (shANO7) samples were normalised to the corresponding control (shScr) MOI. The overall silencing efficacy was poor. The best efficacies were seen in MDA PCa 2b with construct shANO7-1 in MOIs 1 and 3 with 62% reduction of ANO7 transcripts compared to the corresponding control samples, indicated with black arrows. *TBP* bars are showing the mean and standard deviation from the measurement of two technical replicates.

To understand the poor efficacy of the *ANO7* knockdown, we measured the transcripts from nuclear and cytoplasmic compartments, as well as from whole cell lysate. The cell line and shRNA constructs with the highest silencing efficacy were selected for this purpose (MDA PCa 2b; shANO7-1; MOI1, 3). The transcripts of *ANO7*, and control genes *GAPDH* and *MALAT1*, were measured with ddPCR.

The results in Figure 10 show that *GAPDH* transcripts are enriched in the cytoplasm, whereas *MALAT1* transcripts are enriched in the nucleus. *ANO7* shows similar nuclear enrichment to *MALAT1*. A comparison of cytoplasmic enrichment between shScr and shANO7-1 in each MOI, and a comparison of wild-type (WT) MDA PCa 2b cells to siScr samples, shows that the shANO7-1 MOI1 samples contain significantly fewer cytoplasmic transcripts as compared to the corresponding shScr, while no other comparisons were significantly different.

This implies the following: first, the expression of *ANO7* in cell lines is very low, thus the cell lines do not express protein at a detectable level; and second, the residual transcripts are enriched in the nucleus of the cells. Therefore, studying the effect of ANO7 with shRNA silencing is not feasible in prostate cancer cell lines due to the reasons discussed in chapter 6.1, and consequently, the experiment was terminated.

Figure 10. ► Ratio of cytoplasmic *ANO7*, *GAPDH*, and *MALAT1* transcripts in MDA PCa 2b cell line. Values normalised to copies per µg of RNA in samples on the left and the percentage of cytoplasmic transcripts (cytoplasmic transcripts/nuclear transcripts) on the right for each gene. Each dot represents the mean value of two technical replicates and three biological replicates were measured per each construct. In the construct shANO7-1 with MOI1 the proportion of the cytoplasmic transcripts was significantly reduced compared to the control shRNA. Comparison of the cytoplasmic transcripts in WT to shScr samples showed no significant differences in any gene. * p-value >0.05, Tukey's multiple comparisons test. Wc: whole cell; cyt: cytoplasm; nuc: nucleus; RT: reverse transcriptase; NTC: no template control.

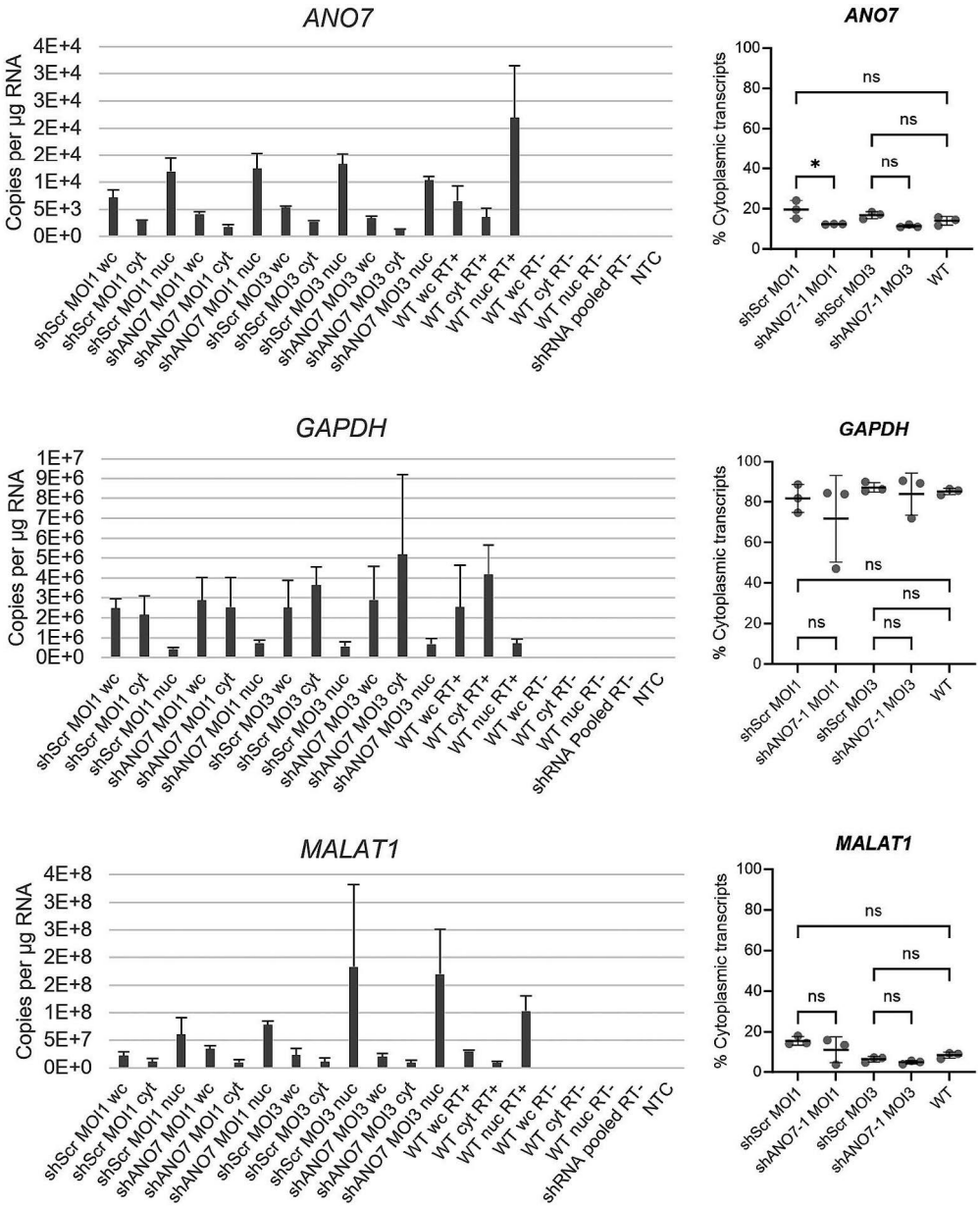
ANO7
Copies per µg RNA
4E+4
3E+4
3E+4
3E+4
2E+4
2E+4
2E+4
1E+4
5E+3
0E+0
shScr MOI1 wc
shScr MOI1 cyt
shScr MOI1 nuc
shANO7 MOI1 wc
shANO7 MOI1 cyt
shANO7 MOI1 nuc
shScr MOI3 wc
shScr MOI3 cyt
shScr MOI3 nuc
shANO7 MOI3 wc
shANO7 MOI3 cyt
shANO7 MOI3 nuc
WT wc RT+
WT cyt RT+
WT nuc RT+
WT wc RT-
WT cyt RT-
WT nuc RT-
shRNA pooled RT-
NTC
ANO7
% Cytoplasmic transcripts
100
80
60
40
20
0
ns
ns
ns
*
shScr MOI1
shANO7-1 MOI1
shScr MOI3
shANO7-1 MOI3
WT
GAPDH
Copies per µg RNA
1E+7
9E+6
8E+6
7E+6
6E+6
5E+6
4E+6
3E+6
2E+6
1E+6
0E+0
GAPDH
% Cytoplasmic transcripts
100
80
60
40
20
0
ns
ns
ns
ns
MALAT1
Copies per µg RNA
4E+8
3E+8
3E+8
2E+8
2E+8
1E+8
5E+7
0E+0
MALAT1
% Cytoplasmic transcripts
100
80
60
40
20
0
ns
ns
ns
ns

5.2 *ANO7* is retained in the nuclei of luminal epithelial cells of the prostate

We next conducted analysis in prostate tissue, which exhibits robust expression of *ANO7*. At the time of this work, there was no fully specific commercial antibody available against ANO7. The antibody, which is also used by others (HPA035730) (Marx et al., 2021) is not fully specific to ANO7 and also stains endothelial cells and, in some cases, basal cells in prostate tissue (Wahlström et al., 2022). Therefore, we utilised fluorescent *in situ* hybridisation to study the expression patterns in prostatic tissue containing both benign and cancerous glands, and to compare the mRNA and protein staining in tissue. The tissue material for the study was obtained from archived FFPE tissue blocks from samples of Finnish patients in the Prosty-trial, containing tissue samples from patients who later developed castration-resistant disease (Kellokumpu-Lehtinen et al., 2013).

5.2.1 The expression of ANO7 protein and mRNA is concordant in luminal epithelial cells

We assessed the expression from benign glands and cancerous glands ranging from Gleason 3 to Gleason 5. The protein staining showed a pattern with high-intensity staining apically in the luminal epithelial cells (I: Figure 2B), similar to what has been described previously (Das et al., 2007; 2008; Wahlström et al., 2022). The mRNA signal displayed a similar pattern to the protein staining in the epithelium. However, the mRNA signal was restricted to the lumen-facing cell layer (luminal cells) in benign epithelium, while the basal cells, which were stained weakly for protein, did not exhibit an mRNA signal (I: Figure 2A-D). The weaker protein staining in high-grade cancer was also reflected in the mRNA signal, with fewer spots detected in high-grade cancer compared to the benign gland and low-grade cancer by visual inspection (I: Figure 2C, D).

5.2.2 ANO7 mRNA localises in the nucleus of the cells

The mRNA signal of *ANO7* displays a very different subcellular pattern compared to the control gene *PPIB*. The majority of the *ANO7* signal spots are localised inside the nuclei, with less dense signal spots in the cytoplasm. Furthermore, the signal spots seem to be concentrated into high-intensity spots within the nuclei (I: Figure 2D). We quantified the nuclear enrichment in the epithelial cells with confocal imaging. The nuclei and mRNA signal spots for *ANO7* and positive control *PPIB* were segmented from the images, and calculated the ratio of nuclear versus cytoplasmic transcripts. The results show that the *ANO7* transcripts are highly enriched in the nuclei in benign glands/low-grade cancer and in high-grade cancer

(89% and 78%, respectively). In contrast, *PPIB* is evenly distributed between the nucleus and cytoplasm (I: Table 1). Neither *ANO7* nor *PPIB* show a statistical difference in the nucleus versus cytoplasm ratio between benign gland/low-grade cancer and high-grade cancer (I: Figure 3).

5.2.3 Nuclear enrichment of ANO7 mRNA was validated in prostate cancer cell lines 22Rv1 and MDA PCa 2b

We validated the the nuclear enrichment of the ANO7 transcripts in two prostate cancer cell lines, 22Rv1 and MDA PCa 2b. We prepared samples containing the cytoplasmic and nuclear fraction of the cells and confirmed the purity of the cell fractions in Western blot, using HOXB13 as a nuclear marker and β-tubulin as a cytoplasmic marker. Both cell lines showed high purity of fractions (I: Figure 4A). We assayed *ANO7*, *MALAT1*, and *GAPDH* mRNA from the cell fractions as well as whole cells. *MALAT1* was highly enriched in the nucleus in both cell lines, as expected. *ANO7* was similarly enriched in the nucleus, with a binary logarithmic fold change of 3.75 in 22Rv1 and 2.63 in MDA PCa 2b (I: Figure 3 and Table 2).

These results confirmed that the majority of the *ANO7* transcripts are retained in the nucleus of prostate epithelial cells. The retention of the transcripts in the nucleus does not change during cancer progression, while the mRNA and protein expression is diminished in high-grade cancer. The potential cause of the strong nuclear retention of *ANO7* transcripts is discussed in Chapter 6.2.1.

5.3 Spatial profiling of ANO7 in the prostate

The *ANO7* expression exhibited a high-contrast on/off expression pattern in the RNA-FISH. This pattern is also detectable in protein staining; however, it is less pronounced and is obscured by issues with antibody specificity. The striking regional difference seen in the mRNA expression (II: Figure 1) provided an excellent setting for studying differences between the ANO7-positive and -negative epithelial regions. Some glands display uniform protein and mRNA expression, while the adjacent gland can be fully negative for the expression. In other cases, a gland may display regional positive or negative expression inside a single gland. These patterns show very high contrast in the RNA-FISH, while it was also detectable in protein staining.

We employed the GeoMX DSP platform to investigate the differences in *ANO7* expression in the epithelium. GeoMX offers the possibility to manually select the ROIs for analysis. This is essential for studying *ANO7*, since the contrasting regions may represent detailed regions in the epithelium, which are challenging to capture in other similar methods based on even spotting. Additionally, the spatial information

and assessment of tissue morphology around the collected regions allow for more accurate annotation of the samples, aiding in the interpretation of the results.

The high-contrast on/off expression pattern is only seen in benign glands and therefore we targeted only benign glands in the analysis. We collected the samples by manually drawing ROIs on the sample collection sections based on ANO7 protein staining in the adjacent slides, and using the pancytokeratin staining to mark the epithelium (II: Supplementary Figure S1A, B, C). The sample set consisted of epithelial regions positive or negative for ANO7 and stromal regions adjacent to the epithelial regions. We split the data into epithelial and stromal subsets, and ran analyses on the subsets separately. The level of immune cell infiltration, assessed from the H&E images, heavily affected the sample clustering in uniform manifold approximation and projection (UMAP) plots as epithelial samples collected from regions with strong infiltration formed separate clusters (II: Figures 2B, C). Consequently, we regrouped the epithelial and stromal samples to low and high inflammation groups based on the level on immune cell infiltrations (II: Supplementary Materials and Methods, Figure S2).

5.3.1 *ANO7* is enriched in the luminal cells of the epithelium, and its expression is diminished in epithelia enriched with club cells

We utilised ssGSEA to investigate the cell composition of the sequenced regions using marker gene sets from scRNA-seq study that analysed tissue with localised prostate cancer (Song et al., 2022). Initially, the analysis was run also with markers from Henry et al. (2018) study with matching results (not shown), however, in the final analysis only the cancerous tissue markers were used. The cell types considered in this analysed were luminal, club, basal, T-cells, and myeloid cells in the epithelium, and fibroblast, smooth muscle, endothelial, T-cells, and myeloid cells in the stroma. The ssGSEA scores per cell type were assessed for differential distribution between the groups.

In low inflammation regions, the luminal scores showed enrichment of luminal cells in *ANO7*-positive epithelial samples (II: Figure 2D). Conversely, the club scores showed enrichment of club cells in *ANO7*-negative regions (II: Figure 2E). High inflammation affected luminal and club scores by showing intermediate luminal score and high club score in *ANO7*-positive epithelium, while luminal and club scores remained similar in *ANO7*-negative epithelium between low and high inflammation regions (II: Figure 2D, E). Basal cells scores indicated enrichment in the low inflammation *ANO7*-negative epithelium compared to other categories (II: Figure 2F). Immune cells (T-cells and myeloid) scores were lowest in *ANO7*-positive epithelium, then proportionally increased in *ANO7*-negative in low inflammation,

ANO7-positive in high inflammation, and were highest in *ANO7*-negative high inflammation epithelium (II: Figure 2G, H).

These results imply that immune cells are infiltrating the epithelium and that inflammation affects both *ANO7* expression and luminal cell identity in the epithelial cells. The epithelial cells react to inflammation by inducing transcriptional programs related to club cell identity. In a correlation analysis of *ANO7* expression and the non-standardised ssGSEA scores for cell types analysed in the epithelium, *ANO7* shows high correlation with luminal cells and high inverse correlation with club and immune cells (II: Figure 2N). The increased infiltration of immune cells was also seen in IF staining, where the CD45-positive cells were more abundant and infiltrating deeper into the epithelium, even into the lumen, in *ANO7*-negative glands (II: Figure 2O and Supplementary Figures 4A-H).

In stroma ssGSEA, fibroblast and smooth muscle scores were enriched in low inflammation regions and reduced in high inflammation regions (II: Figure 2I, J). In contrast, myeloid and T-cell scores showed enrichment of immune cells in high inflammation regions compared to low inflammation regions. Also, the immune cells' scores were significantly higher in samples adjacent to *ANO7*-negative epithelium in low infiltration regions; however, a similar difference was not seen in the high inflammation regions (II: Figure 2L, M). The abundance of immune cells in stroma surrounding the *ANO7*-negative epithelium was also confirmed with IF staining (II: Figure 2O and Supplementary Figures 4A-H). The unchanged endothelial cell scores indicate that vasculature remains similar in all of the analysed regions (II: Figure 2K).

These results imply that immune cell infiltration in the epithelium correlates with the abundance of immune cells in the stroma, and that immune cell infiltration has a significant impact on the epithelium, turning luminal cells into club cells.

5.3.2 CD56bright natural killer cells are enriched in benign *ANO7*-expressing epithelium

We assessed the enrichment of 28 different immune cell subtypes with ssGSEA using gene markers from a pan-cancer analysis of tumour-infiltrating immune cells (Charoentong et al., 2017). While other immune cell marker gene sets exist, for example in a prostate-specific study by Hirz et al. (2023), they do not capture the diversity of the immune cells similarly to the study by Charoentong et al (2017). The marker gene sets for 28 TILs were developed assessing gene expression in purified immune cells and 813 microarrays from 36 studies, as described in Bindea et al. (2013) and Angelova et al. (2015). We conducted the analysis in epithelium and stroma to detect whether immune cells are differentially distributed between the four groups: *ANO7*-positive and negative in low and high inflammation regions. In

general, the results show a similar distribution of immune cells, as seen in the T-cell and myeloid cell analysis (II: Supplementary Figure S7 and Figure 2G, H, L, M). However, we focused on immune cell types that showed differential distribution per *ANO7* status in the samples. Three immune cell types were associated with *ANO7*: CD56bright natural killer (NK) cells were enriched in *ANO7*-positive samples, whereas Th2 (Type 2 T helper cells) and central memory CD8 T-cells were enriched in *ANO7*-negative epithelium (II: Figure 5A, B, C). These enrichments were only seen in the epithelial compartment, while stroma samples did not show a statistically significant difference in the distribution of these three immune cells (II: Figure 5A, B, C).

To confirm the results, we calculated the correlation coefficients of the ssGSEA scores in all GeoMX DSP epithelial samples and analysed them in a hierarchically clustered similarity matrix. The ANO7-signature (II: Figure 4A) grouped with CD56bright NK cells and monocytes in the GeoMX DSP epithelial data (II: Figure 5D). We replicated the calculations in TCGA PRAD STN data, in which the ANO7-signature grouped with CD56bright NK cells, monocytes, activated CD8 T-cells, and CD56dim NK cells (II: Figure 5E). In hierarchical clustering of both data sets, DSP epithelium and TCGA PRAD STN, the nearest neighbour to the ANO7-signature was CD56bright NK cells (II: Figure 5D, E). Other immune cells, apart from CD56bright NK cells, do not show statistically significant correlations in both the TCGA STN and DSP epithelium data (II: Table 4). This makes CD56bright NK cells the only immune cell type analysed in this study that is associated with *ANO7* and the ANO7-signature in benign prostate glands.

5.3.3 5-ARI medication modulates prostate tissue, but does not affect *ANO7* expression in cell types

Two out of four of the patients, whose samples were used in the GeoMX DSP analysis, were taking 5-ARI medication prior to the surgery and collection of tissue samples. 5-ARI medication inhibits the enzyme responsible for the conversion of testosterone into DHT, which is a more potent activator of AR signalling compared to testosterone. In a study using samples from BPH tissue, 5-ARI medication was shown to coincide with luminal-to-club cell transition and to affect cellular morphology, marked by decreased acinus and lumen area, decreased cell height, increased acinus and lumen circularity, and increased cell layer thickness (more than two cells in layer) (Joseph et al., 2022). Furthermore, in that study, the luminal cells from 5-ARI patients had slightly reduced luminal cell markers (*MSMB*, *KLK3*, and *NKX3-1*) and elevated club cell-associated factors, including NF-κB target and anti-apoptotic scores, compared to the luminal cells in non-medicated patients.

In the GeoMX DSP UMAP plots (II: Supplementary Figure S3B, F), 5-ARI had an effect on the clustering of *ANO7*-positive and -negative samples in low inflammation regions, both in epithelial and stromal datasets. However, the expression levels of *ANO7* were similar between 5-ARI medicated and non-medicated patients in *ANO7*-positive and *ANO7*-negative epithelial samples (II: Supplementary Figure S3C, D). This implies that 5-ARI does not affect *ANO7* expression in luminal cells. Therefore, we did not use 5-ARI as a stratifying factor in later analysis since our focus was on the role of *ANO7*.

Furthermore, while Joseph *et al*. (2022) did not detect club cells in untreated patients, whilst in our data, both 5-ARI and untreated patients' tissue contained club cells. Inflammation, however, was detected in club cell-enriched regions in both patient groups in our data.

5.3.4 *ANO7* is associated with AR signalling and cellular processes related to lipid metabolism

We utilised GSEA to analyse the cellular pathways and processes related to *ANO7* using Hallmark gene sets (II: Figure 3D, E). A comparison of *ANO7*-positive and -negative epithelium in low inflammation regions revealed an enrichment of androgen response along with metabolic processes, mainly related to lipids, and spermatogenesis. A similar profile of terms was enriched in *ANO7*-positive epithelium in high inflammation regions. Bile acid metabolism, enriched in high inflammation, is closely related to cholesterol homeostasis, which was enriched in low inflammation. The enriched terms in *ANO7*-positive epithelium indicate that *ANO7* is associated with AR signalling and lipid metabolism, more precisely fatty acid and cholesterol metabolism. In addition, adipogenesis, xenobiotic metabolism, and heme metabolism were enriched in low inflammation regions only. Adipogenesis is related to lipid metabolism, while xenobiotic metabolism involves the processing of exogenous molecules, and heme metabolism involves mitochondrial and cytoplasmic enzymes as well as small molecule transporters.

The terms enriched in *ANO7*-negative regions highlight inflammation and related terms. TNFα signalling via NF-κB associates with club cells (Joseph et al., 2022). Terms including p53 pathway, UV response down, and apoptosis, which were enriched in low and high inflammation tissue regions (II: Figure 3D, E), implicate a response to DNA damage in cells and proliferation. These are characteristics of proliferative inflammatory atrophy, which is also associated with club cells (Huang et al., 2023).

Several of the inflammation-related terms that were enriched in *ANO7*-negative epithelium in low inflammation regions were not enriched in high inflammation. This suggests that *ANO7*-positive epithelium in high inflammation regions is

affected by inflammation, which is also reflected in the increased club cell score in these epithelial samples (II: Figure 2E).

5.3.5 *ANO7*-signature comprises genes that are co-expressed with *ANO7* in benign prostate epithelium

To analyse the cellular pathways and processes associated with *ANO7* in greater detail, we conducted a network analysis with DEGs upregulated in *ANO7*-positive (versus *ANO7*-negative) epithelium in low inflammation regions. To mitigate the variation per individual patients seen in the UMAP plots in *ANO7*-positive epithelium (II: Supplementary Figure S3 A), we calculated the DEGs for each patient separately, resulting in 277 upregulated genes. The genes with expression levels that correlate with *ANO7* ($r > 0.4$) in low inflammation *ANO7*-positive epithelium were assigned as the ANO7-signature (II: Figure 3A). The ANO7-signature represents genes that are co-expressed with *ANO7* in luminal cells of the epithelium with high specificity. The top *ANO7* co-expressing genes along with information about enriched expression across 17 different cancer types, are shown in Table 6.

To confirm the co-expression of the *ANO7*-signature genes, we calculated the correlation coefficient of ANO7-signature ssGSEA scores and *ANO7* expression in all the DSP epithelial samples, including *ANO7*-positive and negative samples from low and high inflammation regions, showing a very strong correlation ($r=0.93$). The correlation coefficient of *ANO7* and the ANO7-signature genes in TCGA PRAD STN was 0.90, which is in concordance with the result in the DSP epithelial data, thus validating the co-expression of the genes in the ANO7-signature (II: Table 1).

Next, we conducted a network analysis using the 277 upregulated genes in *ANO7*-positive epithelium as marker genes, separated into two clusters: cluster 1, the ANO7-signature; and cluster 2, the remaining 177 genes upregulated in *ANO7*-positive epithelium. The analysis was run using gene sets in GO, KEGG, and Reactome in the same analysis, to build a comprehensive representation of terms enriched for the marker genes. In the resulting network, 110 out of 277 genes were mapped into terms in which the marker genes are overrepresented compared to all the genes that were assayed (genes included in the WTA).

Table 6. Top *ANO7* correlating genes (r>0.7) in *ANO7*-signature.

GENE	DISCRIPTION	CC WITH *ANO7*	CANCER SPECIFICITY [1]
DCXR	Dicarbonyl and L-xylulose reductase	0.81	Liver, Prostate
PPM1H	Protein phosphatase, Mg2+/Mn2+ dependent 1H	0.81	-
SPDEF	SAM pointed domain containing ETS transcription factor	0.79	Breast, Prostate
PNPLA7	Patatin like phospholipase domain containing 7	0.77	Prostate
GREB1	Growth regulating estrogen receptor binding 1	0.77	Prostate
TPM3	Tropomyosin 3	0.76	-
LMAN1L	Lectin, mannose binding 1 like	0.76	Prostate
NCAPD3	Non-SMC condensin II complex subunit D3	0.75	Prostate
HMG20B	High mobility group 20B	0.74	-
ACAD8	Acyl-CoA dehydrogenase family member 8	0.73	-
POTEG	POTE ankyrin domain family member G	0.72	-
NTNG2	Netrin G2	0.72	Glioblastoma
ZBTB16	Zinc finger and BTB domain containing 16	0.71	Prostate
FASN	Fatty acid synthase	0.71	-
CENPX	Centromere protein X	0.71	-
NRBP2	Nuclear receptor binding protein 2	0.70	-
PASK	PAS domain containing serine/threonine kinase	0.70	-
GLB1L3	Galactosidase beta 1 like 3	0.70	Lung, Prostate

[1] Annotated in the HPA as exhibiting enriched expression across 17 different cancer types, based on RNA-seq data from TCGA.
CC: correlation coefficient.

The analysis resulted in 65 individual terms, which are further grouped into 23 groups. The grouping is based on similarity per shared genes between the terms by Cohen's kappa score over 0.4, and the groups are named after the term with the highest significance within the group. This makes the interpretation easier as the grouping reduces redundancy in the resulting individual terms and shows which terms represent similar cellular processes and their relationship at the gene level.

The full network of enriched terms and their associated genes is shown in II: Supplementary Figure S5, and all terms are listed in II: Supplementary File S5. A large proportion of the groups are related to metabolism, including fatty acid derivative biosynthetic process, arginine and proline metabolism, alanine, aspartate, and glutamate metabolism, PPAR signalling pathway, and arachidonic acid metabolism. The AR regulation is highlighted in terms such as PKN1 in a complex with AR positively regulating the expression of KLK2 and KLK3 and prostate gland development. The rest of the groups include response to stimuli and signalling

(cellular response to oxygen levels, response to fatty acid, and interleukin-12 signalling), trafficking-related groups (regulated exocytosis, monoamine transport, retrograde transport at the trans-Golgi network, inorganic cation import across the plasma membrane), molecular processes (ferric-chelate reductase [NADPH] activity, protein-disulphide reductase activity, metallocarboxypeptidase activity, insulin processing), and other processes (glandular epithelial cell development, vacuolar acidification, plasma lipoprotein particle organisation). This network provides a landscape of pathways enriched in *ANO7*-positive luminal epithelial cells. Genes with interactions with more than two groups within the network are listed in Table 7, representing hub genes involved in several cellular processes.

The terms containing ANO7-signature genes were extracted from the network and partitioned based on the Kappa scores (II: Figure 4B). The terms that were enriched for ANO7-signature genes (>50% of the associated genes) are arachidonic acid metabolism, prostate gland development, activated PKN1-stimulated transcription of AR (androgen receptor) regulated genes KLK2 and KLK3, PKN1 in complex with AR positively regulated expression of KLK2 and KLK3, glandular epithelial cell development, and monoamine transport. AR signalling relates to the two terms containing AR regulation in addition to the *AR* and *NKX3-1*-linked term prostate gland development (II: Supplementary Figure S5). The term glandular epithelial cell development is linked to SREBP-regulated metabolism via *FASN* (II: Supplementary Figure S5). The term-groups SREBP-regulated metabolism, lipid and amino acid metabolism, and arachidonic acid metabolism form a larger entity (II: Figure 4B). This subnetwork represents processes that are linked with AR regulation via *SREBF1* and serve an important role in prostate cancer progression. The term monoamine transport is linked with alanine, aspartate, and glutamate metabolism via *ABAT* (4-aminobutyrate aminotransferase); however, this term represents hormonal signalling of monoamine neurotransmitters and is the only term enriched for ANO7-signature genes that is not related to AR signalling or lipid metabolism.

Table 7. Hub genes in network analysis of DEGs upregulated in *ANO7*-positive luminal epithelial cells.

GENE	DESCRIPTION	GROUP INTER-SECTIONS	CLUSTER
P4HB	Prolyl 4-hydroxylase subunit beta	6	2
FASN	Fatty acid synthase	4	1, *ANO7*-signature
ACSL3	Acyl-CoA synthetase long chain family member 3	4	2
HMGCS2	3-hydroxy-3-methylglutaryl-CoA synthase 2	4	2
LCP1	Lymphocyte cytosolic protein 1	4	2
SCD	Stearoyl-CoA desaturase	4	2
ACADL	Acyl-CoA dehydrogenase long chain	3	1, *ANO7*-signature
ALOX15B	Arachidonate 15-lipoxygenase type B	3	1, *ANO7*-signature
ARG2	Arginase 2	3	1, *ANO7*-signature
EPHX2	Epoxide hydrolase 2	3	1, *ANO7*-signature
PICK1	Protein interacting with PRKCA 1	3	1, *ANO7*-signature
ALDH4A1	Aldehyde dehydrogenase 4 family member A1	3	2
ARF1	ADP ribosylation factor 1	3	2
FOLH1	Folate hydrolase 1	3	2
FURIN	Furin, paired basic amino acid cleaving enzyme	3	2
GGT1	Gamma-glutamyltransferase 1	3	2
GGTLC1	Gamma-glutamyltransferase light chain 1	3	2
GGTLC2	Gamma-glutamyltransferase light chain 2	3	2
HDLBP	High density lipoprotein binding protein	3	2
LDLR	Low density lipoprotein receptor	3	2
SREBF1	Sterol regulatory element binding transcription factor 1	3	2
STEAP2	STEAP2 metalloreductase	3	2

5.3.6 *ANO7*-signature shows clinical significance

Next, we tested whether the ANO7-signature has clinical relevance in the TCGA PRAD data. The patients were divided into high and low groups based on the z-scores of ANO7-signature ssGSEA scores analysed from gene expression data, with zero as cut-off for division. We then tested for differences in clinical parameters in high versus low ANO7-signature score groups. The selected clinical parameters were age at initial pathological diagnosis, Gleason score, pathological T (describes the

size and invasion of the primary tumour) and N (describes whether cancer cells are present in sentinel lymph nodes) classification, and primary therapy outcome success. The primary therapy outcome success (either chemotherapy or radiation therapy) is divided into four classes: complete remission/response (no evidence of cancer), partial remission/response (reduction of tumour size), stable disease (the tumour size remains about the same), and progressive disease (increasing tumour size). These parameters describe the nature of the disease, and the purpose of the analysis was to evaluate how the expression of the ANO7-signature genes might affect the tumour characteristics.

The results show that the patients belonging to the high signature group at the time of diagnosis were one year younger, had lower Gleason scores, pathologic T and N classifications, and better responses to primary therapy (II: Table 3). These results indicate that the genes identified as the ANO7-signature, as well as the processes they contribute to in benign tissue, are also relevant in cancer progression. More specifically, these genes are expressed more in cases that are possibly less malignant.

5.3.7 *ANO7* in cancer

As the expression of ANO7 has been shown to be reduced during cancer progression at the protein level (Marx et al., 2021) as well as at the RNA level (Sinnott et al., 2017; Figiel et al., 2023), we investigated which pathways are associated with *ANO7* in the TCGA PRAD data, including STN and primary tumour samples. The correlation of *ANO7* expression and the ANO7-signature decreases with increasing Gleason score (II: Table 1), implying that the association between *ANO7* and the processes it is related to in benign tissue becomes impaired in high-grade cancer due to decreased *ANO7* expression (II: Supplementary Figure S6).

We then calculated the genes co-expressed with *ANO7* in STN and Gleason scores 6, 7, 8, and 9-10 combined, and analysed pathways enriched for the co-expression signatures in each of the sample groups. The results show that androgen response is associated with *ANO7* expression only in STN and Gleason 6, while all of the lipid metabolism-related pathways, such as cholesterol biosynthesis and sterol biosynthesis, are enriched with genes co-expressed with *ANO7* in normal samples but not in primary tumour samples (II: Table 2). The primary tumour groups showed enrichment of some metabolism-related pathways, such as bile acid metabolism in Gleason 8 and butanoate metabolism in Gleason 9-10. Overall, the association with metabolism-related pathways is not evident in primary tumour samples, which is concordant with decreased levels of *ANO7*.

6 Discussion

6.1 Finding a suitable setting for studying *ANO7*

Initially, we sought to study the function of ANO7 using cell lines. Cell lines are derived from human tissue and are usually derived from metastatic tumours, such as the ones used in these studies. A few prostate-derived benign cell lines also exist, including a cell line representing benign prostate hyperplasia (Hayward et al., 1995), and histologically normal epithelium-derived cells RWPE-1 (Bello et al., 1997). However, none of these cell lines express *ANO7* mRNA at levels similar to those seen in normal prostate tissue. In fact, the cell lines in the Cancer Cell Line Encyclopedia show that *ANO7* expression is low in all included cell lines ($n > 1000$), and several cell lines derived from other organs, such as breast and lung, show higher expression of *ANO7* compared to prostatic cell lines. The highest expression of *ANO7* among all prostatic cell lines is seen in MDA PCa 2b (Ghandi et al., 2019). The Western blot analysis of the MDA PCa 2b cells, including samples from shRNA-treated cells and nontreated controls, confirm that the cell lines do not express protein at a detectable level. However, what we did notice in the shRNA experiments was the nuclear accumulation of the transcripts.

The decrease of cytoplasmic transcripts in shANO7-1 and shANO7-3, as compared to their corresponding controls, indicates that the shRNA silencing did have a minor effect on the residual *ANO7* transcripts that the cells contain. The shRNA knockdown is based on RNA interference (RNAi). The genome-integrated shRNA is transcribed in the nucleus, then transported into the cytoplasm where it is processed into microRNA, which is loaded into an RNAi effector complex (RISC). The RISC is localised in the cytoplasm, where it targets the mRNA complementary to the microRNA for degradation (Siolas et al., 2005). Therefore, the nuclear mRNA is not affected, and the reduction of target mRNA is seen in the cytoplasm, as we observed. Despite this, the total amount of *ANO7* mRNA expressed by the cell lines is not enough to produce detectable levels of endogenous protein, and therefore it was not feasible to continue with the work with shRNA cell lines. From here, we moved on to investigate the expression in tissue samples in which *ANO7* is actually expressed.

6.2 *ANO7* expression in human tissues

The RNA-FISH experiment demonstrated that *ANO7* mRNA expressing cells are abundantly detected in prostate tissue. More specifically, *ANO7* mRNA was observed in the luminal cell layer, in contrast to basal epithelial cells. It has been previously reported that *ANO7* is expressed in basal and "terminal" epithelial cells in prostate tissue – terminal here likely refers to the luminal cell layer (Bera et al., 2004). The presence of expression in basal cells is contradictory to the observation that we made in the tissue, where the *ANO7* signal was from luminal cell layer and a very strong signal was observed in the nuclei of the luminal cells.

Databases containing bulk RNA-seq and scRNA-seq data of healthy human tissues show that although *ANO7* is enriched in the prostate at the tissue level, other organs also contain cells that express *ANO7* at similar levels to the prostate glandular epithelial cells (Appendices 1, 2). The other organs where *ANO7* is expressed are mainly part of the gastrointestinal tract, and the cell types are mucus-secreting goblet cell and gastric mucus-secreting cell. The intestinal tract digests and absorbs nutrients, and goblet cells produce a mucus barrier that separates the intestinal epithelial layer from the intestinal content, including bacteria and other micro-organisms. Goblet cell differentiation is mediated by transcription factors such as *ATOH1*, *GFI1*, and *SPDEF*. Mucus is primarily composed of mucin, which is secreted by a mechanism involving core components mucin 2 (MUC2), Fcγ binding protein, and calcium-activated chloride channel regulator 1 (Gustafsson and Johansson, 2022). Interestingly, *SPDEF* is one of the top genes co-expressed with *ANO7* in prostate luminal epithelial cells. Furthermore, the intestinal goblet cells and prostatic luminal epithelial cells share a similar functional property as epithelial secretory cells, thus they may share a transcriptional feature that induces *ANO7* expression in both cell types, such as regulation via *SPDEF*. In prostate cancer, *SPDEF* promotes luminal differentiation and associates with better outcome (Wang et al., 2018).

Human prostate tissue samples are typically obtained from patients during medical procedures, often rendering it challenging to ascertain whether the cells reflect a healthy state or are influenced by disease. The study by Henry et al. (2018), however, utilised tissue from organ donors aged 18–31, providing a representation of fully mature prostatic tissue without the pathological changes that typically develop with age. In that paper, the authors report gene markers enriched in prostatic cell types assessed by fluorescent-activated cell sorting (FACS) and scRNA-sequencing. *ANO7* was found to be specific for luminal epithelial cells only in FACS but not in scRNA-seq results. The same group later studied the effects of 5-ARI in BPH patients, and *ANO7* was found among the top differentially expressed genes in luminal cells compared to club cells in a GeoMX analysis, while in the Visium platform the difference was less evident (Joseph et al., 2022). *ANO7* has not been

reported to be specific to luminal cells in scRNA-seq analyses in the literature. This may indicate that *ANO7* is highly expressed in a specific subset of luminal cells in the prostate, and in scRNA-seq the expression is not strongly correlated with the canonical luminal markers, such as *KLK3*, *MSMB*, and *ACP3*. The results in study II indeed shows high variation in the expression level of *ANO7* in *ANO7*-positive epithelium.

6.2.1 Nuclear retention of *ANO7* transcripts is mediated by intronic SINEs

The nuclear enrichment of *ANO7* transcripts is likely caused by the retained introns seen in bulk RNA-seq (Wahlström et al., 2022). The introns are removed, or spliced, from the pre-mRNA by spliceosomes. For effective intron splicing, the splice site must match the consensus motif, and weakly defined splice sites (disparity from the consensus motifs) cause less efficient splicing and intron retention (De Conti, Baralle and Buratti, 2013). Weak definition of some of the exon-intron junctions (*i.e.* splice sites) in *ANO7* likely explains the retained introns seen in RNA-seq (Wahlström et al., 2022).

The retained introns 3, 4, and 19 in *ANO7* contain short interspersed nuclear elements (SINEs), as assessed from the RepeatMasker track in the UCSC Genome Browser (https://genome.ucsc.edu/index.html, last accessed 29/01/2025). These elements are recognised by nuclear proteins that mediate nuclear retention, for example in *MALAT1* (Nguyen et al., 2020). SINEs, and specifically Alu elements (a subcategory of SINE), are abundant in primate genomes and have a significant impact on gene expression in various ways (Deininger, 2011). While the SINEs in *ANO7* retained introns are most likely causing the nuclear retention of the transcripts, the exact mechanism remains to be elucidated. However, as the cytoplasmic:nuclear ratio of *ANO7* transcripts is similar in benign glands, low-grade cancer, and high-grade cancer as shown in Study I, it indicates that changes in intron retention are likely not the cause of decreased protein expression in high-grade prostate cancer.

6.2.2 *ANO7* is expressed in luminal cell and is counteracted by inflammation associated with club cells

To study the differences between the closely residing epithelial regions with strong differences in *ANO7* expression, we conducted spatial transcriptomic profiling. We did not analyse cancerous tissue, since the expression of *ANO7* is usually high in low-grade cancer and gradually decreases during cancer progression. Thus, analysing varying levels of *ANO7* in cancer is likely to reveal changes in cancer progression in general rather than genes and processes related to *ANO7*. Therefore,

we assessed only benign glands. Additionally, some samples were collected from glandular structures containing regions that were positive or negative for *ANO7* within the same gland. These epithelial regions should exhibit minimal biological variation aside from what is related to ANO7. Nevertheless, these samples showed similar differentiation in *ANO7*-positive versus negative comparisons as those collected from separate glands.

At the time when this study was initiated, a few options were available for spatial transcriptomics, including the Visium platform (10X Genomics, Pleasanton, CA, USA), sequencing of laser capture microdissected samples, and the GeoMX platform. Visium is widely used in research and allows for the coverage of large tissue sections. However, Visium assays do not allow for single cell resolution in the investigated portion of tissue, which is an issue for studying *ANO7* as the tissue regions expressing *ANO7* are easily mixed within the Visium collection spots. Two options remained: laser capture microdissection and GeoMX. We tested laser capture microdissection, but the small regions in the epithelium did not yield enough RNA for sequencing. Therefore, GeoMX was an obvious choice for its capability of manually selecting the regions within the tissue to be collected for analysis.

In the analysed epithelial regions, the *ANO7*-positive epithelium was highly enriched for luminal cells, as shown in the ssGSEA results. The luminal features were confirmed with high expression of luminal marker genes and enrichment of luminal cell-associated pathways. Therefore, it is evident that the analysed *ANO7*-positive regions represent the prostatic fluid-secreting epithelial cells.

In contrast, the *ANO7*-negative regions were enriched for club cells and immune cells. Previously, it has been shown that the prostatic epithelium assumes a club cell identity as a consequence of DHT depletion (Joseph et al., 2022) and inflammation in PIA (Huang et al., 2023). The *ANO7*-negative epithelium exhibits several features of PIA, including epithelium-infiltrating lymphocytes, proliferation, and DNA damage (De Marzo et al., 1999). The most prominent inflammation-related pathway differentiating *ANO7*-negative epithelium from the *ANO7*-positive epithelium was TNFα signalling via NF-κB, which is in interplay with AR signalling (Malinen et al., 2017) and may be responsible for the reduction of *ANO7* expression in benign epithelium. The abundance of Th2 and central memory CD8 T-cells showed a negative correlation with *ANO7* in epithelium in spatial profiling. Th2 cells facilitate protective type 2 immune responses and are established in chronic inflammatory diseases like asthma and allergy (Walker and McKenzie, 2018). However, AR signalling inhibits group 2 innate lymphoid cells, including Th2 cells (Laffont et al., 2017), and the negative correlation of these cells with *ANO7*-positive epithelium may be explained by the strong AR signalling in these epithelial regions. Central memory CD8 T-cells, acting in protection against pathogens, are usually found recirculating in lymph nodes and possess high capacity of producing effector CD8

T-cells (Parga-Vidal and Gisbergen, 2020). It is unclear why the Th2 and central memory CD8 T-cells would be enriched in *ANO7*-negative epithelium, however, both cell types are related to prolonged inflammatory responses (Walker and McKenzie, 2018; Parga-Vidal and Gisbergen, 2020). Therefore, the enrichment of Th2 and central memory CD8 T-cells may just be another indication of chronic inflammation in PIA.

The stroma was mainly differentiating by the varying levels of immune cells while no other major differences were detected that would correspond to the epithelial *ANO7* status. This emphasises the effect of immune cell infiltration, especially in the epithelium, influencing *ANO7* expression and epithelial cell type identity.

When the 5-ARI treated patients were compared with untreated patients, the expression of *ANO7* was similar in *ANO7*-positive epithelium, suggesting that 5-ARI does not affect *ANO7* expression in luminal cells. Therefore, we did not investigate further the differences between these two patient groups, although the 5-ARI status seemed to affect the sample distribution in UMAP. Previously, it was shown that 5-ARI medication induced club cell adaptation in a study conducted with samples derived from simple prostatectomy of BPH patients (Joseph et al., 2022). In our data, the *ANO7*-positive epithelium in high inflammation regions exhibits intermediate luminal cell scores and high club cell scores, and these samples were derived from a patient who was not on 5-ARI medication prior to the surgery and sample collection. These samples may represent epithelial cells that are undergoing luminal-to-club cell transition, which was only seen in the 5-ARI treated patients in BPH (Joseph et al., 2022). Therefore, it is possible that inflammation is the main driver of club cell transformation, while 5-ARI medication could render the luminal cells more prone to the transformation. This is due to DHT depletion resulting in less active AR signalling, as the AR and NF-κB share transcription factors (Malinen et al., 2017) and without DHT, NF-κB may become induced by lighter stimuli in luminal cells under 5-ARI medication. However, this hypothesis is based on a small number of samples and requires further testing before it could be considered valid.

6.3 The functional landscape of *ANO7*

The *ANO7*-signature was identified in *ANO7*-positive luminal cells in low inflammation regions to delimit the effect of inflammation (in high inflammation regions). The network analysis conducted with the DEGs upregulated in *ANO7*-positive epithelium provides an overall representation of the processes and pathways that are enriched in these epithelial regions and how they are interconnected. The processes containing or enriched with *ANO7*-signature genes are the ones that are of specific interest within the whole network.

AR signalling is highlighted in the network and in processes enriched for *ANO7*, which suggests that AR regulates the expression of *ANO7*. However, *ANO7* is not directly regulated by AR since *ANO7* has not been identified as an AR target. Therefore, the induction of *ANO7* expression must be indirect in the luminal cell harbouring strong AR signalling. AR plays a significant role in metabolism, which is studied extensively in prostate cancer. AR signalling governs the production and/or intake of fatty acids, cholesterol, and amino acids in concert with other signalling, including the PI3K/AKT pathway (Ahmad, Cherukuri and Choyke, 2021). The network analysis highlighted several of the SREBP-regulated processes (via *SREBF1*), suggesting that *ANO7* is related to fatty acid metabolism in particular. These analyses give a context for the role of *ANO7* in cellular processes; however, without knowing the mechanism of action of the ANO7 protein, it is difficult to evaluate whether ANO7 would enhance or inhibit the metabolic processes that it is related to at the gene expression level.

Our group has studied the effect of ANO7 in an overexpression cell line model in the benign prostate-derived RWPE-1 cells (Löf et al., 2025). These results suggest that ANO7 affects the cell by disrupting mitochondrial function, downregulating fatty acid metabolism genes, and altering the cellular lipid composition, as well as causing cells to utilise glycolysis rather than mitochondrial respiration (oxidative phosphorylation). The mechanism of action, however, is not yet revealed. Nevertheless, these results indicate that ANO7 is in fact inhibiting the fatty acid metabolism regulated by the AR and PI3K/AKT signalling, where mTOR is an important mediator. The tumour-suppressor role of ANO7 related to PI3K/AKT signalling is further supported by the study showing that the prognostic effect of strong ANO7 protein expression remains when comparing biochemical recurrence events in patients that had normal or deleted *PTEN* (Marx et al., 2021).

ANO7 may also take part in other cellular processes besides regulating metabolism. As mentioned before, *SPDEF*, which is included in the ANO7-signature, regulates goblet cell differentiation in the colon (Gustafsson and Johansson, 2022). Interestingly, *ANO7* has been linked with *MUC2* expression and mucin biosynthesis in colon adenocarcinoma (COAD), while the lower expression of both *ANO7* and *MUC2* is prognostic for poor survival in COAD (Chen, Aluksanasuwan and Somsuan, 2023). This suggests that *ANO7* plays a role in other organs besides the prostate, and the function could be related to the secretory pathway in intestinal cells.

The potential diverse roles of ANO7, and other anoctamins, resemble the characterisation of a “moonlighting protein”, which are proteins that convey more than one function, while some of the functions are context dependent. For example, GAPDH serves a role in glycolysis, while in cancer it also promotes survival and proliferation by interacting with AKT (Singh and Bhalla, 2020). Another example is

dicarbonyl/L-xylulose reductase (*DCXR*), which was the top *ANO7* coexpressing gene in Study II. DCXR serves a multifunctional role, for example in metabolism, cell adhesion, and regulating cell division in a context-dependent manner (Ebert, Kisiela and Maser, 2015). The hypothesised roles for ANO7 in vesicle trafficking, cell adhesion (Guo et al., 2021), and the role in regulation of lipid metabolism hypothesised by our group somewhat match the multifaceted roles of a moonlighting protein. However, patients that are heterozygous for the loss-of-protein causing SNP in *ANO7* have morphologically normal prostates and are not diagnosed with prostate cancer at a young age, suggesting that ANO7 protein is not essential for normal prostate development or cancer initiation (Wahlström et al., 2022). Therefore, it may be possible that the ANO7 protein, functioning as a membrane-bound calcium-activated ion channel and/or lipid scramblase, becomes relevant only in certain pathophysiological conditions and under specific transcriptional programs, such as those in low-grade prostate cancer, for instance.

6.3.1 The association of *ANO7* with NK cells

The CD56bright NK cells are a subset of NK cells that represent an early phase in NK cell maturation, which later adapts a highly cytotoxic phenotype, CD56dim NK cell (Netskar et al., 2024). CD56bright NK cells function in immunoregulation of innate immunity together with monocytes and produce several cytokines, most importantly INF-γ, to activate further immune responses (Cooper et al., 2001).

The ANO7-signature genes correlate with the CD56bright NK cells in prostatic tissues not only locally, but at the tissue level in general, as the connection was also seen in bulk RNA-seq data. This may imply that *ANO7*-positive epithelium is relatively clear of inflammatory agents compared to the surrounding *ANO7*-negative epithelium, while the CD56bright NK cell enrichment is related to the normal immunosurveillance task of these cells. The processes related to the ANO7-signature may, however, modulate the immune landscape of the benign prostatic epithelium. Arachidonic acid metabolism, which was highlighted in the network analysis as being associated with the ANO7-signature, is linked with enhanced tumour-promoting auto- and paracrine signalling (Wang et al., 2021) and infiltration of NK cells resulting from aberrant mTORC2 signalling in *PIK3CA*-mutated breast cancer (Koundouros et al., 2020). Furthermore, in primary prostate cancer, increased NK cell infiltration is shown to correlate with better disease outcomes, while reduced infiltration correlates with mutations in *PTEN*, *RB1*, and *TP53* (Zorko et al., 2025). These implications may provide useful insights into how *ANO7* may contribute to the modulation of the immune landscape in benign epithelium and cancer, possibly via the effect of *ANO7* on fatty acid derivative metabolism, such as arachidonic acid metabolism.

6.4 Possible implications in disease

As mentioned, *ANO7* probably is not an essential factor for normal prostate development as the patients carrying the loss-of-protein affecting SNP develop normal prostates (Wahlström et al., 2022). In prostate cancer, lipid metabolism is enhanced resulting from an aberrant TCA cycle and induction of lipid synthesis by AR and PI3K/AKT signalling via SREBP (Audet-Walsh et al., 2018), and is promoted by the mutations occurring early in prostate cancer development, such as *PTEN* deletion and *MYC* amplification (Cotter and Rubin, 2022). Enhanced lipid metabolism then promotes the progression of prostate cancer (Zadra et al., 2019). It is possible that ANO7 has a protective effect in this context, where it disrupts mitochondrial function (Löf et al., 2025) in cells whose energy demand is high during continuous growth mediated by the enhanced mitogenic signalling. The limited energy resources resulting from inefficient mitochondrial function activate the cell's energy-sensing mechanisms, which turn the cell into survival mode and to utilise catabolic metabolism instead of the growth-related anabolic metabolism (Sung, Yu and Han, 2023).

The observed reduction in ANO7 expression during primary tumour progression (Marx et al., 2021) coupled with its absence in prostate cancer metastases (Chandran et al., 2007) provides further evidence of its putative protective function. The downregulation could be due to epigenetic regulation of the gene, or alternatively for example transdifferentation (cells assimilate a different cell lineage identity), which are observed in prostate cancer (Hanahan, 2022; Davies et al., 2023).

Lactate may be an important metabolite mediating the effect of ANO7 in prostate cancer cells. Our group’s results suggest that ANO7 causes the cells to favour glycolytic metabolism and ANO7 exerts a similar effect in the cells as inhibition of the mitochondrial pyruvate carrier MPC (Löf et al., 2025). This could cause an accumulation of lactate, which has been shown to affect the cell by inhibiting luminal cell differentiation and enhancing basal cell differentiation (Giafaglione et al., 2023).

The loss-of-protein SNP rs77559646 carrying patients were shown to have a better response to docetaxel given as a first-line treatment to castration-resistant metastatic prostate cancer patients (Kaikkonen et al., 2019). The mode of action of docetaxel is based on binding to microtubules leading to impaired cell cycle and activation of apoptosis (Rizzo, 2021). This is achieved by inhibiting several signalling pathways, such as the EGFR pathway (Herbst and Khuri, 2003) and inhibiting the translocation of AR into the nucleus (Rizzo, 2021). The docetaxel resistance mechanisms include prosurvival gene activation, autophagy, epithelial-mesenchymal transition, and more (Rizzo, 2021). Therefore, whilst the protective effect of ANO7 may partly overlap with the cytotoxic mechanisms of docetaxel, the lack of ANO7 in prostate cancer cells may render the cell to become more dependent on the docetaxel-targeting mechanisms during cancer progression, thus being more

sensitive to docetaxel treatment. This may explain the higher sensitivity of rs77559646 carrying cases to docetaxel.

The clinical significance of the ANO7-signature is interesting as higher expression of these genes correlate with lower grade prostate cancer cases and better treatment outcome. While AR signalling and arachidonic acid metabolism, both which were highlighted in ANO7-signaure, are shown to enhance prostate cancer progression (Yang et al., 2012; He et al., 2022), it is counterintuitive that the signature correlates with better clinical parameters. *ANO7* likely conveys its beneficial effect on the clinical parameters, however, most probably there are other players contributing to the result as well. Many of the genes that are highly co-expressed with *ANO7* in luminal epithelial cells, such as *DCXR*, *PNPLA7*, *GREB1*, *LMAN1L*, and *NCAPD3*, are also enriched in prostate cancer as compared to other cancers and no cellular processes related to these genes were enriched in the network analysis. *DCXR* has been implicated in breast cancer, promoting glycolysis and cancer growth (Jin et al., 2023). *PNPLA7* has been shown to contribute to phosphatidylcholine catabolism to supply choline for the methionine cycle and it affects gene expression via histone methylation in the liver (Hirabayashi et al., 2023). *NCAPD3* is suggested to contribute to prostate cancer progression via AR interaction (Jing et al., 2022b), while it promotes glycolysis via *MYC* and *E2F1* in colorectal cancer (Jing et al., 2022a). *GREB1* is shown to regulate the PI3K/AKT pathway in breast cancer (Haines et al., 2020). *LMAN1L* is suggested to affect glycosylation and influence the progression of triple-negative breast cancer (Yu et al., 2025). Studying the *ANO7* co-expressing genes in relation to *ANO7* in prostate cancer may provide further insight into cellular mechanisms underlying prostate cancer development.

6.5 *ANO7* as a prognostic marker in prostate cancer

The inverse correlation of *ANO7* mRNA and protein with higher grade tumour and worse clinical outcomes has been shown in many studies (Mohsenzadegan et al., 2013; 2015; Sinnott et al., 2017; Marx et al., 2021; Figiel et al., 2023). Furthermore, several SNPs in *ANO7* correlate with the risk of prostate cancer (Kaikkonen et al., 2018; Conti et al., 2021; Chen et al., 2023), and the accumulation of predictably protein-affecting germline variants is associated with early-onset disease (Jiang et al., 2024). If further biochemical studies confirm the role of *ANO7* in prostate cancer progression, the expression level or the protein-disrupting SNP can be utilised in prognostication of localised prostate cancer at risk for developing into aggressive prostate cancer. It should be noted that the protein-affecting SNPs in *ANO7*, such as rs77559646, will likely influence the mRNA-based prognostication tools, for example the Decipher gene panel, which includes *ANO7* and 21 other genes (Erho

et al., 2013). In the case of rs77559646, the SNP also increases the mRNA expression in carriers versus non-carriers (Kaikkonen et al., 2018). Given that higher *ANO7* expression is used as a prognostic factor for lower risk, the prognostic power likely suffers in patients carrying protein-altering germline SNPs. Therefore, each germline SNP and its effect on the ANO7 protein should be evaluated, and if the SNP is found to disrupt the function of the protein, the germline SNPs could be used to predict aggressiveness in prostate cancer.

6.6 Limitations of the study

A major limitation in studying the function of *ANO7 in vitro* is the specificity of the ANO7 antibodies and the low expression of endogenous protein in the cell lines considered in this study. However, the endogenous mRNA could be studied in prostate cancer cell lines due to the high sensitivity of mRNA measurement methods, such as ddPCR. We were able to measure *ANO7* transcripts in cell lines, but the measurements were not consistent compared to control genes. This inconsistency may be due to the very low mRNA expression, where small differences in absolute expression can cause large relative changes between biological replicate samples or in treatment comparisons. However, this does not affect the comparison of mRNA in cell fractions isolated from the same batches of cells, which was utilised in validating the nuclear enrichment of *ANO7* transcripts.

The material used for the RNA-FISH experiment came from different sources and might have been handled differently prior assaying, especially during tissue fixation. Also, the material had been archived for a period of several years. These factors most likely had an effect on signal intensities; thus, we did not quantify the number of transcripts for comparison of mRNA amount between samples. However, it was evident that the number of *ANO7* transcripts is reduced in high-grade cancer compared to low-grade and benign epithelium, aligning with the protein staining and published data.

The main limitation in the results of spatial profiling is that differential gene expression profiles only indicate associations, not causality. These results need to be further studied in biochemical assays to provide a more precise understanding of the causal relationships between *ANO7* and the genes and processes revealed in the present study. Another limitation of this study is that the epithelial samples contained both luminal/club cells and basal cells, as all epithelial cells express cytokeratin markers used as morphology markers in sample collection. This may have caused a bias in the data, as basal cells were enriched in *ANO7*-negative samples in low inflammation regions. However, this also provides additional information regarding cell distribution in epithelial regions enriched for luminal or club cells. Moreover, it may increase the specificity of the ANO7-signature identified in luminal cells, as

ANO7-negative regions were enriched for both club and basal cells compared to *ANO7*-positive epithelium.

A concern with any antibody or probe-based assays conducted in prostate tissue is that the prostate epithelium seems to contain deposits of unknown material, usually located basolaterally in the luminal cell layer. These deposits can cause nonspecific signals, which can be identified by assessing the positive and negative controls used in the experiment. However, some epithelial regions may need to be excluded entirely, which could bias the results if deposit-enriched regions are not analysed.

6.7 Future prospects

Recent studies, including those by our group and others, have shed light on the potential function of *ANO7* in the prostate and in prostate cancer, with several lines of evidence suggesting a potential tumour-suppressor role. Nonetheless, further research is warranted to determine precisely how ANO7 mediates metabolic inhibition, particularly through its calcium-activated ion channel or lipid scramblase functions. Clarifying these mechanisms will be crucial to fully establish *ANO7*'s role in prostate cancer progression.

Diagnostics leveraging *ANO7*-based biomarkers may refine patient selection for treatment intensification or, conversely, identify individuals who require less intensive treatment, thereby potentially improving long-term survival and quality of life. Although further clinical validation is required, the expanding body of evidence supports incorporating *ANO7* into biomarker panels to enhance prognostication and guide personalised treatment strategies for patients with prostate cancer. The prognostic effect may be especially important for cases with driver genetic alteration, such as those in *PTEN* or *MYC*; however, these or other conditions that may influence the protective role of ANO7 require further investigations.

Beyond its prognostic utility, *ANO7* may help identify patients who could benefit from specific chemotherapeutic agents, such as docetaxel. Furthermore, the metabolic regulation mediated by *ANO7* may modulate the effects of metabolism-targeting therapies, including statins and metformin, in prostate cancer.

7 Summary

Prostate cancer poses a significant burden to healthcare systems globally. While the majority of prostate cancer cases are indolent and not life-threatening, a subset progresses into an aggressive and lethal form. Further research is necessary for better understanding of the mechanisms underlying this rapid progression. ANO7 has been implicated in prostate cancer risk and disease progression. The findings presented in this thesis contribute to the knowledge of ANO7's role in prostate cancer. *ANO7* was found to be associated with androgen receptor regulated lipid metabolism and may exert a protective effect by inhibiting lipid metabolism, a key driver of prostate cancer growth. Several protein-altering germline variants residing in *ANO7* are linked to prostate cancer and faster progression. An understanding of the precise mechanisms through which ANO7 influences cancer growth is still needed for its potential development as a prognostic biomarker in prostate cancer treatment strategies.

Acknowledgements

This work was carried out at the Department of Medical Biochemistry and Genetics, Institute of Biomedicine, Faculty of Medicine, University of Turku. I extend my gratitude to the Institute Director, Professor Sari Mäkelä for providing the excellent facilities to conduct research.

I wholeheartedly thank my supervisors, Professor Johanna Schleutker and Dr. Gudrun Wahlström. Johanna, thank you for providing excellent prerequisites for my research and trusting me to explore ideas and solve problems independently. Through your guidance, I have learned to approach scientific challenges with confidence and creativity, and you have taught me to be ambitious and bold in my work. Gudrun, thank you for your collaborative support and for teaching me patience, critical observation of results without bias, thoughtful consideration before drawing conclusions, and meticulous attention to detail—all crucial elements for conducting rigorous research.

I am grateful to my steering committee members, Professor Klaus Elenius and Docent Otto Ettala, for their valuable comments and encouragement throughout this journey. Special thanks to Otto for introducing me to the clinical aspects of prostate cancer, demonstrating genuine interest in basic science, and offering consistent support.

I thank Docent Tuomas Mirtti and Dr. Alfonso Urbanucci for dedicating time to carefully review my thesis, providing insightful comments, and engaging in stimulating discussion during the review process. Learning from experts like you has been both a privilege and a pleasure. I wish to express my sincere gratitude to Professor Emeritus G. Steven Bova for accepting the invitation to serve as the esteemed opponent in my public defence. It is truly an honour to have you participate in this culmination of my work.

I wish to acknowledge the Turku Doctoral Programme of Molecular Medicine (TuDMM), especially its former and present directors, Professor Kati Elima and Professor Noora Kotaja, and coordinators Dr. Eeva Valve and Dr. Verna Louhivuori, for their support throughout my work.

I acknowledge the financial support provided by the Finnish Cancer Society, Southwestern Finland Cancer Society, Turku University Foundation, and TuDMM.

I express my sincere gratitude to all co-authors of the articles included in my thesis: Professor Pekka Taimen, Professor Emerita Pirkko-Liisa Kellokumpu-Lehtinen, Dr. Neha Goel, and Dr. Mitro Miihkinen. Working with you has been inspirational, and your contributions have made this achievement possible. I also thank my collaborators Associate Professor Pekka Ruusuvuori and Dr. Mira Valkonen for our stimulating partnership, and I look forward to completing our work together in the future.

My warmest thanks to all current and former members of the Schleutker lab: Dr. Christoffer Löf, Dhanaprakash Jambulingam, Dr. Elina Kaikkonen, Dr. Gudrun Wahlström, Venkat Rathinakannan, Dr. Neha Goel, Dr. Vidal Fey, Nasrin Sultana, Dr. Csilla Sipeky, Viivi Kurkilahti, and Jukka Karhu. You have been a wonderful group to work alongside.

I am grateful to the many skilled professionals at the University of Turku who assisted me throughout my projects. Special thanks to Jukka Karhu, Minna Santanen, Bárbara Ramos Artigot, and Ann Sofie Wierda for technical assistance; Dr. Markus Peurla, Dr. Jouko Sandholm, and Dr. Markku Saari for microscopy support; Marja-Riitta Kajaala, Erica Nyman, and Sinikka Collanus for sample preparations and staining; and Dr. Ivana Mikocziova for excellent support with spatial transcriptomics.

I acknowledge all the wonderful colleagues on the 5th and 7th floors of Medisiina D for creating an enjoyable working atmosphere. I express my heartfelt gratitude to Docent Emilia Peuhu for your pivotal support, encouragement, and for keeping the flame of my scientific passion burning bright. Special thanks to Kreetta Paunu, Anni Soikkeli, Oona Paavolainen, Saiganesh Sriraman, Antti Kukkula, and Defne Dinc—your peer support has been invaluable throughout these years. Thanks also to my longtime PhD buddies Dr. Mikko Konki, Dr. Joni Merisaari, Dr. Veera Ojala, Petri Rummukainen, and Anni Hallanheimo for all the wonderful memories we've shared.

I want to thank my mother, Dr. Taina Metsälä, my father, Ilkka Metsälä, and my brothers Visa Metsälä and Matias Metsälä for your support throughout my life. Having you as my loving family means worlds to me. I also acknowledge my godmother, Minna Metsälä, and my late uncle, Tero Karhi, for their encouragement in pursuing my academic endeavours.

To the person who I share my life with, Heli Sihvonen, I present my deepest, most profound gratitude. Your love has been an endless source of strength and comfort to me in this journey.

Turku, May 2025
Olli Metsälä

References

Abida, W., Armenia, J., Gopalan, A., Brennan, R., Walsh, M., Barron, D., Danila, D., Rathkopf, D., Morris, M., Slovin, S., McLaughlin, B., Curtis, K., Hyman, D.M., Durack, J.C., Solomon, S.B., Arcila, M.E., Zehir, A., Syed, A., Gao, J., Chakravarty, D., Vargas, H.A., Robson, M.E., Vijai, J., Offit, K., Donoghue, M.T.A., Abeshouse, A.A., Kundra, R., Heins, Z.J., Penson, A.V., Harris, C., Taylor, B.S., Ladanyi, M., Mandelker, D., Zhang, L., Reuter, V.E., Kantoff, P.W., Solit, D.B., Berger, M.F., Sawyers, C.L., Schultz, N. and Scher, H.I., 2017. Prospective Genomic Profiling of Prostate Cancer Across Disease States Reveals Germline and Somatic Alterations That May Affect Clinical Decision Making. *JCO Precision Oncology*, 1, pp. 1–16. https://doi.org/10.1200/PO.17.00029.

Ahmad, F., Cherukuri, M.K. and Choyke, P.L., 2021. Metabolic reprogramming in prostate cancer. *British Journal of Cancer*, 125(9), pp. 1185–1196. https://doi.org/10.1038/s41416-021-01435-5.

Andersen, L.B., Nørgaard, M., Rasmussen, M., Fredsøe, J., Borre, M., Ulhøi, B.P. and Sørensen, K.D., 2021. Immune cell analyses of the tumor microenvironment in prostate cancer highlight infiltrating regulatory T cells and macrophages as adverse prognostic factors. *The Journal of Pathology*, 255(2), pp. 155–165. https://doi.org/10.1002/path.5757.

Angelova, M., Charoentong, P., Hackl, H., Fischer, M.L., Snajder, R., Krogsdam, A.M., Waldner, M.J., Bindea, G., Mlecnik, B., Galon, J. and Trajanoski, Z., 2015. Characterization of the immunophenotypes and antigenomes of colorectal cancers reveals distinct tumor escape mechanisms and novel targets for immunotherapy. *Genome Biology*, 16(1), 64. https://doi.org/10.1186/s13059-015-0620-6.

Audet-Walsh, É., Vernier, M., Yee, T., Laflamme, C., Li, S., Chen, Y. and Giguère, V., 2018. SREBF1 Activity Is Regulated by an AR/mTOR Nuclear Axis in Prostate Cancer. *Molecular Cancer Research*, 16(9), pp. 1396–1405. https://doi.org/10.1158/1541-7786.MCR-17-0410.

Bader, D.A., Hartig, S.M., Putluri, V., Foley, C., Hamilton, M.P., Smith, E.A., Saha, P.K., Panigrahi, A., Walker, C., Zong, L., Martini-Stoica, H., Chen, R., Rajapakshe, K., Coarfa, C., Sreekumar, A., Mitsiades, N., Bankson, J.A., Ittmann, M.M., O'Malley, B.W., Putluri, N. and McGuire, S.E., 2019. Mitochondrial pyruvate import is a metabolic vulnerability in androgen receptor-driven prostate cancer. *Nature Metabolism*, 1(1), pp. 70–85. https://doi.org/10.1038/s42255-018-0002-y.

Barbie, D.A., Tamayo, P., Boehm, J.S., Kim, S.Y., Moody, S.E., Dunn, I.F., Schinzel, A.C., Sandy, P., Meylan, E., Scholl, C., Fröhling, S., Chan, E.M., Sos, M.L., Michel, K., Mermel, C., Silver, S.J., Weir, B.A., Reiling, J.H., Sheng, Q., Gupta, P.B., Wadlow, R.C., Le, H., Hoersch, S., Wittner, B.S., Ramaswamy, S., Livingston, D.M., Sabatini, D.M., Meyerson, M., Thomas, R.K., Lander, E.S., Mesirov, J.P., Root, D.E., Gilliland, D.G., Jacks, T. and Hahn, W.C., 2009. Systematic RNA interference reveals that oncogenic KRAS-driven cancers require TBK1. *Nature*, 462(7269), pp. 108–112. https://doi.org/10.1038/nature08460.

Baulieu, E.E., Lasnitzki, I. and Robel, P., 1968. Metabolism of Testosterone and Action of Metabolites on Prostate Glands grown in Organ Culture. *Nature*, 219(5159), pp. 1155–1156. https://doi.org/10.1038/2191155a0.

Bell, K.J.L., Del Mar, C., Wright, G., Dickinson, J. and Glasziou, P., 2015. Prevalence of incidental prostate cancer: A systematic review of autopsy studies. *International Journal of Cancer*, 137(7), pp. 1749–1757. https://doi.org/10.1002/ijc.29538.

Bello, D., Webber, M.M., Kleinman, H.K., Wartinger, D.D. and Rhim, J.S., 1997. Androgen responsive adult human prostatic epithelial cell lines immortalized by human papillomavirus 18. *Carcinogenesis*, 18(6), pp.1215–1223. https://doi.org/10.1093/carcin/18.6.1215.

Benarroch, E.E., 2017. Anoctamins (TMEM16 proteins). *Neurology*, 89(7), pp. 722–729. https://doi.org/10.1212/WNL.0000000000004246.

Bera, T.K., Das, S., Maeda, H., Beers, R., Wolfgang, C.D., Kumar, V., Hahn, Y., Lee, B. and Pastan, I., 2004. NGEP, a gene encoding a membrane protein detected only in prostate cancer and normal prostate. *Proceedings of the National Academy of Sciences of the United States of America*, 101(9), pp. 3059–3064. https://doi.org/10.1073/pnas.0308746101.

Bergengren, O., Pekala, K.R., Matsoukas, K., Fainberg, J., Mungovan, S.F., Bratt, O., Bray, F., Brawley, O., Luckenbaugh, A.N., Mucci, L., Morgan, T.M. and Carlsson, S.V., 2023. 2022 Update on Prostate Cancer Epidemiology and Risk Factors—A Systematic Review. *European Urology*, 84(2), pp. 191–206. https://doi.org/10.1016/j.eururo.2023.04.021.

Bernard, D., Pourtier-Manzanedo, A., Gil, J. and Beach, D.H., 2003. Myc confers androgen-independent prostate cancer cell growth. *The Journal of Clinical Investigation*, 112(11), pp. 1724–1731. https://doi.org/10.1172/JCI19035.

Bindea, G., Mlecnik, B., Hackl, H., Charoentong, P., Tosolini, M., Kirilovsky, A., Fridman, W.-H., Pagès, F., Trajanoski, Z. and Galon, J., 2009. ClueGO: a Cytoscape plug-in to decipher functionally grouped gene ontology and pathway annotation networks. *Bioinformatics*, 25(8), pp. 1091–1093. https://doi.org/10.1093/bioinformatics/btp101.

Bindea, G., Mlecnik, B., Tosolini, M., Kirilovsky, A., Waldner, M., Obenauf, A.C., Angell, H., Fredriksen, T., Lafontaine, L., Berger, A., Bruneval, P., Fridman, W.H., Becker, C., Pagès, F., Speicher, M.R., Trajanoski, Z. and Galon, J., 2013. Spatiotemporal Dynamics of Intratumoral Immune Cells Reveal the Immune Landscape in Human Cancer. *Immunity*, 39(4), pp. 782–795. https://doi.org/10.1016/j.immuni.2013.10.003.

Blackburn, J.B., Li, N.F., Bartlett, N.W. and Richmond, B.W., 2023. An update in club cell biology and its potential relevance to chronic obstructive pulmonary disease. *American Journal of Physiology-Lung Cellular and Molecular Physiology*, 324(5), pp. L652–L665. https://doi.org/10.1152/ajplung.00192.2022.

de Bono, J.S., Guo, C., Gurel, B., De Marzo, A.M., Sfanos, K.S., Mani, R.S., Gil, J., Drake, C.G. and Alimonti, A., 2020. Prostate carcinogenesis: inflammatory storms. *Nature Reviews Cancer*, 20(8), pp. 455–469. https://doi.org/10.1038/s41568-020-0267-9.

Braglia, L., Zavatti, M., Vinceti, M., Martelli, A.M. and Marmiroli, S., 2020. Deregulated PTEN/PI3K/AKT/mTOR signaling in prostate cancer: Still a potential druggable target? *Biochimica et Biophysica Acta (BBA) - Molecular Cell Research*, 1867(9), 118731. https://doi.org/10.1016/j.bbamcr.2020.118731.

Britschgi, A., Bill, A., Brinkhaus, H., Rothwell, C., Clay, I., Duss, S., Rebhan, M., Raman, P., Guy, C.T., Wetzel, K., George, E., Popa, M.O., Lilley, S., Choudhury, H., Gosling, M., Wang, L., Fitzgerald, S., Borawski, J., Baffoe, J., Labow, M., Gaither, L.A. and Bentires-Alj, M., 2013. Calcium-activated chloride channel ANO1 promotes breast cancer progression by activating EGFR and CAMK signaling. *Proceedings of the National Academy of Sciences*, 110(11), pp. E1026–E1034. https://doi.org/10.1073/pnas.1217072110.

Burkhart, D.L., Morel, K.L., Sheahan, A.V., Richards, Z.A. and Ellis, L., 2019. The Role of RB in Prostate Cancer Progression. In: S.M. Dehm and D.J. Tindall, eds. *Prostate Cancer: Cellular and Genetic Mechanisms of Disease Development and Progression*. [online] Cham: Springer International Publishing. pp. 301–318. https://doi.org/10.1007/978-3-030-32656-2_13.

Buskin, A., Singh, P., Lorenz, O., Robson, C., Strand, D.W. and Heer, R., 2021. A Review of Prostate Organogenesis and a Role for iPSC-Derived Prostate Organoids to Study Prostate Development

and Disease. *International Journal of Molecular Sciences*, 22(23), 13097. https://doi.org/10.3390/ijms222313097.

Butler, W. and Huang, J., 2021. Neuroendocrine cells of the prostate: Histology, biological functions, and molecular mechanisms. *Precision Clinical Medicine*, 4(1), pp. 25–34. https://doi.org/10.1093/pcmedi/pbab003.

Castoldi, E., Collins, P.W., Williamson, P.L. and Bevers, E.M., 2011. Compound heterozygosity for 2 novel *TMEM16F* mutations in a patient with Scott syndrome. *Blood*, 117(16), pp. 4399–4400. https://doi.org/10.1182/blood-2011-01-332502.

Cereda, V., Poole, D.J., Palena, C., Das, S., Bera, T.K., Remondo, C., Gulley, J.L., Arlen, P.M., Yokokawa, J., Pastan, I., Schlom, J. and Tsang, K.Y., 2010. New gene expressed in prostate: a potential target for T cell-mediated prostate cancer immunotherapy. *Cancer Immunology, Immunotherapy*, 59(1), pp. 63–71. https://doi.org/10.1007/s00262-009-0723-6.

Chandran, U.R., Ma, C., Dhir, R., Bisceglia, M., Lyons-Weiler, M., Liang, W., Michalopoulos, G., Becich, M. and Monzon, F.A., 2007. Gene expression profiles of prostate cancer reveal involvement of multiple molecular pathways in the metastatic process. *BMC Cancer*, 7, 64. https://doi.org/10.1186/1471-2407-7-64.

Charoentong, P., Finotello, F., Angelova, M., Mayer, C., Efremova, M., Rieder, D., Hackl, H. and Trajanoski, Z., 2017. Pan-cancer Immunogenomic Analyses Reveal Genotype-Immunophenotype Relationships and Predictors of Response to Checkpoint Blockade. *Cell Reports*, 18(1), pp. 248–262. https://doi.org/10.1016/j.celrep.2016.12.019.

Chen, C., Aluksanasuwan, S. and Somsuan, K., 2023. Expression of anoctamin 7 (ANO7) is associated with poor prognosis and mucin 2 (MUC2) in colon adenocarcinoma: a study based on TCGA data. *Genomics & Informatics*, 21(4), e46. https://doi.org/10.5808/gi.23071.

Chen, F., Madduri, R.K., Rodriguez, A.A., Darst, B.F., Chou, A., Sheng, X., Wang, A., Shen, J., Saunders, E.J., Rhie, S.K., Bensen, J.T., Ingles, S.A., Kittles, R.A., Strom, S.S., Rybicki, B.A., Nemesure, B., Isaacs, W.B., Stanford, J.L., Zheng, W., Sanderson, M., John, E.M., Park, J.Y., Xu, J., Wang, Y., Berndt, S.I., Huff, C.D., Yeboah, E.D., Tettey, Y., Lachance, J., Tang, W., Rentsch, C.T., Cho, K., Mcmahon, B.H., Biritwum, R.B., Adjei, A.A., Tay, E., Truelove, A., Niwa, S., Sellers, T.A., Yamoah, K., Murphy, A.B., Crawford, D.C., Patel, A.V., Bush, W.S., Aldrich, M.C., Cussenot, O., Petrovics, G., Cullen, J., Neslund-Dudas, C.M., Stern, M.C., Kote-Jarai, Z., Govindasami, K., Cook, M.B., Chokkalingam, A.P., Hsing, A.W., Goodman, P.J., Hoffmann, T.J., Drake, B.F., Hu, J.J., Keaton, J.M., Hellwege, J.N., Clark, P.E., Jalloh, M., Gueye, S.M., Niang, L., Ogunbiyi, O., Idowu, M.O., Popoola, O., Adebiyi, A.O., Aisuodionoe-Shadrach, O.I., Ajibola, H.O., Jamda, M.A., Oluwole, O.P., Nwegbu, M., Adusei, B., Mante, S., Darkwa-Abrahams, A., Mensah, J.E., Diop, H., Van Den Eeden, S.K., Blanchet, P., Fowke, J.H., Casey, G., Hennis, A.J., Lubwama, A., Thompson, I.M., Leach, R., Easton, D.F., Preuss, M.H., Loos, R.J., Gundell, S.M., Wan, P., Mohler, J.L., Fontham, E.T., Smith, G.J., Taylor, J.A., Srivastava, S., Eeles, R.A., Carpten, J.D., Kibel, A.S., Multigner, L., Parent, M.-É., Menegaux, F., Cancel-Tassin, G., Klein, E.A., Andrews, C., Rebbeck, T.R., Brureau, L., Ambs, S., Edwards, T.L., Watya, S., Chanock, S.J., Witte, J.S., Blot, W.J., Michael Gaziano, J., Justice, A.C., Conti, D.V. and Haiman, C.A., 2023. Evidence of Novel Susceptibility Variants for Prostate Cancer and a Multiancestry Polygenic Risk Score Associated with Aggressive Disease in Men of African Ancestry. *European Urology*, 84(1), pp. 13–21. https://doi.org/10.1016/j.eururo.2023.01.022.

Chen, H.-W., Chang, Y.-F., Chuang, H.-Y., Tai, W.-T. and Hwang, J.-J., 2012. Targeted therapy with fatty acid synthase inhibitors in a human prostate carcinoma LNCaP/tk-luc-bearing animal model. *Prostate Cancer and Prostatic Diseases*, 15(3), pp.260–264. https://doi.org/10.1038/pcan.2012.15.

Chen, M., Zhang, J., Sampieri, K., Clohessy, J.G., Mendez, L., Gonzalez-Billalabeitia, E., Liu, X.-S., Lee, Y.-R., Fung, J., Katon, J.M., Menon, A.V., Webster, K.A., Ng, C., Palumbieri, M.D., Diolombi, M.S., Breitkopf, S.B., Teruya-Feldstein, J., Signoretti, S., Bronson, R.T., Asara, J.M., Castillo-Martin, M., Cordon-Cardo, C. and Pandolfi, P.P., 2018. An aberrant SREBP-dependent

lipogenic program promotes metastatic prostate cancer. *Nature Genetics*, 50, pp. 206–218. https://doi.org/10.1038/s41588-017-0027-2.

Conti, D.V., Darst, B.F., Moss, L.C., Saunders, E.J., Sheng, X., Chou, A., Schumacher, F.R., Olama, A.A.A., Benlloch, S., Dadaev, T., Brook, M.N., Sahimi, A., Hoffmann, T.J., Takahashi, A., Matsuda, K., Momozawa, Y., Fujita, M., Muir, K., Lophatananon, A., Wan, P., Le Marchand, L., Wilkens, L.R., Stevens, V.L., Gapstur, S.M., Carter, B.D., Schleutker, J., Tammela, T.L.J., Sipeky, C., Auvinen, A., Giles, G.G., Southey, M.C., MacInnis, R.J., Cybulski, C., Wokołorczyk, D., Lubiński, J., Neal, D.E., Donovan, J.L., Hamdy, F.C., Martin, R.M., Nordestgaard, B.G., Nielsen, S.F., Weischer, M., Bojesen, S.E., Røder, M.A., Iversen, P., Batra, J., Chambers, S., Moya, L., Horvath, L., Clements, J.A., Tilley, W., Risbridger, G.P., Gronberg, H., Aly, M., Szulkin, R., Eklund, M., Nordström, T., Pashayan, N., Dunning, A.M., Ghoussaini, M., Travis, R.C., Key, T.J., Riboli, E., Park, J.Y., Sellers, T.A., Lin, H.-Y., Albanes, D., Weinstein, S.J., Mucci, L.A., Giovannucci, E., Lindstrom, S., Kraft, P., Hunter, D.J., Penney, K.L., Turman, C., Tangen, C.M., Goodman, P.J., Thompson, I.M., Hamilton, R.J., Fleshner, N.E., Finelli, A., Parent, M.-É., Stanford, J.L., Ostrander, E.A., Geybels, M.S., Koutros, S., Freeman, L.E.B., Stampfer, M., Wolk, A., Håkansson, N., Andriole, G.L., Hoover, R.N., Machiela, M.J., Sørensen, K.D., Borre, M., Blot, W.J., Zheng, W., Yeboah, E.D., Mensah, J.E., Lu, Y.-J., Zhang, H.-W., Feng, N., Mao, X., Wu, Y., Zhao, S.-C., Sun, Z., Thibodeau, S.N., McDonnell, S.K., Schaid, D.J., West, C.M.L., Burnet, N., Barnett, G., Maier, C., Schnoeller, T., Luedeke, M., Kibel, A.S., Drake, B.F., Cussenot, O., Cancel-Tassin, G., Menegaux, F., Truong, T., Koudou, Y.A., John, E.M., Grindedal, E.M., Maehle, L., Khaw, K.-T., Ingles, S.A., Stern, M.C., Vega, A., Gómez-Caamaño, A., Fachal, L., Rosenstein, B.S., Kerns, S.L., Ostrer, H., Teixeira, M.R., Paulo, P., Brandão, A., Watya, S., Lubwama, A., Bensen, J.T., Fontham, E.T.H., Mohler, J., Taylor, J.A., Kogevinas, M., Llorca, J., Castaño-Vinyals, G., Cannon-Albright, L., Teerlink, C.C., Huff, C.D., Strom, S.S., Multigner, L., Blanchet, P., Brureau, L., Kaneva, R., Slavov, C., Mitev, V., Leach, R.J., Weaver, B., Brenner, H., Cuk, K., Holleczek, B., Saum, K.-U., Klein, E.A., Hsing, A.W., Kittles, R.A., Murphy, A.B., Logothetis, C.J., Kim, J., Neuhausen, S.L., Steele, L., Ding, Y.C., Isaacs, W.B., Nemesure, B., Hennis, A.J.M., Carpten, J., Pandha, H., Michael, A., De Ruyck, K., De Meerleer, G., Ost, P., Xu, J., Razack, A., Lim, J., Teo, S.-H., Newcomb, L.F., Lin, D.W., Fowke, J.H., Neslund-Dudas, C., Rybicki, B.A., Gamulin, M., Lessel, D., Kulis, T., Usmani, N., Singhal, S., Parliament, M., Claessens, F., Joniau, S., Van den Broeck, T., Gago-Dominguez, M., Castelao, J.E., Martinez, M.E., Larkin, S., Townsend, P.A., Aukim-Hastie, C., Bush, W.S., Aldrich, M.C., Crawford, D.C., Srivastava, S., Cullen, J.C., Petrovics, G., Casey, G., Roobol, M.J., Jenster, G., van Schaik, R.H.N., Hu, J.J., Sanderson, M., Varma, R., McKean-Cowdin, R., Torres, M., Mancuso, N., Berndt, S.I., Van Den Eeden, S.K., Easton, D.F., Chanock, S.J., Cook, M.B., Wiklund, F., Nakagawa, H., Witte, J.S., Eeles, R.A., Kote-Jarai, Z. and Haiman, C.A., 2021. Trans-ancestry genome-wide association meta-analysis of prostate cancer identifies new susceptibility loci and informs genetic risk prediction. *Nature Genetics*, 53(1), pp. 65–75. https://doi.org/10.1038/s41588-020-00748-0.

Continuous Update Project panel, 2018. World Cancer Research Fund/American Institute for Cancer Research. Continuous Update Project Expert Report 2018. Diet, nutrition, physical activity and prostate cancer. [online] World Cancer Research Fund. Available at: <dietandcancerreport.org> [Accessed 2 December 2024].

Conway, J.R.W., Dinç, D.D., Follain, G., Paavolainen, O., Kaivola, J., Boström, P., Hartiala, P., Peuhu, E. and Ivaska, J., 2023. IGFBP2 secretion by mammary adipocytes limits breast cancer invasion. *Science Advances*, 9(28), eadg1840. https://doi.org/10.1126/sciadv.adg1840.

Cooper, M.A., Fehniger, T.A., Turner, S.C., Chen, K.S., Ghaheri, B.A., Ghayur, T., Carson, W.E. and Caligiuri, M.A., 2001. Human natural killer cells: a unique innate immunoregulatory role for the CD56bright subset. *Blood*, 97(10), pp. 3146–3151. https://doi.org/10.1182/blood.V97.10.3146.

Cornford, P., van den Bergh, R.C.N., Briers, E., Van den Broeck, T., Brunckhorst, O., Darraugh, J., Eberli, D., De Meerleer, G., De Santis, M., Farolfi, A., Gandaglia, G., Gillessen, S., Grivas, N., Henry, A.M., Lardas, M., van Leenders, G.J.L.H., Liew, M., Linares Espinos, E., Oldenburg, J.,

van Oort, I.M., Oprea-Lager, D.E., Ploussard, G., Roberts, M.J., Rouvière, O., Schoots, I.G., Schouten, N., Smith, E.J., Stranne, J., Wiegel, T., Willemse, P.-P.M. and Tilki, D., 2024. EAU-EANM-ESTRO-ESUR-ISUP-SIOG Guidelines on Prostate Cancer—2024 Update. Part I: Screening, Diagnosis, and Local Treatment with Curative Intent. *European Urology*, 86(2), pp. 148–163. https://doi.org/10.1016/j.eururo.2024.03.027.

Costello, L.C. and Franklin, R.B., 2006. The clinical relevance of the metabolism of prostate cancer; zinc and tumor suppression: connecting the dots. *Molecular Cancer*, 5, 17. https://doi.org/10.1186/1476-4598-5-17.

Cotter, K. and Rubin, M.A., 2022. The evolving landscape of prostate cancer somatic mutations. *The Prostate*, 82(S1), pp. S13–S24. https://doi.org/10.1002/pros.24353.

Cropp, C.D., Simpson, C.L., Wahlfors, T., Ha, N., George, A., Jones, M.S., Harper, U., Ponciano-Jackson, D., Green, T.A., Tammela, T.L.J., Bailey-Wilson, J. and Schleutker, J., 2011. Genome-wide linkage scan for prostate cancer susceptibility in Finland: Evidence for a novel locus on 2q37.3 and confirmation of signal on 17q21-q22. *International Journal of Cancer*, 129(10), pp. 2400–2407. https://doi.org/10.1002/ijc.25906.

Cunha, G.R., Vezina, C.M., Isaacson, D., Ricke, W.A., Timms, B.G., Cao, M., Franco, O. and Baskin, L.S., 2018. Development of the human prostate. *Differentiation*, 103, pp. 24–45. https://doi.org/10.1016/j.diff.2018.08.005.

Dairo, O., DePaula Oliveira, L., Schaffer, E., Vidotto, T., Mendes, A.A., Lu, J., Huynh, S.V., Hicks, J., Sowalsky, A.G., De Marzo, A.M., Joshu, C.E., Hanratty, B., Sfanos, K.S., Isaacs, W.B., Haffner, M.C. and Lotan, T.L., 2024. FASN Gene Methylation is Associated with Fatty Acid Synthase Expression and Clinical-genomic Features of Prostate Cancer. *Cancer Research Communications*, 4(1), pp. 152–163. https://doi.org/10.1158/2767-9764.CRC-23-0248.

Daksis, J.I., Lu, R.Y., Facchini, L.M., Marhin, W.W. and Penn, L.J., 1994. Myc induces cyclin D1 expression in the absence of de novo protein synthesis and links mitogen-stimulated signal transduction to the cell cycle. *Oncogene*, 9(12), pp. 3635–3645.

D'Amico, A.V., Whittington, R., Malkowicz, S.B., Fondurulia, J., Chen, M.-H., Kaplan, I., Beard, C.J., Tomaszewski, J.E., Renshaw, A.A., Wein, A. and Coleman, C.N., 1999. Pretreatment Nomogram for Prostate-Specific Antigen Recurrence After Radical Prostatectomy or External-Beam Radiation Therapy for Clinically Localized Prostate Cancer. *Journal of Clinical Oncology*, 17(1), pp. 168–168. https://doi.org/10.1200/JCO.1999.17.1.168.

Das, S., Hahn, Y., Nagata, S., Willingham, M.C., Bera, T.K., Lee, B. and Pastan, I., 2007. NGEP, a Prostate-Specific Plasma Membrane Protein that Promotes the Association of LNCaP Cells. *Cancer Research*, 67(4), pp. 1594–1601. https://doi.org/10.1158/0008-5472.CAN-06-2673.

Das, S., Hahn, Y., Walker, D.A., Nagata, S., Willingham, M.C., Peehl, D.M., Bera, T.K., Lee, B. and Pastan, I., 2008. Topology of NGEP, a Prostate-Specific Cell:Cell Junction Protein Widely Expressed in Many Cancers of Different Grade Level. *Cancer Research*, 68(15), pp. 6306–6312. https://doi.org/10.1158/0008-5472.CAN-08-0870.

Davies, A., Zoubeidi, A., Beltran, H. and Selth, L.A., 2023. The Transcriptional and Epigenetic Landscape of Cancer Cell Lineage Plasticity. *Cancer Discovery*, 13(8), pp. 1771–1788. https://doi.org/10.1158/2159-8290.CD-23-0225.

De Conti, L., Baralle, M. and Buratti, E., 2013. Exon and intron definition in pre-mRNA splicing. *WIREs RNA*, 4(1), pp. 49–60. https://doi.org/10.1002/wrna.1140.

De Marzo, A.M., Marchi, V.L., Epstein, J.I. and Nelson, W.G., 1999. Proliferative Inflammatory Atrophy of the Prostate: Implications for Prostatic Carcinogenesis. *The American Journal of Pathology*, 155(6), pp. 1985–1992. https://doi.org/10.1016/S0002-9440(10)65517-4.

Deininger, P., 2011. Alu elements: know the SINEs. *Genome Biology*, 12(12), 236. https://doi.org/10.1186/gb-2011-12-12-236.

Devlin, C.M., Simms, M.S. and Maitland, N.J., 2021. Benign prostatic hyperplasia – what do we know? *BJU International*, 127(4), pp. 389–399. https://doi.org/10.1111/bju.15229.

Di Carlo, E. and Sorrentino, C., 2024. The multifaceted role of the stroma in the healthy prostate and prostate cancer. *Journal of Translational Medicine*, 22, 825. https://doi.org/10.1186/s12967-024-05564-2.

Duran, C., Qu, Z., Osunkoya, A.O., Cui, Y. and Hartzell, H.C., 2012. ANOs 3–7 in the anoctamin/Tmem16 Cl− channel family are intracellular proteins. *American Journal of Physiology-Cell Physiology*, 302(3), pp. C482–C493. https://doi.org/10.1152/ajpcell.00140.2011.

Ebert, B., Kisiela, M. and Maser, E., 2015. Human DCXR – another 'moonlighting protein' involved in sugar metabolism, carbonyl detoxification, cell adhesion and male fertility? *Biological Reviews*, 90(1), pp. 254–278. https://doi.org/10.1111/brv.12108.

Effert, P.J., Bares, R., Handt, S., Wolff, J.M., Bull, U. and Jakse, G., 1996. Metabolic Imaging of Untreated Prostate Cancer by Positron Emission Tomography with sup 18 Fluorine-Labeled Deoxyglucose. *The Journal of Urology*, 155(3), pp. 994–998. https://doi.org/10.1016/S0022-5347(01)66366-3.

Eggener, S.E., Rumble, R.B., Armstrong, A.J., Morgan, T.M., Crispino, T., Cornford, P., van der Kwast, T., Grignon, D.J., Rai, A.J., Agarwal, N., Klein, E.A., Den, R.B. and Beltran, H., 2020. Molecular Biomarkers in Localized Prostate Cancer: ASCO Guideline. *Journal of Clinical Oncology*, 38(13), pp. 1474–1494. https://doi.org/10.1200/JCO.19.02768.

Ehrlich, Y., Foster, R.S., Bihrle, R., Cheng, L., Tong, Y. and Koch, M.O., 2010. Division of Prostatic Anterior Fibromuscular Stroma Reduces Urethral Resistance in an Ex Vivo Human Prostate Model. *Urology*, 76(2), pp. 511.e10-511.e13. https://doi.org/10.1016/j.urology.2010.03.035.

Epstein, J.I., Egevad, L., Amin, M.B., Delahunt, B., Srigley, J.R., Humphrey, P.A. and Committee, the G., 2016. The 2014 International Society of Urological Pathology (ISUP) Consensus Conference on Gleason Grading of Prostatic Carcinoma: Definition of Grading Patterns and Proposal for a New Grading System. *The American Journal of Surgical Pathology*, 40(2), pp. 244–252. https://doi.org/10.1097/PAS.0000000000000530.

Erho, N., Crisan, A., Vergara, I.A., Mitra, A.P., Ghadessi, M., Buerki, C., Bergstralh, E.J., Kollmeyer, T., Fink, S., Haddad, Z., Zimmermann, B., Sierocinski, T., Ballman, K.V., Triche, T.J., Black, P.C., Karnes, R.J., Klee, G., Davicioni, E. and Jenkins, R.B., 2013. Discovery and Validation of a Prostate Cancer Genomic Classifier that Predicts Early Metastasis Following Radical Prostatectomy. *PLOS ONE*, 8(6), p.e66855. https://doi.org/10.1371/journal.pone.0066855.

Falzone, M.E., Malvezzi, M., Lee, B.C. and Accardi, A., 2018. Known structures and unknown mechanisms of TMEM16 scramblases and channels. *The Journal of general physiology*, 150(7), pp.933–947. https://doi.org/10.1085/jgp.201711957.

Figiel, S., Yin, W., Doultsinos, D., Erickson, A., Poulose, N., Singh, R., Magnussen, A., Anbarasan, T., Teague, R., He, M., Lundeberg, J., Loda, M., Verrill, C., Colling, R., Gill, P.S., Bryant, R.J., Hamdy, F.C., Woodcock, D.J., Mills, I.G., Cussenot, O. and Lamb, A.D., 2023. Spatial transcriptomic analysis of virtual prostate biopsy reveals confounding effect of tissue heterogeneity on genomic signatures. *Molecular Cancer*, 22(1), 162. https://doi.org/10.1186/s12943-023-01863-2.

Finley, L.W.S., 2023. What is cancer metabolism? *Cell*, 186(8), pp.1670–1688. https://doi.org/10.1016/j.cell.2023.01.038.

Gao, L., Schwartzman, J., Gibbs, A., Lisac, R., Kleinschmidt, R., Wilmot, B., Bottomly, D., Coleman, I., Nelson, P., McWeeney, S. and Alumkal, J., 2013. Androgen Receptor Promotes Ligand-Independent Prostate Cancer Progression through c-Myc Upregulation. *PLOS ONE*, 8(5), e63563. https://doi.org/10.1371/journal.pone.0063563.

Gao, Q., Liu, X., Ye, L., Lv, T., Teng, Y., Lan, J., Li, T., Tian, M., Chen, J., He, S., Xie, S. and Zou, Y., 2022. Adenosquamous Carcinoma of Skene's Gland: A Case Report and Literature Review. *Frontiers in Oncology*, 12, 893980. https://doi.org/10.3389/fonc.2022.893980.

Gao, Y., Islam, M.S., Tian, J., Lui, V.W.Y. and Xiao, D., 2014. Inactivation of ATP citrate lyase by Cucurbitacin B: A bioactive compound from cucumber, inhibits prostate cancer growth. *Cancer Letters*, 349(1), pp. 15–25. https://doi.org/10.1016/j.canlet.2014.03.015.

Ghandi, M., Huang, F.W., Jané-Valbuena, J., Kryukov, G.V., Lo, C.C., McDonald, E.R., Barretina, J., Gelfand, E.T., Bielski, C.M., Li, H., Hu, K., Andreev-Drakhlin, A.Y., Kim, J., Hess, J.M., Haas, B.J., Aguet, F., Weir, B.A., Rothberg, M.V., Paolella, B.R., Lawrence, M.S., Akbani, R., Lu, Y., Tiv, H.L., Gokhale, P.C., de Weck, A., Mansour, A.A., Oh, C., Shih, J., Hadi, K., Rosen, Y., Bistline, J., Venkatesan, K., Reddy, A., Sonkin, D., Liu, M., Lehar, J., Korn, J.M., Porter, D.A., Jones, M.D., Golji, J., Caponigro, G., Taylor, J.E., Dunning, C.M., Creech, A.L., Warren, A.C., McFarland, J.M., Zamanighomi, M., Kauffmann, A., Stransky, N., Imielinski, M., Maruvka, Y.E., Cherniack, A.D., Tsherniak, A., Vazquez, F., Jaffe, J.D., Lane, A.A., Weinstock, D.M., Johannessen, C.M., Morrissey, M.P., Stegmeier, F., Schlegel, R., Hahn, W.C., Getz, G., Mills, G.B., Boehm, J.S., Golub, T.R., Garraway, L.A. and Sellers, W.R., 2019. Next-generation characterization of the Cancer Cell Line Encyclopedia. *Nature*, 569(7757), pp. 503–508. https://doi.org/10.1038/s41586-019-1186-3.

Giafaglione, J.M., Crowell, P.D., Delcourt, A.M.L., Hashimoto, T., Ha, S.M., Atmakuri, A., Nunley, N.M., Dang, R.M.A., Tian, M., Diaz, J.A., Tika, E., Payne, M.C., Burkhart, D.L., Li, D., Navone, N.M., Corey, E., Nelson, P.S., Lin, N.Y.C., Blanpain, C., Ellis, L., Boutros, P.C. and Goldstein, A.S., 2023. Prostate lineage-specific metabolism governs luminal differentiation and response to antiandrogen treatment. *Nature Cell Biology*, 25(12), pp.1821–1832. https://doi.org/10.1038/s41556-023-01274-x.

Gleason, D.F., 1966. Classification of prostatic carcinomas. *Cancer Chemotherapy Reports*, 50(3), pp.125–128.

Gordon, J.M., Phizicky, D.V. and Neugebauer, K.M., 2021. Nuclear mechanisms of gene expression control: pre-mRNA splicing as a life or death decision. *Current Opinion in Genetics & Development*, 67, pp. 67–76. https://doi.org/10.1016/j.gde.2020.11.002.

Grasso, C.S., Wu, Y.-M., Robinson, D.R., Cao, X., Dhanasekaran, S.M., Khan, A.P., Quist, M.J., Jing, X., Lonigro, R.J., Brenner, J.C., Asangani, I.A., Ateeq, B., Chun, S.Y., Siddiqui, J., Sam, L., Anstett, M., Mehra, R., Prensner, J.R., Palanisamy, N., Ryslik, G.A., Vandin, F., Raphael, B.J., Kunju, L.P., Rhodes, D.R., Pienta, K.J., Chinnaiyan, A.M. and Tomlins, S.A., 2012. The mutational landscape of lethal castration-resistant prostate cancer. *Nature*, 487(7406), pp. 239–243. https://doi.org/10.1038/nature11125.

Grönberg, H., Eklund, M., Picker, W., Aly, M., Jäderling, F., Adolfsson, J., Landquist, M., Haug, E.S., Ström, P., Carlsson, S. and Nordström, T., 2018. Prostate Cancer Diagnostics Using a Combination of the Stockholm3 Blood Test and Multiparametric Magnetic Resonance Imaging. *European Urology*, 74(6), pp. 722–728. https://doi.org/10.1016/j.eururo.2018.06.022.

Gross, N.T., Wang, J., Fiandalo, M.V., Gomez, E.C., Watts, A., Godoy, A.S., Smith, G.J. and Wu, Y., 2020. Recapitulation of prostate tissue cell type-specific transcriptomes by an in vivo primary prostate tissue xenograft model. *PLOS ONE*, 15(6), e0233899. https://doi.org/10.1371/journal.pone.0233899.

Guo, C., Luttrell, L.M. and Price, D.T., 2000. Mitogenic signaling in androgen sensitive and insensitive prostate cancer cell lines. *The Journal of Urology*, 163(3), pp. 1027–1032. https://doi.org/10.1016/S0022-5347(05)67876-7.

Guo, J., Wang, D., Dong, Y., Gao, X., Tong, H., Liu, W., Zhang, L. and Sun, M., 2021. ANO7: Insights into topology, function, and potential applications as a biomarker and immunotherapy target. *Tissue & Cell*, 72, 101546. https://doi.org/10.1016/j.tice.2021.101546.

Gustafsson, J.K. and Johansson, M.E.V., 2022. The role of goblet cells and mucus in intestinal homeostasis. *Nature Reviews Gastroenterology & Hepatology*, 19(12), pp.785–803. https://doi.org/10.1038/s41575-022-00675-x.

Gyobu, S., Ishihara, K., Suzuki, J., Segawa, K. and Nagata, S., 2017. Characterization of the scrambling domain of the TMEM16 family. *Proceedings of the National Academy of Sciences*, 114(24), pp. 6274–6279. https://doi.org/10.1073/pnas.1703391114.

Haines, C.N., Klingensmith, H.D., Komara, M. and Burd, C.J., 2020. GREB1 regulates PI3K/Akt signaling to control hormone-sensitive breast cancer proliferation. *Carcinogenesis*, 41(12), pp. 1660–1670. https://doi.org/10.1093/carcin/bgaa096.

Hamdy, F.C., Donovan, J.L., Lane, J.A., Metcalfe, C., Davis, M., Turner, E.L., Martin, R.M., Young, G.J., Walsh, E.I., Bryant, R.J., Bollina, P., Doble, A., Doherty, A., Gillatt, D., Gnanapragasam, V., Hughes, O., Kockelbergh, R., Kynaston, H., Paul, A., Paez, E., Powell, P., Rosario, D.J., Rowe, E., Mason, M., Catto, J.W.F., Peters, T.J., Oxley, J., Williams, N.J., Staffurth, J. and Neal, D.E., 2023. Fifteen-Year Outcomes after Monitoring, Surgery, or Radiotherapy for Prostate Cancer. *New England Journal of Medicine*, 388(17), pp. 1547–1558. https://doi.org/10.1056/NEJMoa2214122.

Hanahan, D., 2022. Hallmarks of Cancer: New Dimensions. *Cancer Discovery*, 12(1), pp. 31–46. https://doi.org/10.1158/2159-8290.CD-21-1059.

Hanahan, D. and Weinberg, R.A., 2000. The Hallmarks of Cancer. *Cell*, 100(1), pp. 57–70. https://doi.org/10.1016/S0092-8674(00)81683-9.

Hanahan, D. and Weinberg, R.A., 2011. Hallmarks of Cancer: The Next Generation. *Cell*, 144(5), pp. 646–674. https://doi.org/10.1016/j.cell.2011.02.013.

Hartzell, H.C., Yu, K., Xiao, Q., Chien, L.-T. and Qu, Z., 2009. Anoctamin/TMEM16 family members are Ca2+-activated Cl− channels. *The Journal of Physiology*, 587(10), pp. 2127–2139. https://doi.org/10.1113/jphysiol.2008.163709.

Hayward, S.W., Dahiya, R., Cunha, G.R., Bartek, J., Deshpande, N. and Narayan, P., 1995. Establishment and characterization of an immortalized but non-transformed human prostate epithelial cell line: BPH-1. *In Vitro Cellular & Developmental Biology - Animal*, 31(1), pp. 14–24. https://doi.org/10.1007/BF02631333.

He, Y., Sun, M.M., Zhang, G.G., Yang, J., Chen, K.S., Xu, W.W. and Li, B., 2021. Targeting PI3K/Akt signal transduction for cancer therapy. *Signal Transduction and Targeted Therapy*, 6(1), pp. 1–17. https://doi.org/10.1038/s41392-021-00828-5.

He, Y., Xu, W., Xiao, Y.-T., Huang, H., Gu, D. and Ren, S., 2022. Targeting signaling pathways in prostate cancer: mechanisms and clinical trials. *Signal Transduction and Targeted Therapy*, 7(1), pp. 1–31. https://doi.org/10.1038/s41392-022-01042-7.

Henry, G.H., Malewska, A., Joseph, D.B., Malladi, V.S., Lee, J., Torrealba, J., Mauck, R.J., Gahan, J.C., Raj, G.V., Roehrborn, C.G., Hon, G.C., MacConmara, M.P., Reese, J.C., Hutchinson, R.C., Vezina, C.M. and Strand, D.W., 2018. A Cellular Anatomy of the Normal Adult Human Prostate and Prostatic Urethra. *Cell Reports*, 25(12), pp. 3530-3542.e5. https://doi.org/10.1016/j.celrep.2018.11.086.

Herbst, R.S. and Khuri, F.R., 2003. Mode of action of docetaxel – a basis for combination with novel anticancer agents. *Cancer Treatment Reviews*, 29(5), pp. 407–415. https://doi.org/10.1016/S0305-7372(03)00097-5.

Hewitt, R.J. and Lloyd, C.M., 2021. Regulation of immune responses by the airway epithelial cell landscape. *Nature Reviews Immunology*, 21(6), pp. 347–362. https://doi.org/10.1038/s41577-020-00477-9.

Hirabayashi, T., Kawaguchi, M., Harada, S., Mouri, M., Takamiya, R., Miki, Y., Sato, H., Taketomi, Y., Yokoyama, K., Kobayashi, T., Tokuoka, S.M., Kita, Y., Yoda, E., Hara, S., Mikami, K., Nishito, Y., Kikuchi, N., Nakata, R., Kaneko, M., Kiyonari, H., Kasahara, K., Aiba, T., Ikeda, K., Soga, T., Kurano, M., Yatomi, Y. and Murakami, M., 2023. Hepatic phosphatidylcholine catabolism driven by PNPLA7 and PNPLA8 supplies endogenous choline to replenish the methionine cycle with methyl groups. *Cell Reports*, 42(2), 111940. https://doi.org/10.1016/j.celrep.2022.111940.

Hirz, T., Mei, S., Sarkar, H., Kfoury, Y., Wu, S., Verhoeven, B.M., Subtelny, A.O., Zlatev, D.V., Wszolek, M.W., Salari, K., Murray, E., Chen, F., Macosko, E.Z., Wu, C.-L., Scadden, D.T., Dahl, D.M., Baryawno, N., Saylor, P.J., Kharchenko, P.V. and Sykes, D.B., 2023. Dissecting the immune suppressive human prostate tumor microenvironment via integrated single-cell and spatial

transcriptomic analyses. *Nature Communications*, 14(1), 663. https://doi.org/10.1038/s41467-023-36325-2.

Horoszewicz, J.S., Leong, S.S., Kawinski, E., Karr, J.P., Rosenthal, H., Chu, T.M., Mirand, E.A. and Murphy, G.P., 1983. LNCaP model of human prostatic carcinoma. *Cancer Research*, 43(4), pp. 1809–1818.

Huang, F.W., Song, H., Weinstein, H.N., Xie, J., Cooperberg, M.R., Hicks, J., Mummert, L., De Marzo, A.M. and Sfanos, K.S., 2023. Club-like cells in proliferative inflammatory atrophy of the prostate. *The Journal of Pathology*, 261(1), pp. 85–95. https://doi.org/10.1002/path.6149.

Huang, W.-C., Li, X., Liu, J., Lin, J. and Chung, L.W.K., 2012. Activation of Androgen Receptor, Lipogenesis, and Oxidative Stress Converged by SREBP-1 Is Responsible for Regulating Growth and Progression of Prostate Cancer Cells. *Molecular Cancer Research*, 10(1), pp. 133–142. https://doi.org/10.1158/1541-7786.MCR-11-0206.

Hyun, J.S., 2017. Clinical Significance of Prostatic Calculi: A Review. *The World Journal of Men's Health*, 36(1), pp. 15–21. https://doi.org/10.5534/wjmh.17018.

Ippolito, L., Comito, G., Parri, M., Iozzo, M., Duatti, A., Virgilio, F., Lorito, N., Bacci, M., Pardella, E., Sandrini, G., Bianchini, F., Damiano, R., Ferrone, L., la Marca, G., Serni, S., Spatafora, P., Catapano, C.V., Morandi, A., Giannoni, E. and Chiarugi, P., 2022. Lactate Rewires Lipid Metabolism and Sustains a Metabolic–Epigenetic Axis in Prostate Cancer. *Cancer Research*, 82(7), pp. 1267–1282. https://doi.org/10.1158/0008-5472.CAN-21-0914.

Ishiguro, H. and Kawahara, T., 2014. Nonsteroidal Anti-Inflammatory Drugs and Prostatic Diseases. *BioMed Research International*, 2014(1), 436123. https://doi.org/10.1155/2014/436123.

James, N.D., Tannock, I., N'Dow, J., Feng, F., Gillessen, S., Ali, S.A., Trujillo, B., Al-Lazikani, B., Attard, G., Bray, F., Compérat, E., Eeles, R., Fatiregun, O., Grist, E., Halabi, S., Haran, Á., Herchenhorn, D., Hofman, M.S., Jalloh, M., Loeb, S., MacNair, A., Mahal, B., Mendes, L., Moghul, M., Moore, C., Morgans, A., Morris, M., Murphy, D., Murthy, V., Nguyen, P.L., Padhani, A., Parker, C., Rush, H., Sculpher, M., Soule, H., Sydes, M.R., Tilki, D., Tunariu, N., Villanti, P. and Xie, L.-P., 2024. The Lancet Commission on prostate cancer: planning for the surge in cases. *The Lancet*, 403(10437), pp.1683–1722. https://doi.org/10.1016/S0140-6736(24)00651-2.

Jia, Y., Liu, X., Yan, J., Chong, L., Li, L., Ma, A., Zhou, L. and Sun, Z., 2015. The alteration of inflammatory markers and apoptosis on chronic prostatitis induced by estrogen and androgen. *International Urology and Nephrology*, 47(1), pp. 39–46. https://doi.org/10.1007/s11255-014-0845-4.

Jiang, J., Soh, P.X.Y., Mutambirwa, S.B.A., Bornman, M.S.R., Haiman, C.A., Hayes, V.M. and Jaratlerdsiri, W., 2024. ANO7 African-ancestral genomic diversity and advanced prostate cancer. *Prostate Cancer and Prostatic Diseases*, 27(3), pp.558–565. https://doi.org/10.1038/s41391-023-00722-x.

Jin, R., Yi, Y., Yull, F.E., Blackwell, T.S., Clark, P.E., Koyama, T., Smith, J.A., Jr and Matusik, R.J., 2014. NF-κB Gene Signature Predicts Prostate Cancer Progression. *Cancer Research*, 74(10), pp. 2763–2772. https://doi.org/10.1158/0008-5472.CAN-13-2543.

Jin, Y., Zhang, M., Tong, Y., Qiu, L., Ye, Y. and Zhao, B., 2023. DCXR promotes cell proliferation by promoting the activity of aerobic glycolysis in breast cancer. *Molecular Medicine Reports*, 27(2), pp. 1–10. https://doi.org/10.3892/mmr.2022.12918.

Jing, Z., Liu, Q., He, X., Jia, Z., Xu, Z., Yang, B. and Liu, P., 2022a. NCAPD3 enhances Warburg effect through c-myc and E2F1 and promotes the occurrence and progression of colorectal cancer. *Journal of Experimental & Clinical Cancer Research*, 41(1), 198. https://doi.org/10.1186/s13046-022-02412-3.

Jing, Z., Liu, Q., Xie, W., Wei, Y., Liu, J., Zhang, Y., Zuo, W., Lu, S., Zhu, Q. and Liu, P., 2022b. NCAPD3 promotes prostate cancer progression by up-regulating EZH2 and MALAT1 through STAT3 and E2F1. *Cellular Signalling*, 92, 110265. https://doi.org/10.1016/j.cellsig.2022.110265.

Joseph, D.B., Henry, G.H., Malewska, A., Reese, J.C., Mauck, R.J., Gahan, J.C., Hutchinson, R.C., Mohler, J.L., Roehrborn, C.G. and Strand, D.W., 2022. 5-Alpha reductase inhibitors induce a

prostate luminal to club cell transition in human benign prostatic hyperplasia. *The Journal of Pathology*, 256(4), pp. 427–441. https://doi.org/10.1002/path.5857.

Kaikkonen, E., Ettala, O., Nikulainen, I., Taimen, P., Lehtinen, I., Boström, P.J., Kellokumpu-Lehtinen, P.-L. and Schleutker, J., 2019. ANO7 rs77559646 Is Associated With First-line Docetaxel Treatment Response in Metastatic Castration-resistant Prostate Cancer. *Anticancer Research*, 39(10), pp. 5353–5359. https://doi.org/10.21873/anticanres.13728.

Kaikkonen, E., Rantapero, T., Zhang, Q., Taimen, P., Laitinen, V., Kallajoki, M., Jambulingam, D., Ettala, O., Knaapila, J., Boström, P.J., Wahlström, G., Sipeky, C., Pursiheimo, J.-P., Tammela, T., Kellokumpu-Lehtinen, P.-L., Fey, V., Maehle, L., Wiklund, F., Wei, G.-H. and Schleutker, J., 2018. ANO7 is associated with aggressive prostate cancer. *International Journal of Cancer*, 143(10), pp. 2479–2487. https://doi.org/10.1002/ijc.31746.

Kaikkonen, E., Takala, A., Pursiheimo, J.-P., Wahlström, G. and Schleutker, J., 2020. The interactome of the prostate-specific protein Anoctamin 7. *Cancer Biomarkers*, 28(1), pp. 91–100. https://doi.org/10.3233/CBM-190993.

Kalienkova, V., Clerico Mosina, V. and Paulino, C., 2021. The Groovy TMEM16 Family: Molecular Mechanisms of Lipid Scrambling and Ion Conduction. *Journal of Molecular Biology*, 433(16), 166941. https://doi.org/10.1016/j.jmb.2021.166941.

Kallio, M.A., Tuimala, J.T., Hupponen, T., Klemelä, P., Gentile, M., Scheinin, I., Koski, M., Käki, J. and Korpelainen, E.I., 2011. Chipster: user-friendly analysis software for microarray and other high-throughput data. *BMC Genomics*, 12(1), 507. https://doi.org/10.1186/1471-2164-12-507.

Kellokumpu-Lehtinen, P.-L., Harmenberg, U., Joensuu, T., McDermott, R., Hervonen, P., Ginman, C., Luukkaa, M., Nyandoto, P., Hemminki, A., Nilsson, S., McCaffrey, J., Asola, R., Turpeenniemi-Hujanen, T., Laestadius, F., Tasmuth, T., Sandberg, K., Keane, M., Lehtinen, I., Luukkaala, T. and Joensuu, H., 2013. 2-weekly versus 3-weekly docetaxel to treat castration-resistant advanced prostate cancer: a randomised, phase 3 trial. *The Lancet Oncology*, 14(2), pp. 117–124. https://doi.org/10.1016/S1470-2045(12)70537-5.

Korenchuk, S., Lehr, J.E., MClean, L., Lee, Y.G., Whitney, S., Vessella, R., Lin, D.L. and Pienta, K.J., 2001. VCaP, a cell-based model system of human prostate cancer. *In Vivo (Athens, Greece)*, 15(2), pp. 163–168.

Koundouros, N., Karali, E., Tripp, A., Valle, A., Inglese, P., Perry, N.J.S., Magee, D.J., Anjomani Virmouni, S., Elder, G.A., Tyson, A.L., Dória, M.L., van Weverwijk, A., Soares, R.F., Isacke, C.M., Nicholson, J.K., Glen, R.C., Takats, Z. and Poulogiannis, G., 2020. Metabolic Fingerprinting Links Oncogenic *PIK3CA* with Enhanced Arachidonic Acid-Derived Eicosanoids. *Cell*, 181(7), pp. 1596-1611.e27. https://doi.org/10.1016/j.cell.2020.05.053.

Kukkonen, K., Taavitsainen, S., Huhtala, L., Uusi-Makela, J., Granberg, K.J., Nykter, M. and Urbanucci, A., 2021. Chromatin and Epigenetic Dysregulation of Prostate Cancer Development, Progression, and Therapeutic Response. *Cancers*, 13(13), p.3325. https://doi.org/10.3390/cancers13133325.

Kukurugya, M.A., Rosset, S. and Titov, D.V., 2024. The Warburg Effect is the result of faster ATP production by glycolysis than respiration. *Proceedings of the National Academy of Sciences*, 121(46), e2409509121. https://doi.org/10.1073/pnas.2409509121.

Kumar, T., Nee, K., Wei, R., He, S., Nguyen, Q.H., Bai, S., Blake, K., Pein, M., Gong, Y., Sei, E., Hu, M., Casasent, A.K., Thennavan, A., Li, J., Tran, T., Chen, K., Nilges, B., Kashikar, N., Braubach, O., Ben Cheikh, B., Nikulina, N., Chen, H., Teshome, M., Menegaz, B., Javaid, H., Nagi, C., Montalvan, J., Lev, T., Mallya, S., Tifrea, D.F., Edwards, R., Lin, E., Parajuli, R., Hanson, S., Winocour, S., Thompson, A., Lim, B., Lawson, D.A., Kessenbrock, K. and Navin, N., 2023. A spatially resolved single-cell genomic atlas of the adult human breast. *Nature*, 620(7972), pp. 181–191. https://doi.org/10.1038/s41586-023-06252-9.

Kunisaki, C., 2020. Role of the Anoctamin Family in Various Carcinomas. *Annals of Surgical Oncology*, 27(9), pp. 3112–3114. https://doi.org/10.1245/s10434-020-08371-3.

Laffont, S., Blanquart, E., Savignac, M., Cénac, C., Laverny, G., Metzger, D., Girard, J.-P., Belz, G.T., Pelletier, L., Seillet, C. and Guéry, J.-C., 2017. Androgen signaling negatively controls group 2 innate lymphoid cells. *Journal of Experimental Medicine*, 214(6), pp. 1581–1592. https://doi.org/10.1084/jem.20161807.

Lavallée, E., Bergeron, M., Buteau, F.-A., Blouin, A.-C., Duchesnay, N., Dujardin, T., Tiguert, R., Lacombe, L., Fradet, V., Makao-Nguile, M., Fradet, Y., Beauregard, J.-M. and Pouliot, F., 2019. Increased Prostate Cancer Glucose Metabolism Detected by 18F-fluorodeoxyglucose Positron Emission Tomography/Computed Tomography in Localised Gleason 8–10 Prostate Cancers Identifies Very High–risk Patients for Early Recurrence and Resistance to Castration. *European Urology Focus*, 5(6), pp.998–1006. https://doi.org/10.1016/j.euf.2018.03.008.

Lee, S.H. and Shen, M.M., 2015. Cell types of origin for prostate cancer. *Current Opinion in Cell Biology*, 37, pp. 35–41. https://doi.org/10.1016/j.ceb.2015.10.002.

van Leenders, G.J.L.H., van der Kwast, T.H., Grignon, D.J., Evans, A.J., Kristiansen, G., Kweldam, C.F., Litjens, G., McKenney, J.K., Melamed, J., Mottet, N., Paner, G.P., Samaratunga, H., Schoots, I.G., Simko, J.P., Tsuzuki, T., Varma, M., Warren, A.Y., Wheeler, T.M., Williamson, S.R. and Iczkowski, K.A., 2020. The 2019 International Society of Urological Pathology (ISUP) Consensus Conference on Grading of Prostatic Carcinoma. *The American Journal of Surgical Pathology*, 44(8), pp. e87–e99. https://doi.org/10.1097/PAS.0000000000001497.

Leibovitz, A., Baumoehl, Y. and Segal, R., 2004. Increased incidence of pathological and clinical prostate cancer with age: age related alterations of local immune surveillance. *The Journal of Urology*, 172(2), pp. 435–437. https://doi.org/10.1097/01.ju.0000131908.19114.d3.

Liberzon, A., Birger, C., Thorvaldsdóttir, H., Ghandi, M., Mesirov, J.P. and Tamayo, P., 2015. The Molecular Signatures Database Hallmark Gene Set Collection. *Cell Systems*, 1(6), pp. 417–425. https://doi.org/10.1016/j.cels.2015.12.004.

Lin, B., Shah, V.S., Chernoff, C., Sun, J., Shipkovenska, G.G., Vinarsky, V., Waghray, A., Xu, J., Leduc, A.D., Hintschich, C.A., Surve, M.V., Xu, Y., Capen, D.E., Villoria, J., Dou, Z., Hariri, L.P. and Rajagopal, J., 2024. Airway hillocks are injury-resistant reservoirs of unique plastic stem cells. *Nature*, 629(8013), pp. 869–877. https://doi.org/10.1038/s41586-024-07377-1.

Löf, C., Sultana, N., Goel, N., Heron, S., Wahlström, G., House, A., Holopainen, M., Käkelä, R. and Schleutker, J., 2025. ANO7 expression in the prostate modulates mitochondrial function and lipid metabolism. *Cell Communication and Signaling*, 23(1), 71. https://doi.org/10.1186/s12964-025-02081-7.

Lucas, J.M., Heinlein, C., Kim, T., Hernandez, S.A., Malik, M.S., True, L.D., Morrissey, C., Corey, E., Montgomery, B., Mostaghel, E., Clegg, N., Coleman, I., Brown, C.M., Schneider, E.L., Craik, C., Simon, J.A., Bedalov, A. and Nelson, P.S., 2014. The androgen-regulated protease TMPRSS2 activates a proteolytic cascade involving components of the tumor microenvironment and promotes prostate cancer metastasis. *Cancer Discovery*, 4(11), pp. 1310–1325. https://doi.org/10.1158/2159-8290.CD-13-1010.

Mah, C.Y., Nassar, Z.D., Swinnen, J.V. and Butler, L.M., 2020. Lipogenic effects of androgen signaling in normal and malignant prostate. *Asian Journal of Urology*, 7(3), pp. 258–270. https://doi.org/10.1016/j.ajur.2019.12.003.

Malinen, M., Niskanen, E.A., Kaikkonen, M.U. and Palvimo, J.J., 2017. Crosstalk between androgen and pro-inflammatory signaling remodels androgen receptor and NF-κB cistrome to reprogram the prostate cancer cell transcriptome. *Nucleic Acids Research*, 45(2), pp. 619–630. https://doi.org/10.1093/nar/gkw855.

Maratt, J.K. and Stoffel, E., 2022. Identification of Lynch Syndrome. *Gastrointestinal Endoscopy Clinics of North America*, 32(1), pp. 45–58. https://doi.org/10.1016/j.giec.2021.09.002.

Marx, A., Koopmann, L., Höflmayer, D., Büscheck, F., Hube-Magg, C., Steurer, S., Eichenauer, T., Clauditz, T.S., Wilczak, W., Simon, R., Sauter, G., Izbicki, J.R., Huland, H., Heinzer, H., Graefen, M., Haese, A., Schlomm, T., Bernreuther, C., Lebok, P. and Bonk, S., 2021. Reduced anoctamin 7 (ANO7) expression is a strong and independent predictor of poor prognosis in prostate cancer.

Cancer Biology & Medicine, 18(1), pp. 245–255. https://doi.org/10.20892/j.issn.2095-3941.2019.0324.

McNeal, J.E., 1968. Regional morphology and pathology of the prostate. *American Journal of Clinical Pathology*, 49(3), pp.347–357. https://doi.org/10.1093/ajcp/49.3.347.

McNeal, J.E., 1981. The zonal anatomy of the prostate. *The Prostate*, 2(1), pp. 35–49. https://doi.org/10.1002/pros.2990020105.

Meng, J., Mostaghel, E.A., Vakar-Lopez, F., Montgomery, B., True, L. and Nelson, P.S., 2011. Testosterone Regulates Tight Junction Proteins and Influences Prostatic Autoimmune Responses. *Hormones & Cancer*, 2(3), p.145. https://doi.org/10.1007/s12672-010-0063-1.

Minnery, C.H. and Getzenberg, R.H., 2005. Benign prostatic hyperplasia cell line viability and modulation of jm-27 by doxazosin and Ibuprofen. *The Journal of Urology*, 174(1), pp. 375–379. https://doi.org/10.1097/01.ju.0000161598.24740.34.

Mizuno, K. and Beltran, H., 2022. Future directions for precision oncology in prostate cancer. *The Prostate*, 82(S1), pp. S86–S96. https://doi.org/10.1002/pros.24354.

Mohsenzadegan, M., Madjd, Z., Asgari, M., Abolhasani, M., Shekarabi, M., Taeb, J. and Shariftabrizi, A., 2013. Reduced expression of NGEP is associated with high-grade prostate cancers: a tissue microarray analysis. *Cancer Immunology, Immunotherapy*, 62(10), pp. 1609–1618. https://doi.org/10.1007/s00262-013-1463-1.

Mohsenzadegan, M., Shekarabi, M., Madjd, Z., Asgari, M., Abolhasani, M., Tajik, N. and Farajollahi, M.M., 2015. Study of NGEP expression pattern in cancerous tissues provides novel insights into prognostic marker in prostate cancer. *Biomarkers in Medicine*, 9(4), pp. 391–401. https://doi.org/10.2217/bmm.14.106.

Mucci, L.A., Hjelmborg, J.B., Harris, J.R., Czene, K., Havelick, D.J., Scheike, T., Graff, R.E., Holst, K., Möller, S., Unger, R.H., McIntosh, C., Nuttall, E., Brandt, I., Penney, K.L., Hartman, M., Kraft, P., Parmigiani, G., Christensen, K., Koskenvuo, M., Holm, N.V., Heikkilä, K., Pukkala, E., Skytthe, A., Adami, H.-O., Kaprio, J., and for the Nordic Twin Study of Cancer (NorTwinCan) Collaboration, 2016. Familial Risk and Heritability of Cancer Among Twins in Nordic Countries. *JAMA*, 315(1), pp. 68–76. https://doi.org/10.1001/jama.2015.17703.

Navone, N.M., Olive, M., Ozen, M., Davis, R., Troncoso, P., Tu, S.M., Johnston, D., Pollack, A., Pathak, S., Eschenbach, A.C. von and Logothetis, C.J., 1997. Establishment of two human prostate cancer cell lines derived from a single bone metastasis. *Clinical Cancer Research*, 3(12), pp. 2493–2500.

Netskar, H., Pfefferle, A., Goodridge, J.P., Sohlberg, E., Dufva, O., Teichmann, S.A., Brownlie, D., Michaëlsson, J., Marquardt, N., Clancy, T., Horowitz, A. and Malmberg, K.-J., 2024. Pan-cancer profiling of tumor-infiltrating natural killer cells through transcriptional reference mapping. *Nature Immunology*, 25(8), pp. 1445–1459. https://doi.org/10.1038/s41590-024-01884-z.

Nguyen, T.M., Kabotyanski, E.B., Reineke, L.C., Shao, J., Xiong, F., Lee, J.-H., Dubrulle, J., Johnson, H., Stossi, F., Tsoi, P.S., Choi, K.-J., Ellis, A.G., Zhao, N., Cao, J., Adewunmi, O., Ferreon, J.C., Ferreon, A.C.M., Neilson, J.R., Mancini, M.A., Chen, X., Kim, J., Ma, L., Li, W. and Rosen, J.M., 2020. The SINEB1 element in the long non-coding RNA Malat1 is necessary for TDP-43 proteostasis. *Nucleic Acids Research*, 48(5), pp. 2621–2642. https://doi.org/10.1093/nar/gkz1176.

Nickel, J.C., Roehrborn, C.G., O'Leary, M.P., Bostwick, D.G., Somerville, M.C. and Rittmaster, R.S., 2008. The Relationship between Prostate Inflammation and Lower Urinary Tract Symptoms: Examination of Baseline Data from the REDUCE Trial. *European Urology*, 54(6), pp. 1379–1384. https://doi.org/10.1016/j.eururo.2007.11.026.

Nussinov, R., Zhang, W., Liu, Y. and Jang, H., 2024. Mitogen signaling strength and duration can control cell cycle decisions. *Science Advances*, 10(27), eadm9211. https://doi.org/10.1126/sciadv.adm9211.

Parad, R.B., 2022. An oversight regarding the club cell? *Pediatric Pulmonology*, 57(9), pp. 2252–2252. https://doi.org/10.1002/ppul.25970.

Parga-Vidal, L. and Gisbergen, K.P. van, 2020. Area under Immunosurveillance: Dedicated Roles of Memory CD8 T-Cell Subsets. *Cold Spring Harbor Perspectives in Biology*, 12(11), a037796. https://doi.org/10.1101/cshperspect.a037796.

Pelletier, G., 2008. Expression of steroidogenic enzymes and sex-steroid receptors in human prostate. *Best Practice & Research Clinical Endocrinology & Metabolism*, 22(2), pp. 223–228. https://doi.org/10.1016/j.beem.2008.02.004.

Pitkäniemi, J., Malila, N., Heikkinen, S. and Seppa, K., 2024. *Cancer in Finland 2022*.

Pletcher, A. and Shibata, M., 2022. Prostate organogenesis. *Development*, 149(12), dev200394. https://doi.org/10.1242/dev.200394.

Rajendran, M., Dane, E., Conley, J. and Tantama, M., 2016. Imaging Adenosine Triphosphate (ATP). *The Biological Bulletin*, 231(1), pp. 73–84. https://doi.org/10.1086/689592.

Rebbeck, T.R., Devesa, S.S., Chang, B.-L., Bunker, C.H., Cheng, I., Cooney, K., Eeles, R., Fernandez, P., Giri, V.N., Gueye, S.M., Haiman, C.A., Henderson, B.E., Heyns, C.F., Hu, J.J., Ingles, S.A., Isaacs, W., Jalloh, M., John, E.M., Kibel, A.S., Kidd, L.R., Layne, P., Leach, R.J., Neslund-Dudas, C., Okobia, M.N., Ostrander, E.A., Park, J.Y., Patrick, A.L., Phelan, C.M., Ragin, C., Roberts, R.A., Rybicki, B.A., Stanford, J.L., Strom, S., Thompson, I.M., Witte, J., Xu, J., Yeboah, E., Hsing, A.W. and Zeigler-Johnson, C.M., 2013. Global Patterns of Prostate Cancer Incidence, Aggressiveness, and Mortality in Men of African Descent. *Prostate Cancer*, 2013(1), 560857. https://doi.org/10.1155/2013/560857.

Risbridger, G.P., 2018. Prostate Disease Overview. In: M.K. Skinner, ed. *Encyclopedia of Reproduction (Second Edition)*. [online] Oxford: Academic Press. pp. 334–340. https://doi.org/10.1016/B978-0-12-801238-3.64373-8.

Rizzo, M., 2021. Mechanisms of docetaxel resistance in prostate cancer: The key role played by miRNAs. *Biochimica et Biophysica Acta (BBA) - Reviews on Cancer*, 1875(1), 188481. https://doi.org/10.1016/j.bbcan.2020.188481.

Robinson, D., Van Allen, E.M., Wu, Y.-M., Schultz, N., Lonigro, R.J., Mosquera, J.-M., Montgomery, B., Taplin, M.-E., Pritchard, C.C., Attard, G., Beltran, H., Abida, W., Bradley, R.K., Vinson, J., Cao, X., Vats, P., Kunju, L.P., Hussain, M., Feng, F.Y., Tomlins, S.A., Cooney, K.A., Smith, D.C., Brennan, C., Siddiqui, J., Mehra, R., Chen, Y., Rathkopf, D.E., Morris, M.J., Solomon, S.B., Durack, J.C., Reuter, V.E., Gopalan, A., Gao, J., Loda, M., Lis, R.T., Bowden, M., Balk, S.P., Gaviola, G., Sougnez, C., Gupta, M., Yu, E.Y., Mostaghel, E.A., Cheng, H.H., Mulcahy, H., True, L.D., Plymate, S.R., Dvinge, H., Ferraldeschi, R., Flohr, P., Miranda, S., Zafeiriou, Z., Tunariu, N., Mateo, J., Perez-Lopez, R., Demichelis, F., Robinson, B.D., Schiffman, M., Nanus, D.M., Tagawa, S.T., Sigaras, A., Eng, K.W., Elemento, O., Sboner, A., Heath, E.I., Scher, H.I., Pienta, K.J., Kantoff, P., de Bono, J.S., Rubin, M.A., Nelson, P.S., Garraway, L.A., Sawyers, C.L. and Chinnaiyan, A.M., 2015. Integrative Clinical Genomics of Advanced Prostate Cancer. *Cell*, 161(5), pp. 1215–1228. https://doi.org/10.1016/j.cell.2015.05.001.

Saxton, R.A. and Sabatini, D.M., 2017. mTOR Signaling in Growth, Metabolism, and Disease. *Cell*, 168(6), pp. 960–976. https://doi.org/10.1016/j.cell.2017.02.004.

Saydullaeva, I., Butuner, B.D. and Korkmaz, K.S., 2023. NKX3.1 Expression Contributes to Epithelial–Mesenchymal Transition of Prostate Cancer Cells. *ACS Omega*, 8(36), pp. 32580–32592. https://doi.org/10.1021/acsomega.3c03127.

Schreiber, R., Ousingsawat, J. and Kunzelmann, K., 2024. Epithelial Anoctamins. *Cell Calcium*, 120, 102885. https://doi.org/10.1016/j.ceca.2024.102885.

Scott, K.E.N., Wheeler, F.B., Davis, A.L., Thomas, M.J., Ntambi, J.M., Seals, D.F. and Kridel, S.J., 2012. Metabolic Regulation of Invadopodia and Invasion by Acetyl-CoA Carboxylase 1 and De novo Lipogenesis. *PLOS ONE*, 7(1), e29761. https://doi.org/10.1371/journal.pone.0029761.

Sena, L.A. and Denmeade, S.R., 2021. Fatty Acid Synthesis in Prostate Cancer: Vulnerability or Epiphenomenon? *Cancer Research*, 81(17), pp. 4385–4393. https://doi.org/10.1158/0008-5472.CAN-21-1392.

Shannon, P., Markiel, A., Ozier, O., Baliga, N.S., Wang, J.T., Ramage, D., Amin, N., Schwikowski, B. and Ideker, T., 2003. Cytoscape: a software environment for integrated models of biomolecular interaction networks. *Genome Research*, 13(11), pp. 2498–2504. https://doi.org/10.1101/gr.1239303.

Siegel, R.L., Giaquinto, A.N. and Jemal, A., 2024. Cancer statistics, 2024. *CA: A Cancer Journal for Clinicians*, 74(1), pp. 12–49. https://doi.org/10.3322/caac.21820.

Sigorski, D., Gulczyński, J., Sejda, A., Rogowski, W. and Iżycka-Świeszewska, E., 2021. Investigation of Neural Microenvironment in Prostate Cancer in Context of Neural Density, Perineural Invasion, and Neuroendocrine Profile of Tumors. *Frontiers in Oncology*, 11, 710899. https://doi.org/10.3389/fonc.2021.710899.

Singh, K.B., Hahm, E.-R., Kim, S.-H., Wendell, S.G. and Singh, S.V., 2021. A novel metabolic function of Myc in regulation of fatty acid synthesis in prostate cancer. *Oncogene*, 40(3), pp. 592–602. https://doi.org/10.1038/s41388-020-01553-z.

Singh, N. and Bhalla, N., 2020. Moonlighting Proteins. *Annual Review of Genetics*, 54, pp. 265–285. https://doi.org/10.1146/annurev-genet-030620-102906.

Sinnott, J.A., Peisch, S.F., Tyekucheva, S., Gerke, T., Lis, R., Rider, J.R., Fiorentino, M., Stampfer, M.J., Mucci, L.A., Loda, M. and Penney, K.L., 2017. Prognostic Utility of a New mRNA Expression Signature of Gleason Score. *Clinical Cancer Research*, 23(1), pp. 81–87. https://doi.org/10.1158/1078-0432.CCR-16-1245.

Siolas, D., Lerner, C., Burchard, J., Ge, W., Linsley, P.S., Paddison, P.J., Hannon, G.J. and Cleary, M.A., 2005. Synthetic shRNAs as potent RNAi triggers. *Nature Biotechnology*, 23(2), pp. 227–231. https://doi.org/10.1038/nbt1052.

Smyth, G.K., 2004. Linear Models and Empirical Bayes Methods for Assessing Differential Expression in Microarray Experiments. *Statistical Applications in Genetics and Molecular Biology*, 3(1). https://doi.org/10.2202/1544-6115.1027.

Smyth, G.K., Michaud, J. and Scott, H.S., 2005. Use of within-array replicate spots for assessing differential expression in microarray experiments. *Bioinformatics*, 21(9), pp. 2067–2075. https://doi.org/10.1093/bioinformatics/bti270.

Song, H., Weinstein, H.N.W., Allegakoen, P., Wadsworth, M.H., Xie, J., Yang, H., Castro, E.A., Lu, K.L., Stohr, B.A., Feng, F.Y., Carroll, P.R., Wang, B., Cooperberg, M.R., Shalek, A.K. and Huang, F.W., 2022. Single-cell analysis of human primary prostate cancer reveals the heterogeneity of tumor-associated epithelial cell states. *Nature Communications*, 13(1), 141. https://doi.org/10.1038/s41467-021-27322-4.

Sramkoski, R.M., Pretlow, T.G., Giaconia, J.M., Pretlow, T.P., Schwartz, S., Sy, M.-S., Marengo, S.R., Rhim, J.S., Zhang, D. and Jacobberger, J.W., 1999. A new human prostate carcinoma cell line, 22Rv1. *In Vitro Cellular & Developmental Biology - Animal*, 35(7), pp. 403–409. https://doi.org/10.1007/s11626-999-0115-4.

Subramanian, A., Tamayo, P., Mootha, V.K., Mukherjee, S., Ebert, B.L., Gillette, M.A., Paulovich, A., Pomeroy, S.L., Golub, T.R., Lander, E.S. and Mesirov, J.P., 2005. Gene set enrichment analysis: A knowledge-based approach for interpreting genome-wide expression profiles. *Proceedings of the National Academy of Sciences*, 102(43), pp. 15545–15550. https://doi.org/10.1073/pnas.0506580102.

Sung, H., Ferlay, J., Siegel, R.L., Laversanne, M., Soerjomataram, I., Jemal, A. and Bray, F., 2021. Global Cancer Statistics 2020: GLOBOCAN Estimates of Incidence and Mortality Worldwide for 36 Cancers in 185 Countries. *CA: A Cancer Journal for Clinicians*, 71(3), pp. 209–249. https://doi.org/10.3322/caac.21660.

Sung, Y., Yu, Y.C. and Han, J.M., 2023. Nutrient sensors and their crosstalk. *Experimental & Molecular Medicine*, 55(6), pp.1076–1089. https://doi.org/10.1038/s12276-023-01006-z.

Suzuki, J., Umeda, M., Sims, P.J. and Nagata, S., 2010. Calcium-dependent phospholipid scrambling by TMEM16F. *Nature*, 468(7325), pp. 834–838. https://doi.org/10.1038/nature09583.

Swinnen, J.V., Van Veldhoven, P.P., Esquenet, M., Heyns, W. and Verhoeven, G., 1996. Androgens markedly stimulate the accumulation of neutral lipids in the human prostatic adenocarcinoma cell line LNCaP. *Endocrinology*, 137(10), pp. 4468–4474. https://doi.org/10.1210/endo.137.10.8828509.

Tian, Y., Schreiber, R. and Kunzelmann, K., 2012. Anoctamins are a family of Ca2+-activated Cl− channels. *Journal of Cell Science*, 125(21), pp.4991–4998. https://doi.org/10.1242/jcs.109553.

Toivanen, R. and Shen, M.M., 2017. Prostate organogenesis: tissue induction, hormonal regulation and cell type specification. *Development*, 144(8), pp. 1382–1398. https://doi.org/10.1242/dev.148270.

Uren, P.J., Bahrami-Samani, E., Araujo, P.R. de, Vogel, C., Qiao, M., Burns, S.C., Smith, A.D. and Penalva, L.O.F., 2016. High-throughput analyses of hnRNP H1 dissects its multi-functional aspect. *RNA Biology*, 13(4), pp.400–411. https://doi.org/10.1080/15476286.2015.1138030.

Verze, P., Cai, T. and Lorenzetti, S., 2016. The role of the prostate in male fertility, health and disease. *Nature Reviews Urology*, 13(7), pp. 379–386. https://doi.org/10.1038/nrurol.2016.89.

Wahlström, G., Heron, S., Knuuttila, M., Kaikkonen, E., Tulonen, N., Metsälä, O., Löf, C., Ettala, O., Boström, P.J., Taimen, P., Poutanen, M. and Schleutker, J., 2022. The variant rs77559646 associated with aggressive prostate cancer disrupts ANO7 mRNA splicing and protein expression. *Human Molecular Genetics*, 31(12), pp. 2063–2077. https://doi.org/10.1093/hmg/ddac012.

Walker, J.A. and McKenzie, A.N.J., 2018. TH2 cell development and function. *Nature Reviews Immunology*, 18(2), pp. 121–133. https://doi.org/10.1038/nri.2017.118.

Wang, B., Wu, L., Chen, J., Dong, L., Chen, C., Wen, Z., Hu, J., Fleming, I. and Wang, D.W., 2021. Metabolism pathways of arachidonic acids: mechanisms and potential therapeutic targets. *Signal Transduction and Targeted Therapy*, 6(1), pp. 1–30. https://doi.org/10.1038/s41392-020-00443-w.

Wang, F., Koul, S., Shanmugam, P.S.T., Dong, Q. and Koul, H.K., 2018. Prostate-Derived Ets Factor (PDEF) Inhibits Metastasis by Inducing Epithelial/Luminal Phenotype in Prostate Cancer Cells. *Molecular Cancer Research*, 16(9), pp. 1430–1440. https://doi.org/10.1158/1541-7786.MCR-18-0010.

Wang, M., Wisniewski, C.A., Xiong, C., Chhoy, P., Goel, H.L., Kumar, A., Zhu, L.J., Li, R., St. Louis, P.A., Ferreira, L.M., Pakula, H., Xu, Z., Loda, M., Jiang, Z., Brehm, M.A. and Mercurio, A.M., 2023. Therapeutic blocking of VEGF binding to neuropilin-2 diminishes PD-L1 expression to activate antitumor immunity in prostate cancer. *Science Translational Medicine*, 15(694), eade5855. https://doi.org/10.1126/scitranslmed.ade5855.

Wang, Y. and Kinoshita, T., 2023. The role of lipid scramblases in regulating lipid distributions at cellular membranes. *Biochemical Society Transactions*, 51(5), pp. 1857–1869. https://doi.org/10.1042/BST20221455.

Warburg, O., 1956. On the Origin of Cancer Cells. *Science*, 123(3191), pp. 309–314. https://doi.org/10.1126/science.123.3191.309.

Weber, J.D., Raben, D.M., Phillips, P.J. and Baldassare, J.J., 1997. Sustained activation of extracellular-signal-regulated kinase 1 (ERK1) is required for the continued expression of cyclin D1 in G1 phase. *Biochemical Journal*, 326(1), pp. 61–68. https://doi.org/10.1042/bj3260061.

Wedge, D.C., Gundem, G., Mitchell, T., Woodcock, D.J., Martincorena, I., Ghori, M., Zamora, J., Butler, A., Whitaker, H., Kote-Jarai, Z., Alexandrov, L.B., Van Loo, P., Massie, C.E., Dentro, S., Warren, A.Y., Verrill, C., Berney, D.M., Dennis, N., Merson, S., Hawkins, S., Howat, W., Lu, Y.-J., Lambert, A., Kay, J., Kremeyer, B., Karaszi, K., Luxton, H., Camacho, N., Marsden, L., Edwards, S., Matthews, L., Bo, V., Leongamornlert, D., McLaren, S., Ng, A., Yu, Y., Zhang, H., Dadaev, T., Thomas, S., Easton, D.F., Ahmed, M., Bancroft, E., Fisher, C., Livni, N., Nicol, D., Tavaré, S., Gill, P., Greenman, C., Khoo, V., Van As, N., Kumar, P., Ogden, C., Cahill, D., Thompson, A., Mayer, E., Rowe, E., Dudderidge, T., Gnanapragasam, V., Shah, N.C., Raine, K., Jones, D., Menzies, A., Stebbings, L., Teague, J., Hazell, S., Corbishley, C., de Bono, J., Attard, G., Isaacs, W., Visakorpi, T., Fraser, M., Boutros, P.C., Bristow, R.G., Workman, P., Sander, C., Hamdy, F.C., Futreal, A., McDermott, U., Al-Lazikani, B., Lynch, A.G., Bova, G.S., Foster, C.S.,

Brewer, D.S., Neal, D.E., Cooper, C.S. and Eeles, R.A., 2018. Sequencing of prostate cancers identifies new cancer genes, routes of progression and drug targets. *Nature Genetics*, 50(5), pp. 682–692. https://doi.org/10.1038/s41588-018-0086-z.

Xu, Y., Chen, S.-Y., Ross, K.N. and Balk, S.P., 2006. Androgens Induce Prostate Cancer Cell Proliferation through Mammalian Target of Rapamycin Activation and Post-transcriptional Increases in Cyclin D Proteins. *Cancer Research*, 66(15), pp. 7783–7792. https://doi.org/10.1158/0008-5472.CAN-05-4472.

Yang, P., Cartwright, C.A., Li, J., Wen, S., Prokhorova, I.N., Shureiqi, I., Troncoso, P., Navone, N.M., Newman, R.A. and Kim, J., 2012. Arachidonic acid metabolism in human prostate cancer. *International Journal of Oncology*, 41(4), pp.1495–1503. https://doi.org/10.3892/ijo.2012.1588.

Yebes, A., Toribio-Vazquez, C., Martinez-Perez, S., Quesada-Olarte, J.M., Rodriguez-Serrano, A., Álvarez-Maestro, M. and Martinez-Piñeiro, L., 2023. Prostatitis: A Review. *Current Urology Reports*, 24(5), pp. 241–251. https://doi.org/10.1007/s11934-023-01150-z.

Yu, K., Whitlock, J.M., Lee, K., Ortlund, E.A., Yuan Cui, Y. and Hartzell, H.C., 2015. Identification of a lipid scrambling domain in ANO6/TMEM16F. *eLife*, 4, e06901. https://doi.org/10.7554/eLife.06901.

Yu, Q., Zhong, H., Zhu, X., Liu, C., Zhang, X., Wang, J., Li, Z., Shi, S., Zhao, H., Zhou, C. and Zhao, Q., 2025. Glycosylation profiling of triple-negative breast cancer: clinical and immune correlations and identification of LMAN1L as a biomarker and therapeutic target. *Frontiers in Immunology*, 15, 1521930. https://doi.org/10.3389/fimmu.2024.1521930.

Yue, S., Li, J., Lee, S.-Y., Lee, H.J., Shao, T., Song, B., Cheng, L., Masterson, T.A., Liu, X., Ratliff, T.L. and Cheng, J.-X., 2014. Cholesteryl Ester Accumulation Induced by PTEN Loss and PI3K/AKT Activation Underlies Human Prostate Cancer Aggressiveness. *Cell Metabolism*, 19(3), pp. 393–406. https://doi.org/10.1016/j.cmet.2014.01.019.

Zadra, G. and Loda, M., 2019. When fat goes down, prostate cancer is on the ropes. *Molecular & Cellular Oncology*, 6(3), 1595308. https://doi.org/10.1080/23723556.2019.1595308.

Zadra, G., Ribeiro, C.F., Chetta, P., Ho, Y., Cacciatore, S., Gao, X., Syamala, S., Bango, C., Photopoulos, C., Huang, Y., Tyekucheva, S., Bastos, D.C., Tchaicha, J., Lawney, B., Uo, T., D'Anello, L., Csibi, A., Kalekar, R., Larimer, B., Ellis, L., Butler, L.M., Morrissey, C., McGovern, K., Palombella, V.J., Kutok, J.L., Mahmood, U., Bosari, S., Adams, J., Peluso, S., Dehm, S.M., Plymate, S.R. and Loda, M., 2019. Inhibition of de novo lipogenesis targets androgen receptor signaling in castration-resistant prostate cancer. *Proceedings of the National Academy of Sciences*, 116(2), pp. 631–640. https://doi.org/10.1073/pnas.1808834116.

Zlotta, A.R., Egawa, S., Pushkar, D., Govorov, A., Kimura, T., Kido, M., Takahashi, H., Kuk, C., Kovylina, M., Aldaoud, N., Fleshner, N., Finelli, A., Klotz, L., Lockwood, G., Sykes, J. and Kwast, T. van der, 2014. Prevalence of Inflammation and Benign Prostatic Hyperplasia on Autopsy in Asian and Caucasian Men. *European Urology*, 66(4), pp. 619–622. https://doi.org/10.1016/j.eururo.2014.06.026.

Zorko, N.A., Makovec, A., Elliott, A., Kellen, S., Lozada, J.R., Arafa, A.T., Felices, M., Shackelford, M., Barata, P., Zakharia, Y., Narayan, V., Stein, M.N., Zarrabi, K.K., Patniak, A., Bilen, M.A., Radovich, M., Sledge, G., El-Deiry, W.S., Heath, E.I., Hoon, D.S.B., Nabhan, C., Miller, J.S., Hwang, J.H. and Antonarakis, E.S., 2025. Natural Killer Cell Infiltration in Prostate Cancers Predict Improved Patient Outcomes. *Prostate Cancer and Prostatic Diseases*, 28(1), pp. 129–137. https://doi.org/10.1038/s41391-024-00797-0.

List of Figures, Tables and Appendices

Figures

Tables

Appendices

Appendices

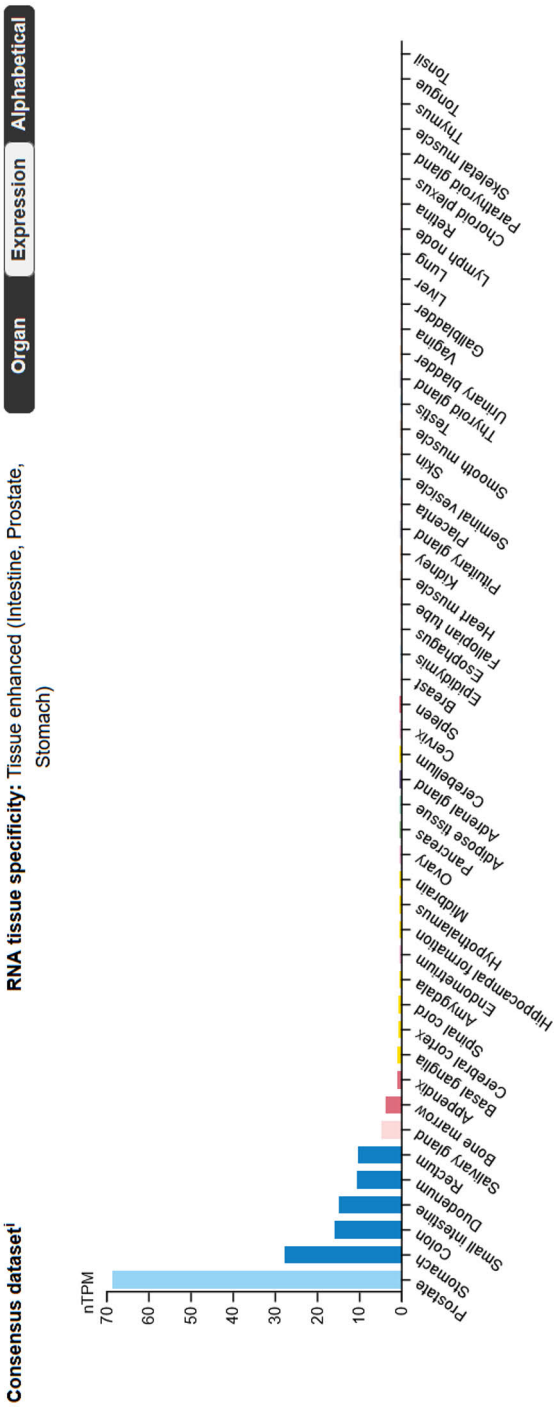

Appendix 1. *ANO7* expression in bulk RNA-seq data from normal tissues. The tissue types are organized from left to right by highest expression. The highest expression is seen in the prostate. Stomach, colon, small intestine, duodenum, and rectum exhibit moderate expression levels. The values represent a consensus data of GTEx and HPA transcriptomics data. Data source (HPA version 24 freeze): https://v24.www.proteinatlas.org/ENSG00000146205-ANO7/tissue#rna_expression

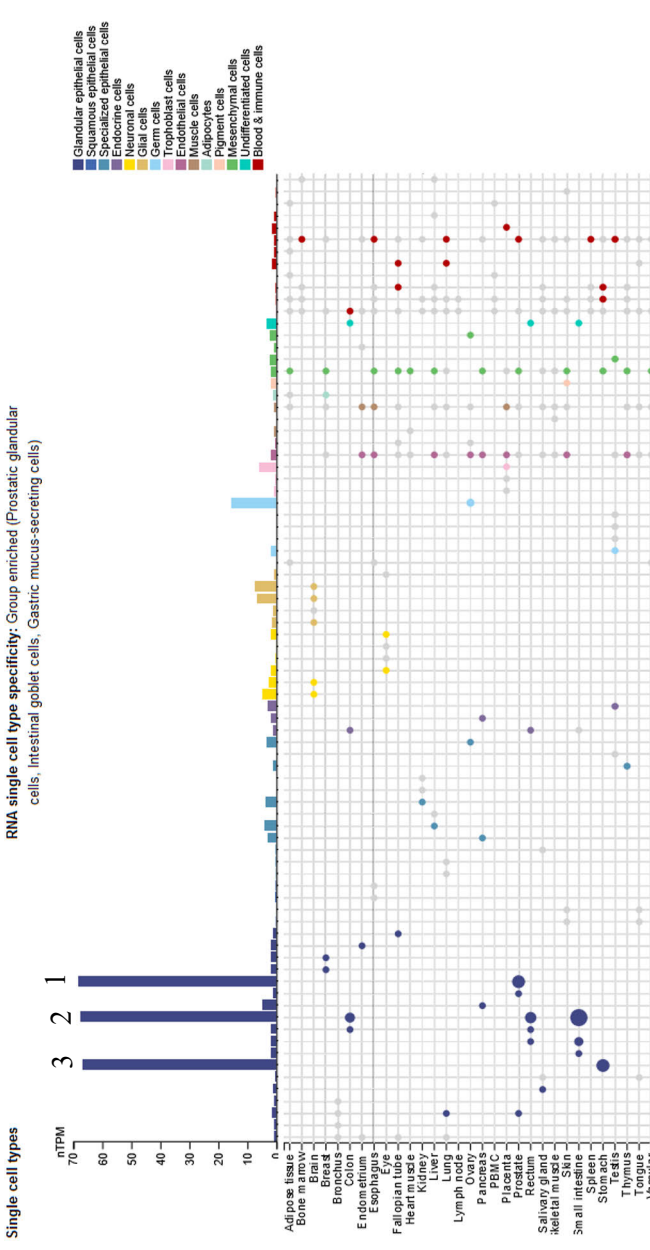

Appendix 2. Single-cell expression of ANO7 in single cell RNA-seq data, organised by tissue and cell type. ANO7 is enriched in prostatic glandular cells (1), intestinal goblet cells (2), and gastric mucus secreting cells (3). Data Source (HPA version 24 freeze): https://v34.proteinatlas.org/ENSG00000146205-ANO7/single+cell

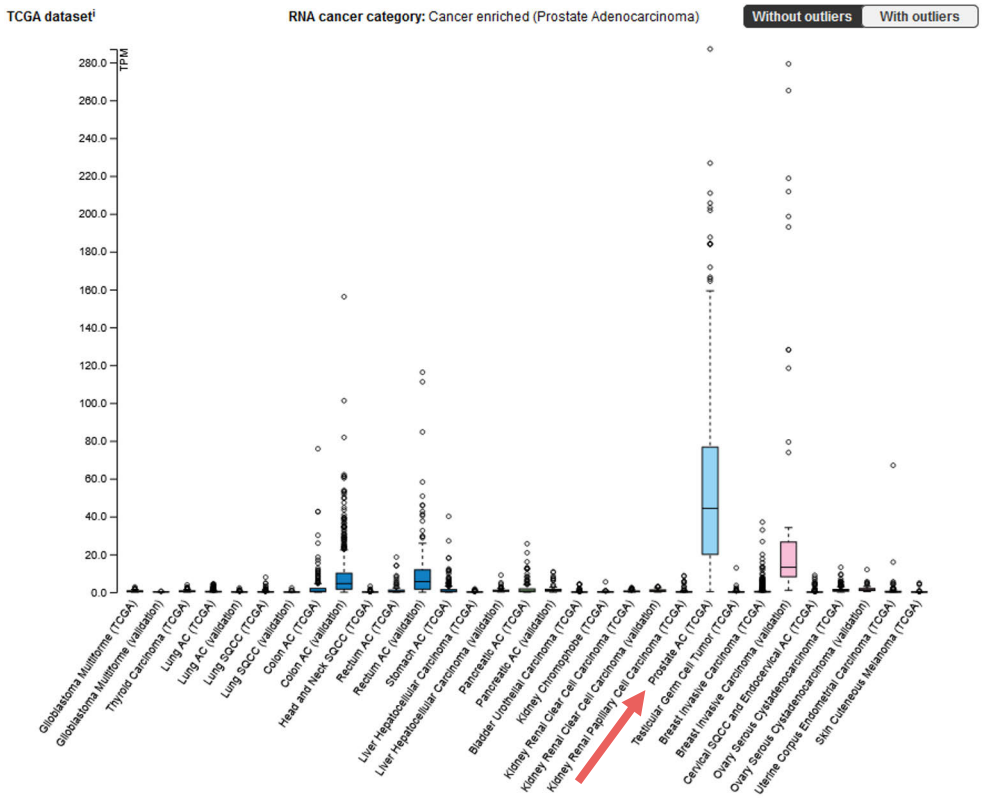

Appendix 3. ANO7 expression in The Cancer Genome Atlas Program (TCGA) pan-cancer data. ANO7 is enriched in prostate adenocarcinoma (marked with a red arrow). Data source (HPA version 24 freeze): https://v24.proteinatlas.org/ENSG00000146205-ANO7/cancer

Appendix 4. The cell fractionation protocol.

Step 1 is done in room temperature. After that, use pre-chilled buffers, keep the buffers and samples on ice throughout the rest of the protocol and run centrifugations at 4°C with slow stop.

1. Step 1 in cell culture. Collect growth media from 10cm dish into 15ml tube and trypsinise cells from the dish. Combine the cells into the 15ml tube and centrifuge at 125g 5min, discard supernatant. Wash the cells with PBS and pellet again at 125g 5min. Leave the supernatant in the tube for transportation.
2. Transport the cells to lab bench or fume hood. Discard the supernatant and wash the pellet with 500ul buffer HT by resuspending pellet into buffer, transfer the cell suspension into a 1,5 ml tube and centrifuge at 125g for 5min. Discard the supernatant.
3. Resuspend the pellet into 500ul of buffer HT. Incubate 15min on ice.
4. Using a 1 ml syringe *gently* pass cell suspension through a 27-gauge needle 10 times. Avoid foaming. Incubate 20 min on ice. Monitor the cells for nuclei disruption.
5. Disperse the cells by pipetting few times and take 167µl into a fresh a. 2 ml or b. 1,5 ml tube. This in the <u>total cell fraction</u>. Add to fractions (a. RNA, b. protein):
    a. 1700µl of TRIreagent
    b. 19,4µl 10% SDS and 7,8µl 25X protease inhibitor cocktail
    →Extract RNA/measure protein.
6. Centrifuge the rest of the sample at 720g for 5min. <u>The pellet contains nuclei</u> and the <u>supernatant contains cytoplasm</u>, membrane and mitochondria.

- Do the steps 7 and 8 in parallel.

7. Transfer 300µl of supernatant into a fresh 1,5 ml tube and centrifuge at 720g for 10min. Transfer 250µl of the supernatant into a fresh 1,5 ml tube and repeat centrifugation at 720g for 10min. Take a. 200µl /b. 172µl of supernatant into a fresh a. 2ml /b. 1,5ml tube. Add to fractions:
    a. 1800µl TRIreagent
    b. 20µl 10% SDS and 8µl 25X protease inhibitor cocktail
    → Extract RNA/measure protein.
8. Wash nuclear pellet from Step 6 with 500µl of buffer HT with 0,15% NP-40. Resuspend the pellet by pipetting and using a 1ml syringe *gently* pass the sample through a 25-gauge needle 5 times. Centrifuge at 720g for 10min and discard the supernatant. Repeat the wash without the needle treatment and centrifuge at 720g for 10min. Discard the supernatant.
    a. Resuspend the pellet in 200µl of buffer HT and transfer the suspension into 2 ml tube with 1800µl of TRIreagent.
    b. Resuspend the pellet in 172µl of buffer HT. Add 20ul 10% SDS and 8µl 25X protease inhibitor cocktail.
    → Extract RNA/measure protein.

Table 8. Buffer HT (Hypotonic buffer) recipe

Reagent	Final concentration (mM)	volume to 10 ml
Nuclease Free Water	-	8701 µl
HEPES pH 7,4 0,1 M	10	1000 µl
$MgCl^2$ 0,1 M	1,5	150 µl
KCl 1 M	10	100 µl
EDTA 0,5 M	1	20 µl
DTT 300 mM*	0,5	16,7 µl
RNase Inhibitor 40 U/µl*	50 U/ml	12,5 µl

*Add just prior to use. Do not store complete buffer.

For the buffer HT with 0.15% NP-40, add NP-40 into buffer HT accordingly. For example: 992,50µl buffer HT + 7,5µl 20% NP-40 (w/v).

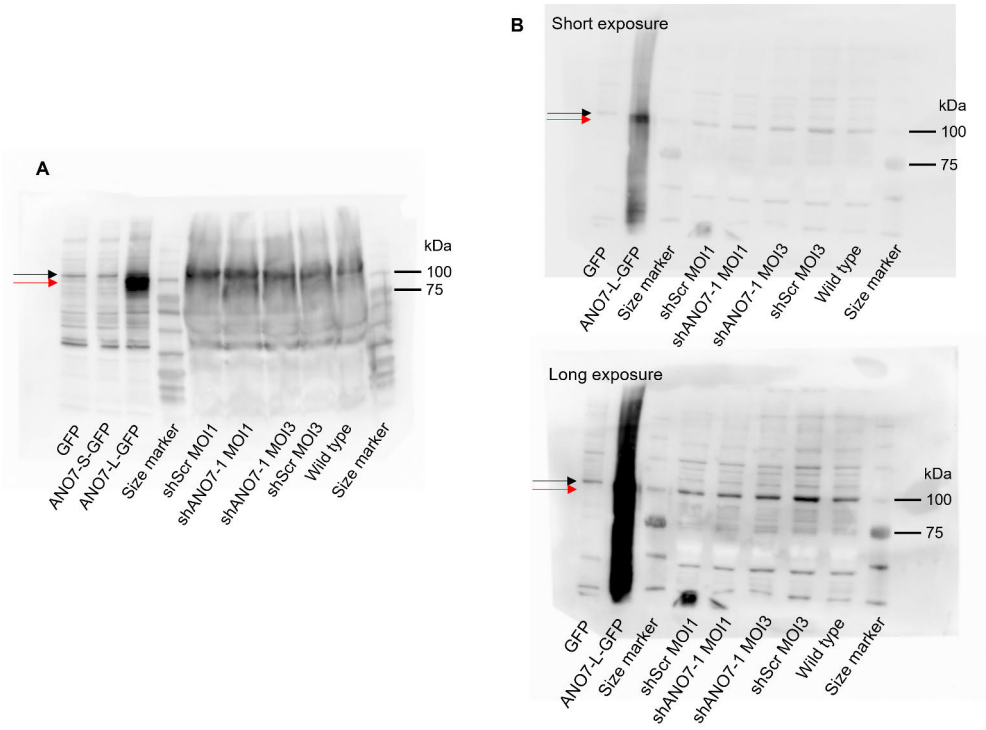

Appendix 5. ANO7 Western blot from MDA PCa 2b shRNA samples. The samples with highest shRNA knock-down efficacy were analysed. Samples were run in a gradient gel with control samples (A). The control samples were collected from COS-7 cells over-expressing GFP, ANO7-S-GFP and ANO7-L-GFP. The ANO7-L is recognised by the antibody (red arrow), and an unspecific band is located just above the ANO7-L band (black arrow). The samples were run in a homogenous (7% acrylamide) gel for better resolution (short and long exposures) (B). The unspecific band and the ANO7-L positive control bands were seen adjacently also in the 7% gel. No band was changed in the shRNA samples in the 100 kDa region, which corresponds to the size of ANO7. GFP: green-fluorescent protein; kDa: kilo dalton.

TURUN
YLIOPISTO
UNIVERSITY
OF TURKU

Painosalama, Turku, Finland 2025

ISBN 978-952-02-0152-4 (PRINT)
ISBN 978-952-02-0153-1 (PDF)
ISSN 0355-9483 (Print)
ISSN 2343-3213 (Online)